OPTICAL PROPERTIES OF EXCITED SILICON AND GERMANIUM

AT LOW TEMPERATURES

Thesis by

Stephen Aplin Lyon

In Partial Fulfillment of the Requirements

for the Degree of

Doctor of Philosophy

California Institute of Technology

Pasadena, California

1979

(Submitted July 24, 1978)

TO MY FATHER

Finally, and most importantly, I would like to thank my wife, Gail, for her encouragement and support during my years as a graduate student.

ABSTRACT

Part I of this thesis deals with 3 topics concerning the luminescence from bound multi-exciton complexes in Si. Part II presents a model for the decay of electron-hole droplets in pure and doped Ge.

Part I.

We present high resolution photoluminescence data for Si doped with Al, Ga, and In. We observe emission lines due to recombination of electron-hole pairs in bound excitons and satellite lines which have been interpreted in terms of complexes of several excitons bound to an impurity. The bound exciton luminescence in Si:Ga and Si:Al consists of three emission lines due to transitions from the ground state and two low lying excited states. In Si:Ga, we observe a second triplet of emission lines which precisely mirror the triplet due to the bound exciton. This second triplet is interpreted as due to decay of a two exciton complex into the bound exciton. The observation of the second complete triplet in Si:Ga conclusively demonstrates that more than one exciton will bind to an impurity. Similar results are found for Si:Al. The energy of the lines show that the second exciton is less tightly bound than the first in Si:Ga. Other lines are observed at lower energies. The assumption of ground-state to ground-state transitions for the lower energy lines is shown to produce a complicated dependence of binding energy of the last exciton on the number of excitons in a complex. No line attributable to the decay of a two exciton complex is observed in Si:In.

We present measurements of the bound exciton lifetimes for the four common acceptors in Si and for the first two bound multi-exciton complexes in Si:Ga and Si:Al. These results are shown to be in agreement with a calculation by Osbourn and Smith of Auger transition rates for acceptor bound excitons in Si. Kinetics determine the relative populations of complexes of various sizes and work functions, at temperatures which do not allow them to thermalize with respect to one another. It is shown that kinetic limitations may make it impossible to form two-exciton complexes in Si:In from a gas of free excitons.

We present direct thermodynamic measurements of the work functions of bound multi-exciton complexes in Al, B, P and Li doped Si. We find that in general the work functions are smaller than previously believed. These data remove one obstacle to the bound multi-exciton complex picture which has been the need to explain the very large apparent work functions for the larger complexes obtained by assuming that some of the observed lines are ground-state to ground-state transitions. None of the measured work functions exceed that of the electron-hole liquid.

Part II

A new model for the decay of electron-hole-droplets in Ge is presented. The model is based on the existence of a cloud of droplets within the crystal and incorporates exciton flow among the drops in the cloud and the diffusion of excitons away from the cloud. It is

able to fit the experimental luminescence decays for pure Ge at dif-
ferent temperatures and pump powers while retaining physically
reasonable parameters for the drops. It predicts the shrinkage of
the cloud at higher temperatures which has been verified by spatially
and temporally resolved infrared absorption experiments. The model
also accounts for the nearly exponential decay of electron-hole-droplets
in lightly doped Ge at higher temperatures.

Parts of this thesis have been or will be published under the following titles:

Chapter 2: Edge Luminescence Spectra of Acceptors in Si; Implications for Multiexciton Complexes, S. A. Lyon, D. L. Smith and T. C. McGill, Phys. Rev. B17, 2620 (1978).

Chapter 3: Bound Exciton Lifetimes for Acceptors in Si, S. A. Lyon, G. C. Osbourn, D. L. Smith and T. C. McGill, Solid State Commun. 23, 425 (1977).

Chapter 4: Thermodynamic Determination of Work Functions of Bound Multiexciton Complexes, S. A. Lyon, D. L. Smith, and T. C. McGill, Phys. Rev. Lett. 41, 56 (1978).

Temperature Dependence and Work Functions of Bound Multiexciton Complexes in Si, S. A. Lyon, D. L. Smith and T. C. McGill, (in preparation).

Chapter 5: Transients of the Photoluminescence from EHD in Doped and Undoped Ge, M. Chen, S. A. Lyon, K. R. Elliott, D. L. Smith and T. C. McGill, Il Nuovo Cimento 39B #2, 622 (1977).

Transients of the Photoluminescence Intensities of the Electron-Hole-Droplets in Pure and Doped Ge, M. Chen, S. A. Lyon, D. L. Smith and T. C. McGill, Phys. Rev. B17, (1978).

Publications not included in this thesis are:

Temperature Dependence of Relative Emission Intensities Via Symmetry Allowed Phonon Processes in Si and Ge, D. L. Smith, R. B. Hammond, M. Chen, S. A. Lyon and T. C. McGill, Proceedings of the Thirteenth International Conference on the Physics of Semiconductors, Rome, 1976, p. 1077.

Transient Decay of Satellite Lines of Bound Excitons in Si:P, A. Hunter, S. A. Lyon, D. L. Smith, and T. C. McGill (in preparation).

Fine Structure in the Photoluminescence Spectra of Lithium Doped Silicon, S. A. Lyon, D. L. Smith and T. C. McGill (in preparation).

TABLE OF CONTENTS

CHAPTER 1

INTRODUCTION

I. Background

One of the important aspects in attempting to understand a material is determining its electronic properties. In general this means gaining some knowledge of the possible electronic excitations of the system. Since a complete description of 10^{23} interacting atoms is impossible, the first approach is to determine the single particle excitations in a solid. This approach corresponds to a determination of the band structure. This one electron picture is very powerful and is the basis for much of our understanding and most of the technology associated with semiconductors. However, treating the electronic excitations of a semiconductor as being in-dependent of one another is an approximation which becomes invalid at low temperatures and high excitation densities. Under these conditions it is possible to produce electronic excited states of the solid which are qualitatively different from those described in the single particle, or Hartree-Fock, picture. This thesis will be concerned with properties of excitations of this type in crystals of silicon and germanium.

One of the simplest excitations of a semiconductor not con-tained in the usual Hartree-Fock picture is the free exciton (FE)[1]. The FE consists of an electron and hole bound together by their mutual coulomb attraction. Typical ionization energies for excitons in semiconductors range from about 1 to 20 meV (see Table 1.1). At low temperatures where kT is small compared to the exciton ionization energy, free electrons and holes in a crystal will bind to form

Table 1.1

Free Excitons

	Silicon	Germanium
Bohr radius, a_o^* ($\overset{o}{A}$)	43 [a]	114 [a]
Dissociation Energy E_D (meV)	14.7 [b]	4.15 [c]
Effective mass, m_{ex}^*	$.6m_o$	$.335m_o$
Lifetime, τ_{ex} (μs)	~2	~7

EHD

	Silicon	Germanium
Work function, ϕ_{EHD} (meV)	8.2 [d]	1.8 [c]
Pair density, n_o (cm^{-3})	3.3×10^{18} [d]	2.4×10^{17} [e]
Pairs per droplet, ν	6.6×10^6 [f]	10^6-10^8 [g]
Total Fermi energy, E_F ($E_{F_e} + E_{F_h}$) (meV)	22.2 [d]	6.43 [e]
Lifetime, τ(μs)	~.2	37
Critical Temperature T_c (^{o}K)	~28	6.5 [h]
Radius, R_D (μm)	<1	2-10 [i]

a) obtained using $E_D = e^2/2\epsilon_o a_o^*$

b) K. L. Shaklee and B. Nahory, Phys. Rev. Lett. 24, 942 (1970).

c) G. A. Thomas, A. Frova, J. C. Hensel, R. E. Miller, and P. A. Lee, Phys. Rev. B13, 1692 (1976).

d) Ref. 28.

e) Ref. 16.

f) M. Capizzi, M. Voos, C. Benoit a la Guillaume and J. C. McGroddy, Solid State Commun. 16, 709 (1975).

g) T. K. Lo, B. J. Feldman, and C. D. Jeffries, Phys. Rev. Lett. 31, 221 (1973).

h) Ref. 12.

i) V. S. Bagaev, et al, [Fiz. Tverd. Tela. 15, 3269 (1973)] [Sov. Phys. Solid State 15, 2179 (1974)].

excitons. The ratio of the density of free carriers to the density of excitons is given by mass action,

$$\frac{n_e n_h}{n_{ex}} \propto e^{-E_D/kT} \quad , \tag{1.1}$$

where n_e is the density of free electrons, n_h the density of free holes, n_{ex} the density of free excitons, and E_D the dissociation energy of an exciton.

In order to understand the optical properties of an exciton, we need an approximation to its wave-function. In a two band model, and neglecting spin, the wave-function can be written [2] in terms of the Hartree-Fock basis as,

$$\psi_{FE} = \sum_{k_e, k_h} A(k_e, k_h) \psi_{ck_e} \chi_{vk_h} \quad , \tag{1.2}$$

where ψ_{ck_e} is the one-particle wave-function for an electron in the conduction band with wavevector k_e, and χ_{vk_h} is for a hole in the valence band with wave-vector k_h. The sum on k_e and k_h range over the Brillouin zone for each band. The Fourier transform of $A(k_e, k_h)$, $F(r_1, r_2)$, is the "envelope function", or slowly varying part of the wave-function, giving its extent in space, and ψ and χ contain the rapidly varying periodic parts of the Bloch functions. Putting this form for ψ_{FE} into Schrodinger's equation with the potential $e^2/\varepsilon_o r$, with ε_o the static dielectric constant, and assuming isotropic effective masses, we obtain an equation for $F(r_1, r_2)$ whose form is the same as that for a hydrogen atom. Thus

the exciton acts as a free particle with an effective mass m_{ex}^{*}, and associated center-of-mass energy, and has internal degrees of freedom described by hydrogenic wave-functions. The size of the wave-function is characterized by a Bohr radius and the energy scale is set by an excitonic Rydberg. Values for these parameters for silicon and germanium are given in Table 1.1.

Free excitons are excited states in silicon and germanium and therefore have a finite lifetime. One decay route is for the electron and hole to recombine, emitting a photon. In the indirect materials such as Si and Ge a momentum-conserving phonon is also emitted, and thus the energy of the photon is given by,

$$h\nu = E_{ex} - \hbar\Omega_{phonon} \tag{1.3}$$

where E_{ex}, the energy of the exciton, is made up of a part due to the center-of-mass kinetic energy and a part due to the creation from the ground state of the electron-hole pair in the exciton. This last part is just the energy of an exciton with zero kinetic energy, $E_o \equiv E_{gap} - E_D$, and since $E_{gap} \gg E_D$ and $E_{gap} \gg \hbar\Omega_{phonon}$, the emitted photon has an energy just slightly less than the band gap. We expect the photons emitted in the decay of free excitons to have an energy distribution starting at $E_{gap} - E_D - \hbar\Omega_{phonon}$ and extending to slightly higher energies due to their center-of-mass motion. At low densities the excitons exhibit a Boltzmann distribution of kinetic energies which gives a luminescence lineshape [3],

$$I_{FE}(h\nu) \propto (h\nu + \hbar\Omega_{ph} - E_0)^{\frac{1}{2}} e^{-(h\nu + \hbar\Omega_{ph} - E_0)/kT} \qquad (1.4)$$

where $I_{FE}(h\nu)$ is the intensity of the luminescence emitted at ν. The spectrum in Fig. 1.1 was taken on high purity Si, and the electrons and holes were generated by exciting the crystal with above band gap light. The line at highest energy is due to the decay of free excitons. From the inset it can be seen that the theoretical curve from Eq. 1.4 (convolved with the instrumental response function) describes the lineshape extremely well.

At an energy lower than the free exciton in Fig. 1.1, we see a broad line labeled Electron-Hole Liquid. This luminescence line was first observed in 1966 by Haynes [4] and interpreted as the decay of one exciton in a bound pair of excitons, a biexciton. In 1968 Keldysh [5] suggested that at high exciton densities, the excitons could condense into a highly correlated, Fermi-degenerate plasma of electrons and holes. Further work [6,7] has shown that the line originally ascribed to the decay of biexcitons actually arises from the recombination of pairs within a droplet of this plasma (EHD). Observation of this metallic liquid within a crystal has been reported for several semiconductors, including Si, Ge, GaP, [8] SiC [9], and CdS [10]. Theoretical calculations show that the liquid phase should be more stable than the free exciton in many semiconductors [11]. There is now a large body of data which shows conclusively that the condensate is a degenerate Fermi-liquid in thermal equilibrium with the surrounding gas of free excitons [12].

Figure 1.1

Photoluminescence spectrum of high purity Si at
low temperatures. The inset shows the FE at higher
resolution and the solid dots are a fit using the
theoretical lineshape discussed in the text. (from
R. B. Hammond, et al, Phys. Rev. B13, 3566 (1976).)
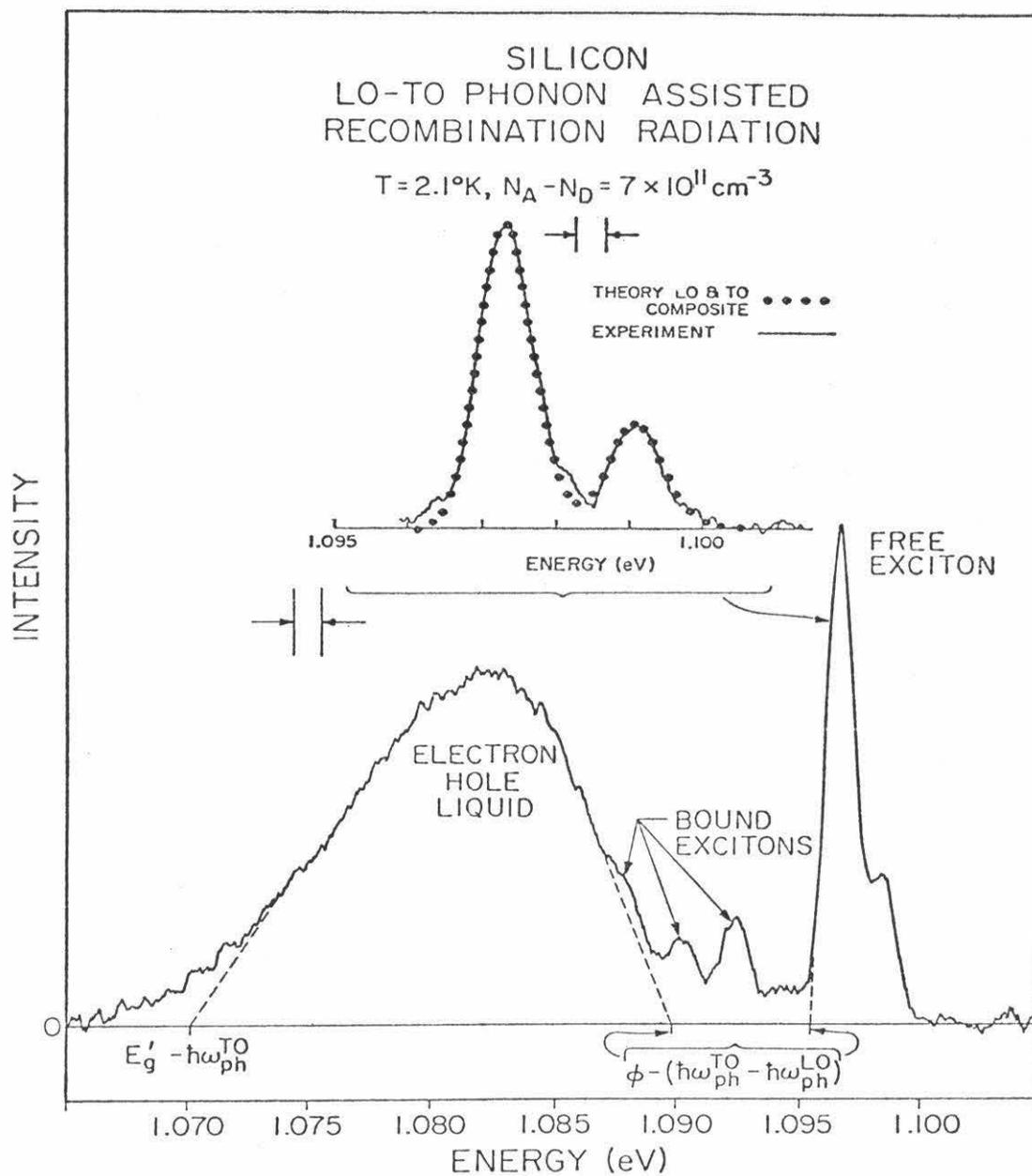
Figure 1.1

At low excitation intensities (low exciton densities) no liquid is formed. If the sample is below the liquid critical temperature and the excitation intensity is increased, a threshold for production of droplets is reached. Further increases in excitation increase the fraction of the volume occupied by EHD without increasing the exciton density. From measurements of the excitation threshold and liquid density as a function of temperature, approximate phase diagrams have been determined for the exciton-EHD system [12].

The EHD has been studied by a number of techniques, one of the most important being the observation of its luminescence as in Fig. 1.1. An above band-gap light source was used to create the electron-hole pairs for Fig. 1.1, but other methods of excitation such as high energy electron beams [13] or electrical injection [14,15] of carriers have also been used. A simple model for the lineshape shows that its width is determined by the electron and hole Fermi energies and the temperature [16]. From the Fermi energies and ef-fective masses of the carriers, the density of pairs within the liquid can be determined. Also, the energy difference between the free exciton edge and the high energy edge of the EHD gives the work function for a pair in the liquid, ϕ_{EHD} (see Fig. 1.1). From careful fitting of luminescence as a function of temperature, these parameters have been measured as well as their variation with temperature for Si and Ge (see Table 1.1).

Another fruitful approach to the study of EHD in Ge has been the scattering and absorption of infrared light [17]. Typically a

wavelength of 3.39 μm is used due to the large absorption coefficient in EHD, and the availability of a laser (He-Ne) at this wavelength. The presence of the condensed phase within a crystal will locally change the real part of the index of refraction. The unexcited Ge crystal is transparent at these wavelengths, but the local index changes will Rayleigh scatter a probe beam. From the angular dependence of this scattering the radii of the droplets of liquid in unstrained Ge are found to range from about 2 to 10 μm depending on temperature. Measurements of the spatial dependence of the scattering and absorption show that the droplets form a cloud within the crystal with a pump-power dependent radius as large as several mm. From measurements of the absolute absorption, it has been determined that the fill factor (fraction of the crystal volume occupied by liquid) within the cloud is typically about 1%. Recent doppler-shifted light scattering experiments [18] show that the droplets are pushed into the crystal, probably through their interaction with phonons.

A third experimental method has been to look at the break-up of EHD in a large electric field[19]. A device is made with a pn junction in one part of the crystal. EHD are created in another area and allowed to drift into the junction where they are pulled apart by the high fields present. This produces a current spike in the external circuit, and the number of carriers in the droplet is approximately equal to the total charge within the spike. From the luminescence and light scattering we know the density and size of a droplet and thus the total number of carriers. The value obtained from the junction noise

experiment is in good agreement with the value calculated from the other two experiments.

Until now we have been discussing experiments performed on crystals with very low concentrations of electrically active impurities ($<10^{12} cm^{-3}$ for Si, $<10^{10} cm^{-3}$ for Ge). However, probably the most important aspect (at least technologically) of semiconductors is our ability to change their electrical properties through the introduction of small amounts of impurities. If a small amount of a shallow impurity ($\sim 10^{13}/cm^3$ for Si or about 1 part per billion) is added to a crystal, it becomes much easier to generate EHD [20]. The excitation threshold for production of the liquid is reduced although these impurity concentrations are insufficient to cause significant changes in such macroscopic properties of the droplets as their work function, density, or radius. It is thought that the impurities are acting as nucleation sites for the droplets [20] and reduce the supersaturation of the excitonic gas needed to produce the liquid. If in fact excitons are building up on impurities to form EHD, then we should be able to detect "embryonic droplets" consisting of only a few excitons bound to an impurity. In Fig. 1.1 we do see some lines labeled "Bound Excitons" which are due to the binding of excitons to impurities. We know that the pair in the initial state is immobile, for otherwise we would expect a characteristic broadening towards higher energies at increased temperatures due to increased kinetic energy as seen for the FE. The "Bound Exciton" lines of Fig. 1.1 show no significant broadening with temperature, however.

The binding of a single exciton to an impurity is a common phenomenon in semiconductors. These bound excitons (BE) occur in both direct and indirect materials. It has been found experimentally that a neutral shallow impurity will bind an exciton with about one-tenth the ionization energy of the impurity [21]. In Si ionization energies of common shallow impurities range from about 30 meV to over 100 meV, and thus from this phenomenological "Haynes rule" we expect excitons to bind with from about 3 to over 10 meV as observed (see Table 1.2). The BE lines in Si are typically less than .5 meV in width and it is possible to resolve the BE due to each of the shallow impurities in a Si crystal. Impurity ionization energies in Ge are about 10 meV or less, which implies that the BE work functions are all about 1 meV or less and since the widths are comparable to those in Si, the lines are difficult to separate. The line positions for luminescence from excitons bound to various impurities in Si are known (see Table 1.2). We find that the highest energy line of the three "Bound Excitons" in Fig. 1.1 is due to the decay of a single exciton bound to residual boron impurities. The two lower energy lines in Fig. 1.1 do not correspond to BE on any known impurities, and studies have shown that they are associated with boron[22]. It is thought that these lines arise from decays within "embryonic droplets" consisting of 2 excitons bound to a boron for the higher lying line and 3 excitons for the lower lying line.

A series of luminescence lines associated with phosphorous is shown in Fig. 1.2. Again the highest energy line is due to the decay of a single exciton bound to the impurity, while the lower lying

Table 1.2

Shallow Impurities in Si

Donors	Impurity Ionization Energy, E_I, (meV)[a]	BE work function ϕ_{BE}, (meV)	BE(NP) line position, $h\nu_{BE}$,(meV)[b]
Li	33[c]	3.4[d]	1151.21±.02
Sb	42.7	4.64[e]	1149.97±.11
P	45.5	4.69	1149.92±.05
As	53.7	5.51[e]	1149.1 ±.11
Bi	69 [c]	7.71[e]	1146.9 ±.11
Acceptors			
B	44.5	3.94	1150.67±.05
Al	68.5	5.08	1149.53±.05
Ga	72	5.66	1148.95±.05
In	155	13.68	1140.93±.05
Tl	260 [c]	44.2 [f]	1110.4 ±.1 [f]

a) F. Bassani, G. Iadonisi, and B. Preziosi, Rep. Prog. Phys. 37, 1099 (1974).

b) Obtained assuming FE(NP) threshold = 1154.61 meV and ϕ_{BE} from (e) for Sb, As, Bi. For Li used BE(TO) from (d) and assumed E_{TO}=58 meV.

c) Sze, Physics of Semiconductor Devices, (Wiley-Interscience, New York, 1969) p. 30.

d) K. Kosai and M. Gershenzon, Phys. Rev. B9, 723 (1974).

e) E. C. Lightowlers, M. O. Henry, and M. A. Vouk, J. Phys. C. 10, L713 (1977).

f) K. R. Elliott, D. L. Smith, and T. C. McGill (to be published).

Figure 1.2

Photoluminescence spectrum of the no-phonon replicas of the BE and the first four BMEC in Si:P. The τ_m (from R. Sauer, W. Schmid, and J. Weber, Solid State Commun. 24, 507 (1977)) are the measured lifetimes of the lines. The splittings between the FE threshold and the phosphorous related lines are shown in the lower part of the figure.
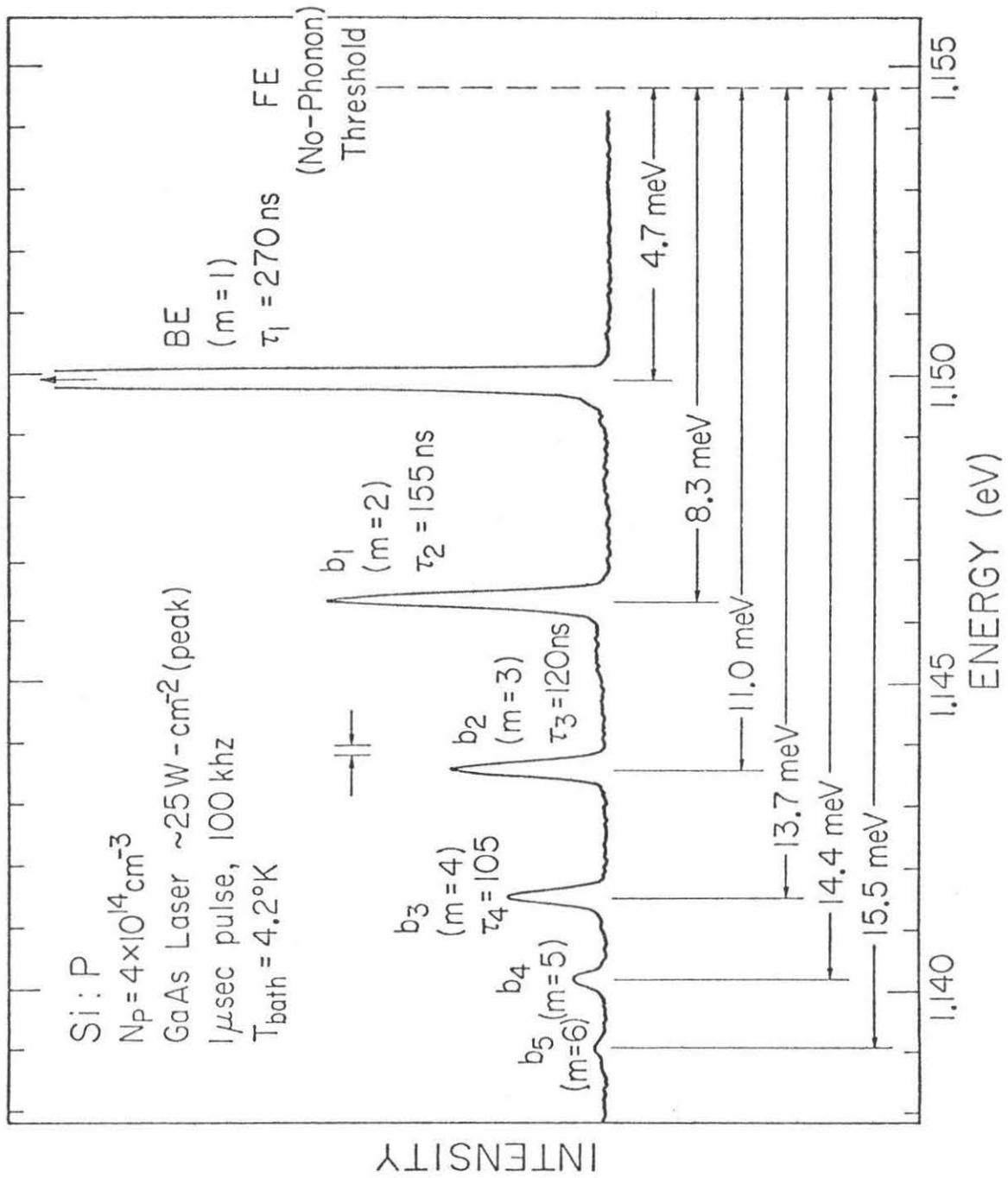
Figure 1.2

lines arise from decays within groups of excitons bound to a single impurity, a Bound Multi-Exciton Complex (BMEC). Luminescence lines from the decay of a BMEC were first observed by Pokrovskii [23] in connection with the nucleation of EHD in silicon, as mentioned earlier, and have subsequently been studied extensively [24]. To date they have been reported in Si associated with the donor impurities: Li, Sb, P, As, and the acceptors B, Al, Ga. Analogous lines have also been reported in Ge [25], cubic SiC, [26] and GaP [27]. If we assume that the lines in Fig. 1.2 are in fact due to these multi-exciton complexes, then we can label each line with an index, m, which tells how many excitons are bound to the impurity in the initial state. Thus the luminescence we observe is due to the recombination of one electron-hole pair, out of m pairs, leaving us with m-1 pairs on the site. One of the first questions that arises is that of how tightly can a complex bind an exciton. This work function for a complex with m-excitons, ϕ_m, is just the difference in energy between the state consisting of an exciton with zero momentum and an m-1 exciton complex in its ground state, and the state consisting of an m exciton complex.

If we assume that the radiative decay of an m-complex leaves the final (m-1) complex in its ground state, then we can determine the work function spectroscopically. The work function under this assumption is the spectroscopic difference, δ_m, between the complex's luminescence line and the free exciton edge. These spectroscopic differences are diagrammed in the bottom half of Fig. 1.2. For the BE

(m=1) we know that the final state of the transition is the ground state of the neutral impurity since the luminescence and absorption lines occur at exactly the same energy. Thus for the bound exciton, the spectroscopic difference, δ_1, and the work function, ϕ_1, are the same. For the BMEC the δ_m increase monotonically with m. If the transitions are, in fact, ground state to ground state, then this says that each exciton binds to the complex more tightly than the last exciton. Also, since we know that the work function of the EHD is about 8.2 meV [28], these data would seem to show that excitons will bind more tightly to a complex than to an EHD. This is somewhat disconcerting since it would be expected that a large complex would look very much like an EHD to an incoming exciton; the other carriers would have screened out the impurity potential. Furthermore, if these complexes do bind excitons more tightly than the EHD, then under certain conditions droplets should be unstable with respect to breaking up into BMEC. However, EHD luminescence is seen with doped Si.

Another problem with the BMEC model has been the observed splittings of the lines with the crystal under stress or in a magnetic field [29,30]. It is found that each line splits into the same number of components and that the components have the same energy separations for every complex. The only differences between complexes are the relative intensities of the components and the variation of these ratios with temperature. It is difficult to understand why a complex with several excitons should show essentially the same simple splittings as those for a single exciton bound to the impurity. These

work function and field splitting arguments have convinced one of the early proponents of the BMEC model to abandon the concept [29], although no new model for the lines has been proposed.

Despite these problems, there are some reasons one would like to retain the BMEC model. First, as shown in Fig. 1.2 each of the lines has a different lifetime, τ_m. The luminescence decays are found to be exponential over at least two decades. Since the τ_m are all different, we know that each line arises from a different initial state, and further the fact that $\tau_{m-1} > \tau_m$ seems consistent with a multi-pair picture. Another piece of evidence for the BMEC picture is that absorption lines corresponding to the luminescence lines for $m \neq 1$ are not observed. In Si:B, for example, the intensity of the luminescence for m=1 and m=2 is comparable, as are the decay times, which indicates that the two processes have similar oscillator strengths. However, in absorption only the bound exciton (m=1) is seen. This is to be expected in the BMEC model since to produce a 2-exciton complex with the absorption beam there must be bound excitons in the crystal to start with.

The third and most important piece of data in support of the BMEC picture concerns the variation of intensity of the lines with excitation intensity. It is found that the intensities are proportional to some power of the excitation, and the exponent, α, is larger for the bigger complexes. A log-log plot of luminescence intensity versus excitation level for Si:Al is shown in Fig. 1.3. The upper curve is for the BE and we see that its intensity varies approximately linearly with the excitation. The curves labeled b_1 (J=2) and b_2 are for the

Figure 1.3

Data on the pump power dependence of the BE and first two BMEC in Si:Al. The straight lines were fit to the data assuming Intensity $\propto$ (Excitation)$^\alpha$. The values obtained for α are shown.
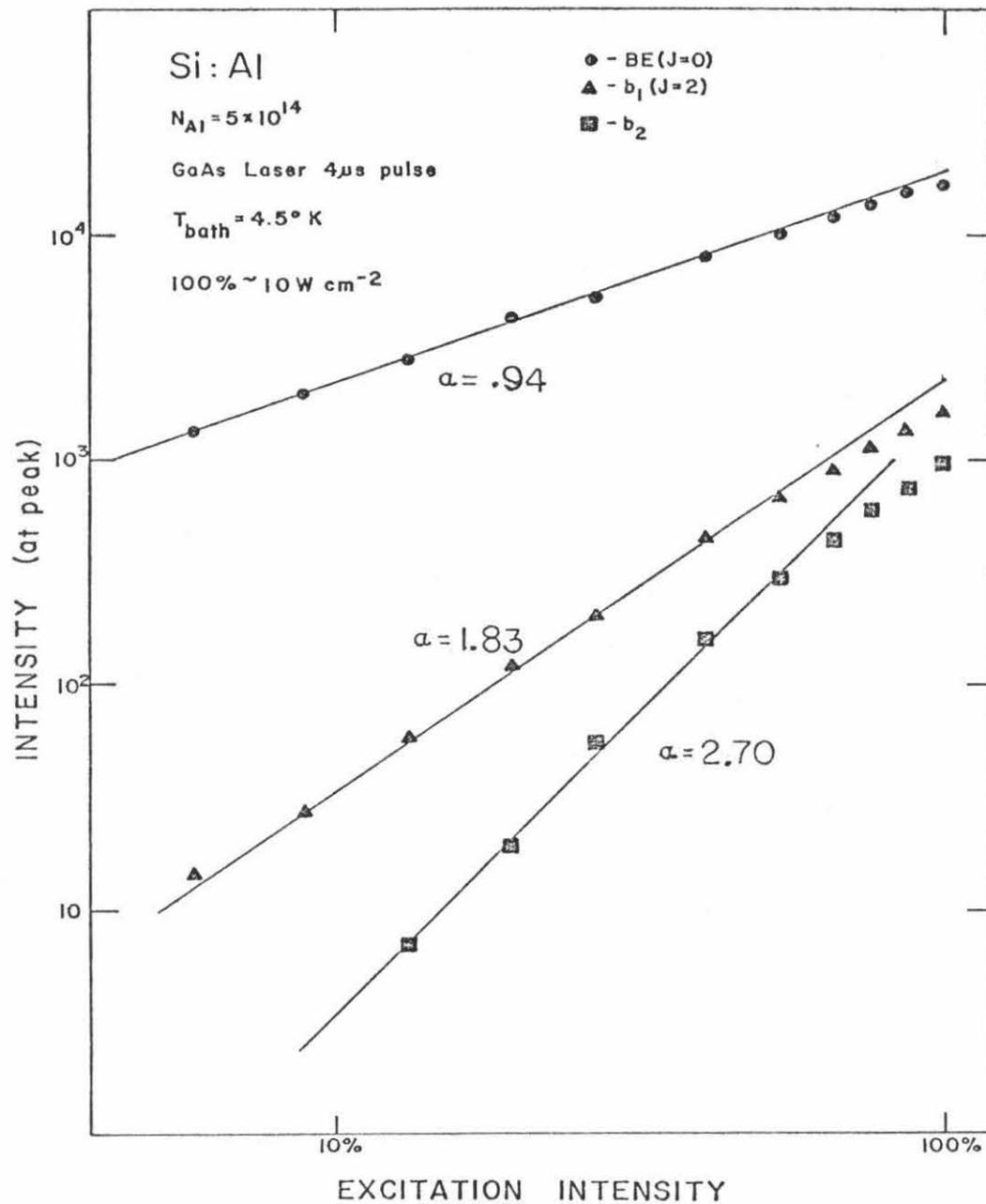
Figure 1.3

m=2 and m=3 complexes, respectively. We see that these lines have a faster than linear dependence on excitation. The rate equations based on the BMEC model predict this superlinear behavior. However, in that picture the exponent for the m-exciton complex should be m, the number of excitons on the site. The experimental numbers do not exactly reproduce this 1, 2, 3 sequence, however, the excitation is only at the surface, not homogeneous, so that some deviation could be expected. Furthermore, the rate equations predict that the intensities should saturate at high excitations as all the impurities are occupied and this behavior is seen in Fig. 1.3 for the b_1 and b_2 lines. The superlinear intensity dependence on excitation does suggest that more than one exciton is involved for the processes in which m > 1 and also establishes an ordering of the lines according to their exponent, α. This is the origin of the assignment of m values to the lines in Fig. 2 up through m=4.

II. Outline of Thesis

This thesis is divided into two parts: Part I deals with some experimental investigations of bound multi-exciton complexes in Si. Part II is a discussion of a new model for the decay of electron-hole-droplets in pure and lightly doped Ge.

Part I.

It has been suggested that acceptors in Si offer a test of the BMEC concept. [26] Some of the acceptor BE have low lying excited states. If a 2-exciton complex decays, it could leave the BE in one of the excited states as well as the ground state. In Chapter 2 we present experimental evidence that this does occur for Si:Ga and Si:Al. The data conclusively demonstrate that more than one exciton will bind to an impurity. However, the apparent work functions do not show a simple dependence upon the number of excitons on the site. No BMEC are observed in Si:In.

Measurements of the lifetimes of BE and BMEC on acceptors are presented in Chapter 3. We find that the BE lifetimes vary by almost three orders of magnitude depending on the impurity and that this variation can be accounted for by assuming that the dominant decay mechanism is a phononless Auger process. The measured lifetimes have important implications for the kinetics of BMEC formation. It is shown that it may be impossible to form 2-exciton complexes in Si:In from a gas of FE due to kinetic limitations.

In Chapter 4 we present direct thermodynamic measurements of the

work functions of BMEC in Si doped with B, Al, Li, and P. We find that the second exciton in Si:P and the third in Si:B are the most tightly bound and thereafter each exciton binds with less energy than the last. This is in contrast to the monotonically increasing work functions for the larger complexes one obtains by assuming that the observed lines are due to ground-state to ground-state transitions. None of the measured work functions exceeds that of the EHD. The data eliminate the problem of accounting for unphysically large binding energies of BMEC.

Part II.

Measurements of the decay of EHD in pure Ge exhibit an excitation dependence which is not explained by the "average drop" model. Attempts to use this model produce unphysical results. In Chapter 5 a new model is presented which takes into account exciton diffusion and the fact that the EHD form a "cloud" within the crystal. The model is able to fit the experimental results while retaining physically reasonable parameters, and the excitation dependence is a natural consequence. In lightly doped Ge EHD decay much more slowly than in pure Ge under the same conditions. The model presented here is also able to fit these data by assuming the impurities reduce the exciton diffusion length.

III. Optical Processes in Indirect Semiconductors

In order to study aggregates of nonequilibrium carriers within a semiconductor we need some way of generating them. One of the simplest methods, and the one used for the experiments discussed in this thesis, is to illuminate the crystal with above band-gap radiation. In Fig. 1.4 the optical absorption curves for Si, Ge, and GaAs are shown. At a photon energy below E_g for a particular semiconductor, the absorption coefficient is very small. For GaAs, a direct gap material, the absorption coefficient is large for photons with energies only slightly above E_g. The absorption turns on more slowly for Si and Ge since they have indirect gaps. The difference between the 77°K and 300°K curves is due to the change in band-gap with temperature. For the experiments to be discussed the excitation was either a GaAs laser (1.46 eV) or an Ar^+ laser (2.41 eV). Since the gaps change only slightly with temperature below 77°K we can use those curves to estimate the penetration depth of our exciting light. Thus for Si the absorption length for the GaAs laser is ~50 μm while for the Ar^+ laser it is ~2 μm. For Ge both lasers emit photons with an energy above the direct gap and thus are absorbed within less than 1 μm.

When the laser photons are absorbed they create electron-hole pairs with energies considerably larger than the band gap. This plasma probably relaxes to the lattice temperature in fractions of a nanosecond [31], or at longest, a few nanoseconds [32]. The free carriers
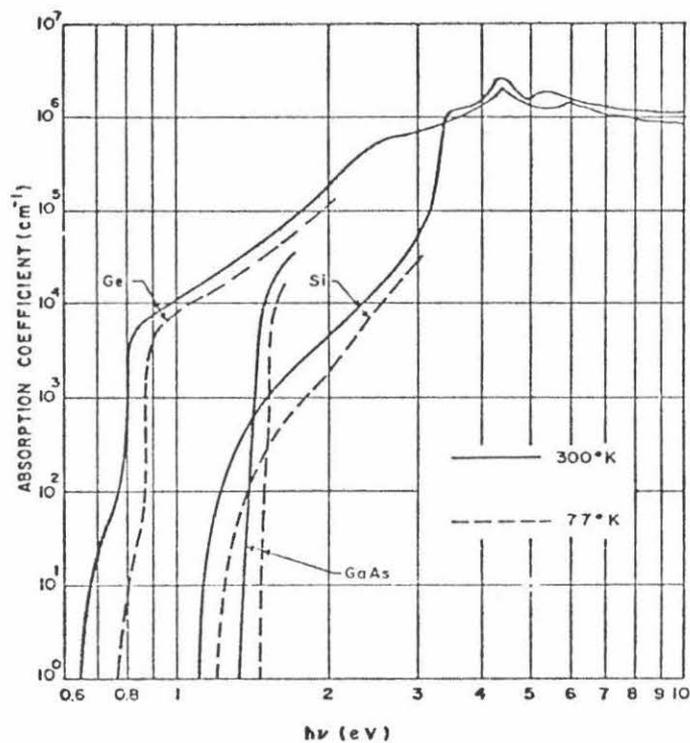
Figure 1.4

Measurements of near-gap optical absorption at 77°K
and 300°K in Si, Ge, and GaAs (from Sze, _Physics of Semi-conductor Devices_, (Wiley-Interscience, New York, 1969)
p. 54.)

bind into excitons on these same time scales. These thermalization times are in general short compared to typical decay times for EHD, excitons, and BMEC, often making it possible to use equilibrium thermodynamics in the analysis.

In radiative recombination the indirect gaps of Si and Ge play an essential role [2]. A photon with an energy of about 1 eV (comparable to the bandgaps for Si or Ge) has a wave-vector of about 10^{-3}Å^{-1}. This is to be compared with the wave-vector at the edge of the Brillouin Zone which is usually $\sim 1\text{Å}^{-1}$. The crystal momentum of the photon is negligible with respect to typical carrier momenta. This leads to the conclusion that the dipole matrix element for recombina-tion of free carriers is,

$$M \sim \left\langle \psi_{vk_1} \middle| \hat{\varepsilon} \cdot p \middle| \psi_{ck_2} \right\rangle , \tag{1.5}$$

where $\hat{\varepsilon}$ is the polarization of the photon and $p = -i\hbar\nabla$. This matrix element is zero unless $k_1 = k_2$. The band structure for Si is shown in Fig. 1.5. We see that the valence band maximum occurs at $k = 0$; however, the conduction band minimum occurs at $k \sim (.85,0,0)\frac{2\pi}{a}$. Thus the matrix element of Eq. 1.5 is zero for an electron-hole pair at the band edges. It is necessary to go to higher order to make this transition allowed. This accounts for the long radiative lifetimes and correspondingly small radiative efficiencies of Si and Ge. To recombine radiatively, the pair emits both a phonon and a photon;

Figure 1.5

A calculation of the band structure of Si, neglecting spin-orbit effects. The top of the valence band is labeled $\Gamma_{25'}$ (E=0). The conduction band minimum is near the point labeled X_1. The minimum occurs approximately at $\overline{k}=(.85,0,0)$ $2\pi/a$. The band gap at T=0 is 1.169 eV. (from D. J. Chadi, Phys. Rev. B$\underline{16}$, 3572 (1977)).
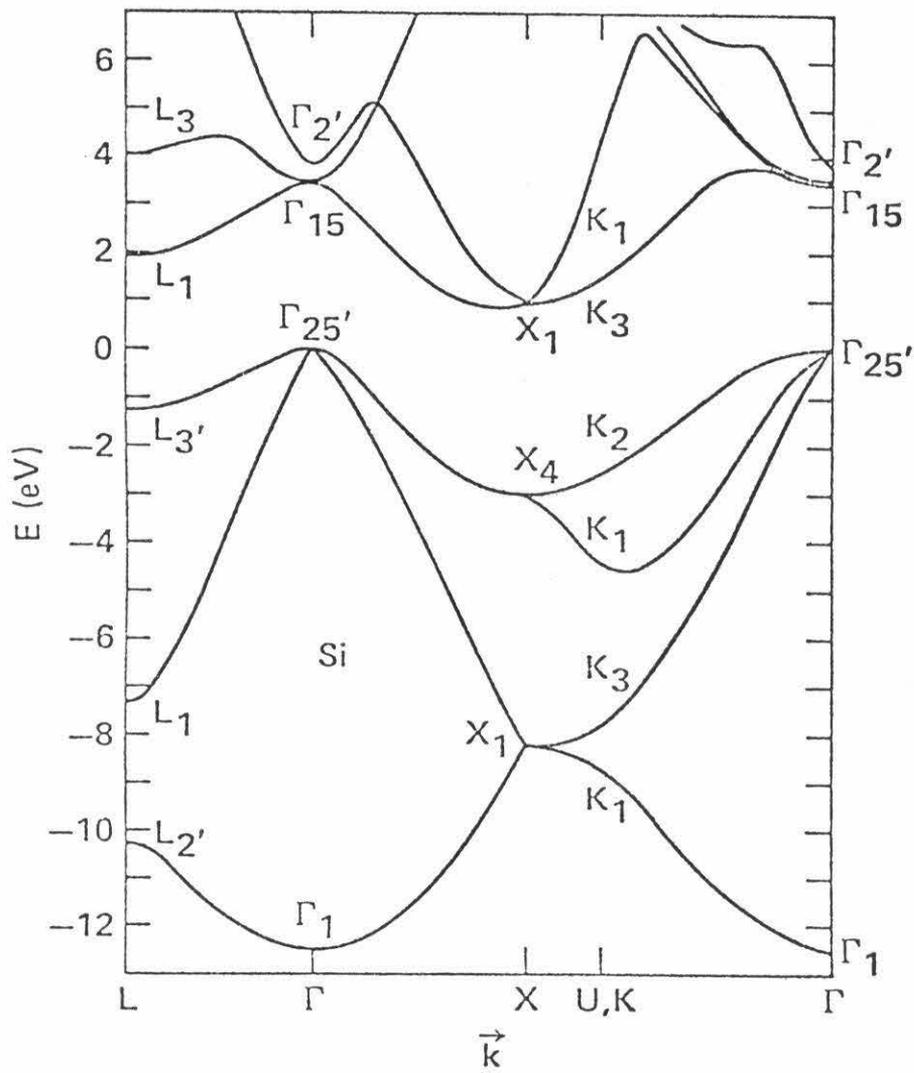
Figure 1.5

the photon carrying off most of the energy and the phonon carrying off the crystal momentum. (The process involving phonon capture is only important at higher temperatures). The rate for this process looks like,

$$R \propto \left| \sum_{k_I} \frac{\langle \psi_{vk_1} | \hat{\epsilon} \cdot p | \psi_{ck_I} \rangle \langle \psi_{ck_I} | H_{e-p} | \psi_{ck_2} \rangle}{(E_{ck_2} - \hbar\Omega_{ph} - E_{ck_I})} \right.$$

$$\left. + \sum_{k_{I'}} \frac{\langle \psi_{vk_1} | H_{e-p} | \psi_{vk_{I'}} \rangle \langle \psi_{vk_{I'}} | \hat{\epsilon} \cdot p | \psi_{ck_2} \rangle}{(E_{vk_1} - \hbar\Omega_{ph} - E_{vk_{I'}})} \right|^2 , \quad (1.6)$$

where H_{e-p} is the electron-phonon interaction, and $k_I, k_{I'}$ label the intermediate states. Phonon assisted recombination is illustrated schematically in Fig. 1.6a. This process requires the emission of a phonon with wave-vector (.85,0,0) for Si, and from the dispersion curves of Fig. 1.6b we see that there are several phonons which can participate. The possibilities are a TA phonon (19 meV), an LA (~41 meV), an LO (56 meV), and a TO (58 meV). Luminescence is seen associated with all of these phonons except the LA. (The absence of LA phonon assisted lines is not well understood.)

The requirement in Eq. 1.5 for conservation of $\vec{k}$ is only strictly true for free particles. For bound states the crystal momentum of a single electron or hole is no longer a conserved quantity. These states must be made up of a linear combination of Bloch functions with different $\vec{k}$. Thus the wave functions exhibit a spreading in

Figure 1.6

a) Schematic illustration of phonon assisted radiative recombination in an indirect semiconductor.

b) Phonon dispersion curves for Si in the (1,0,0)-direction (from G. Dolling, <u>Inelastic Scattering of Neutrons in Solids and Liquids</u> (International Atomic Energy Agency, Vienna 1962), Vol. II, p. 37.)
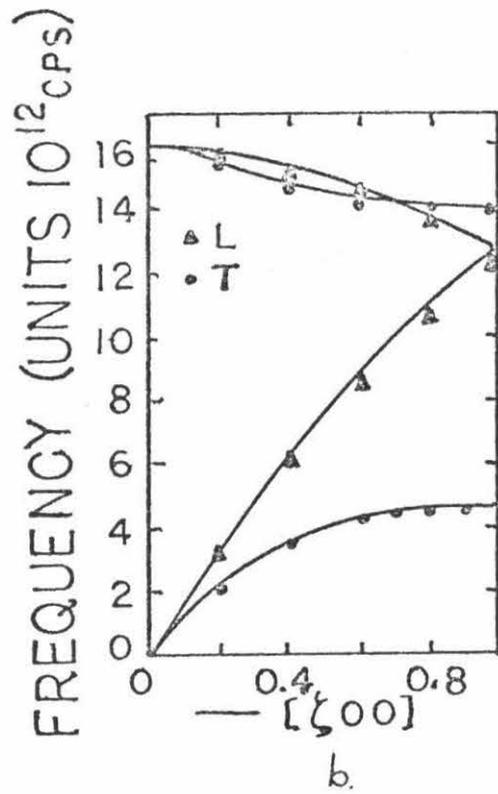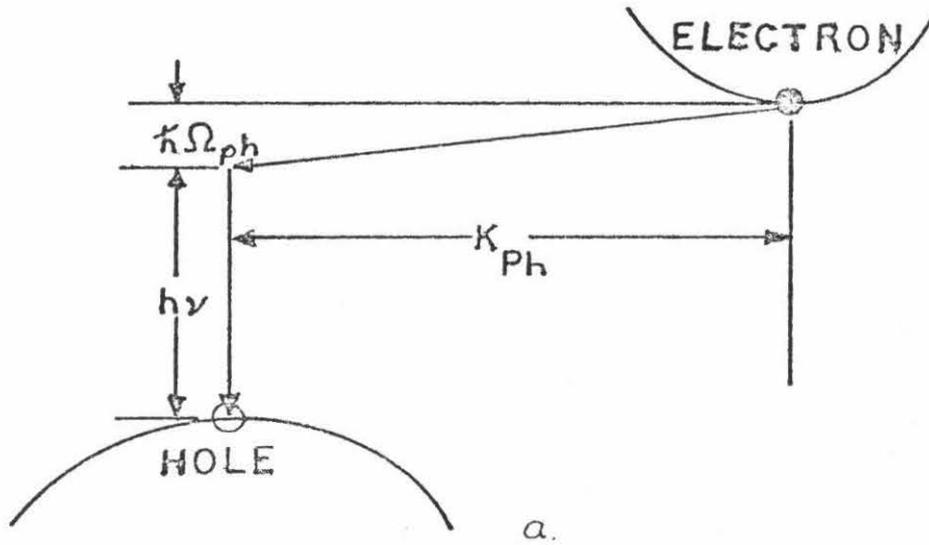
Figure 1.6

k-space, and the extent of this spreading depends upon the nature of the potential which is causing the binding. In particular, part of the potential of an impurity is very short range (central cell part) and consequently mixes states from over much of the zone into the wave functions of the particles bound to it. If, for example, we have an exciton bound to a neutral donor, the electrons will have a finite amplitude at the zone center. Therefore, it is possible to have the exciton recombine radiatively without emitting a phonon. The strength of this "no-phonon" (NP) process depends upon the strength of the short range part of the impurity potential and thus on the particular impurity involved.

In the luminescence spectra of Si or Ge we will find replicas of each feature due to the participation of different phonons. Using the case of a BE on a donor in Si as an example, we expect four replicas. At the highest energy we see a no-phonon replica. Nineteen meV lower in energy we observe luminescence from the BE again but now through a TA-phonon assisted process. At 56 and 58 meV below the NP line we find the LO and TO assisted replicas, respectively. Other replicas involving 2 phonons are also seen, but they are much weaker than the single phonon processes.

References

1. R. S. Knox, Theory of Excitons, (Academic Press, New York, 1963).

2. F. Bassani and G. Pastori Parravicini, Electronic States and Optical Transitions in Solids, (Pergamon Press, Oxford, 1975).

3. R.J. Elliott, Phys. Rev. 108, 1384 (1957).

4. J. R. Haynes, Phys. Rev. Lett. 17, 860 (1966).

5. L. V. Keldysh, in Proc. 9th Int. Conf. Phys. of Semicond., Moscow, 1968. (Nauka, Leningrad, 1968), p. 1303.

6. Y. E. Pokrovskii and K. I. Svistunova, Fiz. Tek. Polup. 4, 691 (1970) [Sov. Phys. - Semicond. 4, 409 (1970)].

7. C. D. Jeffries, Science 189, 955 (1975), and references therein.

8. Jagdeep Shah, R. F. Leheny, W. R. Harding, and D. R. Wight, Phys. Rev. Lett. 38, 1164 (1977).

9. D. Bimberg, M. S. Skolnick, and W. J. Choyke, Phys. Rev. Lett. 40, 56 (1978).

10. R. F. Leheny and Jagdeep Shah, Phys. Rev. Lett. 38 511 (1977).

11. G. Beni and T. M. Rice, Phys. Rev. Lett. 37, 874 (1976), and references therein .

12. G. A. Thomas, T. M. Rice and J. C. Hensel, Phys. Rev. Lett. 33, 219 (1974).

13. M. A. Vouk and E. C. Lightowlers, J. Phys. C8, 3695 (1975).

14. V. Marrello, T. F. Lee, R. N. Silver, T. C. McGill and J. W. Mayer, Phys. Rev. Lett. 31, 593 (1973).

15. R. B. Hammond, V. Marrello, R. N. Silver, T. C. McGill and J. W. Mayer, Solid State Comm. 15, 251 (1974).

16. G. A. Thomas, T. G. Phillips, T. M. Rice and J. C. Hensel, Phys. Rev. Lett. 31, 386 (1973).

17. J. C. V. Mattos, K. L. Shaklee, M. Voos, T. C. Damen and J. M. Worlock, Phys. Rev. B13, 5603 (1976), and references therein.

18. J. Doehler, J. C. V. Mattos, and J. M. Worlock, Phys. Rev. Lett. 38, 726 (1977).

19. J. M. Hvam and O. Christenson, Solid State Comm. 15, 929 (1974), and references therein.

20. V. S. Bagaev, T. I. Galkina, and O. V. Gogolin, in Proc. 10th Int. Conf. Phys. of Semicond., Cambridge, 1970. (USAEC, Oak Ridge, 1970).

21. J. R. Haynes, Phys. Rev. Lett. 4, 361 (1960).

22. R. Sauer, Phys. Rev. Lett. 31, 376 (1973).

23. A. S. Kaminskii, Y. E. Pokrovskii, and N. V. Alkeev, Zh. Eksp. Teor. Fiz. 59, 1937 (1970) [Sov. Phys. - JETP. 32, 1048 (1971)].

24. S. A. Lyon, D. L. Smith and T. C. McGill, Phys. Rev. B17, 2620 (1978), and references therein.

25. R. W. Martin, Solid State Comm. 14, 369 (1974).

26. P. J. Dean, D. C. Herbert, D. Bimberg, and W. J. Choyke, Phys. Rev. Lett. 37, 1635 (1976).

27. Private communication from M. Pilkuhn.

28. R. B. Hammond, T. C. McGill and J. W. Mayer, Phys. Rev. B13, 3566 (1976).

29. R. Sauer and J. Weber, Phys. Rev. Lett. 36, 48 (1976).

30. R. Sauer and J. Weber, Phys. Rev. Lett. $\underline{39}$, 770 (1977).

31. R.F. Leheny (Private Communication).

32. J. C. Hensel and K. Suzuki, Phys. Rev. $\underline{B9}$, 4219 (1974).

PART I

CHAPTER 2

FINE STRUCTURE OF ACCEPTOR

BE AND BMEC IN Si

I. Introduction

As was explained in Chapter 1, the luminescence spectra of silicon doped with shallow impurities contain several emission lines at slightly lower energy than the BE [1-3]. One explanation of the origin of these satellites of the BE is that they result from electron-hole recombination within bound multiple exciton complexes of different sizes. As discussed in Chapter 1, this interpretation is strongly supported by the excitation dependence of the lines and is consistent with the lifetime and absorption measurements. However, if the lines are interpreted as ground-state to ground-state transitions, then the BMEC appear to have work functions which increase with the size of the complex and can become over twice the EHD work function [1-3]. Furthermore, the stress and Zeeman splittings seem much too simple for an entity as complicated as a BMEC [4,5]. Thus, there are data which argue in a circumstantial way both for and against the BMEC picture, but none of these data definitively address the question of whether more than one exciton can bind to an impurity.

The acceptors in Si offer an ideal test of the BMEC model, as suggested by Dean and coworkers [6,7]. The BE in Ga and Al doped Si give a luminescence spectrum which consists of three closely spaced lines corresponding to emission from the BE ground state and two low lying excited states [9-11]. (In Si:In, two BE emission lines are observed and a third is seen in absorption experiments.) The three states for the acceptor BE are due to a coupling of the two spin 3/2 holes in the BE [11]. The ground state corresponds to the J=0 state,

and the two excited states correspond to the J=2 state which is further split by the crystal field. If the BMEC picture is correct, an optical transition from the two exciton complex to a BE should mirror the BE luminescence spectrum, because there are three available final states for the transition.

In Si:Ga we see three such lines in high-resolution photo-luminescence spectra. The energy positions of the lines are well within the experimental resolution of the positions expected for the BMEC model. The observation of these three emission lines conclu-sively demonstrates that, at least in Si:Ga, two excitons will bind to the impurity. The data for Si:Al are similar to those for Si:Ga, however, only one 2-exciton complex line is observed. For Si:In a line at somewhat lower energies than the BE is observed, but it is probably not associated with the decay of a two-exciton complex.

II. J-J Splitting of Acceptor BE

The top of the valence band in silicon is made up of p-type atomic wave-functions on the Si cores. When the electronic spin is included with this orbital part, the total angular momentum of the electrons is either J=3/2 or J=1/2. The J=1/2 states are moved to lower energy by the spin-orbit interaction, making the top of the valence band consist of J=3/2 states. (Actually, since the symmetry is cubic in the crystal, the states should not be labeled by J. With cubic symmetry J=3/2 becomes a Γ_8 state and J=1/2 is a Γ_7 state. This distinction is not important at the moment, and we will continue to use J as a label.) For an effective mass acceptor in Si, the wave-function for a hole bound to the impurity is a linear combination of states near the top of the valence band. Thus, this hole will act like a J=3/2 particle.

When an exciton binds to an acceptor, there are two holes and one electron bound to the impurity. It is thought that the two holes are highly localized near the impurity atom due to its strong attractive potential, while the electron is spread out over a larger region [12]. The holes will interact with one another through their mutual coulomb repulsion, and thus we expect their angular momenta to be coupled [13]. Two J=3/2 particles can couple into J=3,2,1,0 states, but only the J=2,0 states are allowed for the holes by the Pauli exclusion principle. Thus, we expect the ground state of the BE to be split into two states corresponding to the total angular momentum of the holes being either

J=2 or J=0. A more careful treatment including the cubic crystal environment shows that the J=2 state is split into two, giving us three states (Γ_1, Γ_3 and Γ_5) for our BE.

An analogous splitting has been observed experimentally for acceptors in InP [14] and GaAs [15]. Careful measurements of the behavior of the lines with stress has established the J-J coupling interpretation for the splittings. For shallow acceptors in GaAs, the J=0 line lies at higher energies as one would expect from results in atomic physics [13]. However, for the deeper acceptors the J=0 line moves to lower energies and becomes the ground state [15]. Measurements of the oscillator strengths for the three BE lines in Si:Al, Si:Ga, and Si:In (The splitting is small in Si:B.) are in agreement with the relative strengths predicted by assuming the splitting is due to the J-J coupling and that the ground state is J=0 [16,17]. The ordering of the states is the same for all three acceptors in Si, and like the deeper acceptors in GaAs this ordering is different from what one sees in atomic physics.

A schematic illustration of the photoluminescence spectrum we expect to see is shown in Fig. 2.1. On the left is an energy level diagram (not to scale). The states are labeled by the total angular momentum of the holes. Thus, at the bottom we have the ground state of the acceptor (A^0) with J=3/2. Approximately one band gap in energy above the A^0 is the BE which consists of the three states discussed above. When the exciton decays the three different initial states lead to three luminescence lines as shown on the right. The lowest lying

Figure 2.1

Illustration of the J-J coupling of the two holes in the acceptor BE and its effect on the luminescence spectra. In the energy level diagram on the left, J labels the total angular momentum of the holes. The expected luminescence from these levels is shown schematically on the right.
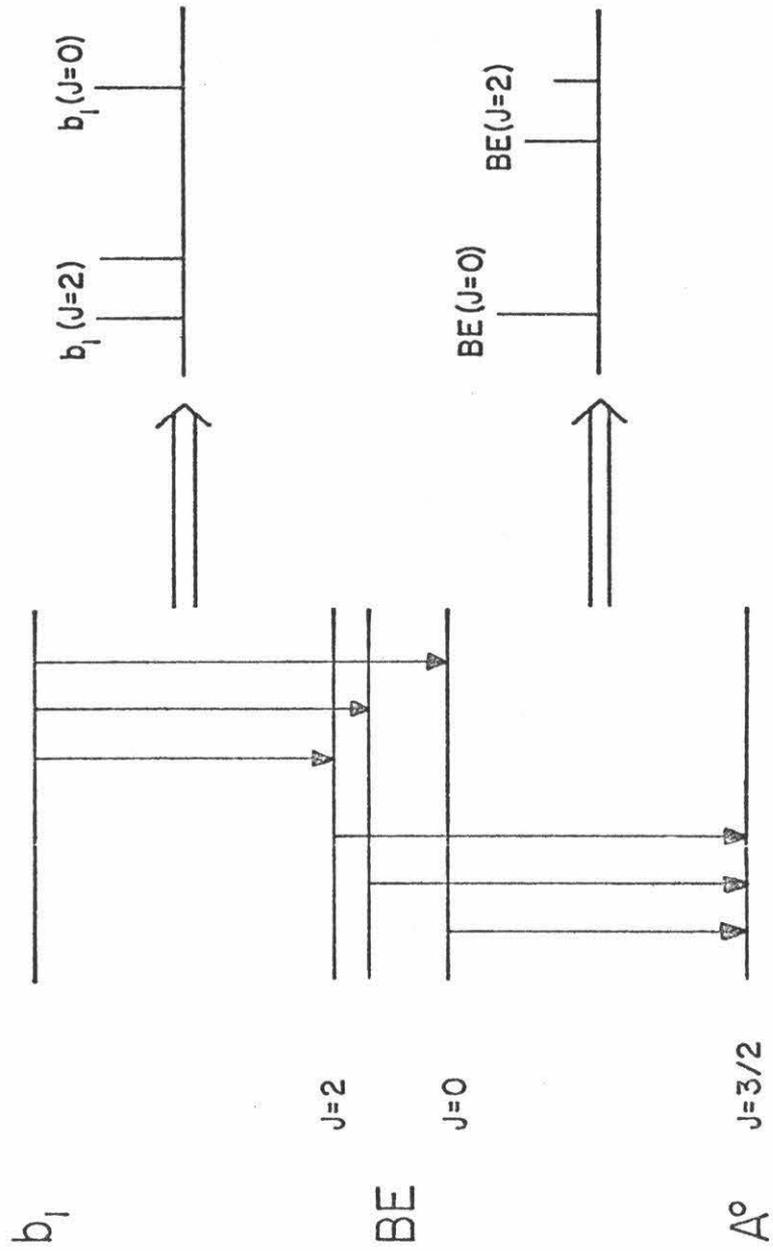
Figure 2.1

line is the ground-state to ground-state transition (J=0), and the higher lying lines arise from excited-state to ground-state transitions (J=2). The three lines are shown with different heights to indicate that the ratio of the line intensities is temperature dependent, since the splitting is in the initial state.

At the top of Fig. 2.1, on the left, is a state labeled b_1, which is our hypothetical 2-exciton complex bound to the impurity. A J-value has not been assigned to this state since we do not know its structure. As discussed in the last section, we expect to see lines due to the decay of one exciton in this complex leaving a BE. Since the BE has two low-lying excited states the decay of b_1 should give three lines for the three final states. (In principle one or more of these lines could be forbidden though probably the complex contains a sufficient mix of states to make all the transitions allowed. In the simple picture of adding a third hole to the J=3/2 shell, b_1 would be a J=3/2 state, and all the transitions would be allowed.) A schematic of the expected spectrum is shown on the right of Fig. 2.1. (The lines are labeled by the J of the final BE state.) Again there are three lines, but since the splitting is in the final state we should see a mirror of the BE spectrum. There will be two ground-state to excited-state transitions at lower energy, and the ground-state to ground-state transition produces the higher lying line. Since the splitting is due entirely to the BE, the energy differences between the lines should be exactly the same as the energy differences in the BE luminescence spectrum. Also, the splitting is in the final state

making the relative intensities of the lines independent of temperature.

III.   Experiment

The experiments were performed using samples of single crystal silicon.   The crystals were grown by the Float-Zone method, and the dopants were introduced during growth.   The impurity concentrations were determined by Hall measurements.   All samples, except the Si:Al, were discs about 1 cm in diameter and 3 mm thick.   The Si:Al crystal was a wafer approximately 450 µm thick.   The samples were lapped and etched with HNO_3:HF (7:1) to remove surface damage.   The crystals were cleaned with methanol before being mounted in the dewar for an experiment.

A diagram of the experimental apparatus is shown in Fig. 2.2. The crystals were mounted on a copper sample block and placed in a Janis variable-temperature dewar.   Temperatures above $4.2^{o}K$ were obtained by heating the sample block in the He-vapor and regulated with a commercial temperature regulator.   For the experiments discussed in this section, a calibrated Ge temperature sensor held in mechanical contact with the sample was used to read the temperature, as opposed to the Si diode shown in the figure.   Experience has shown that the Ge sensor used in this configuration reads the sample temperature to within $2^{o}K$ at the laser powers employed.   The results in this chapter are insensitive to this magnitude of uncertainty in the temperature.

For most of the experiments the excitation source was an Ar-ion laser operating at 5145 $\overset{o}{A}$.   As shown in Fig. 2.2 the beam was filtered to remove any infrared lines in the region of interest and brought to

EXPERIMENTAL SETUP
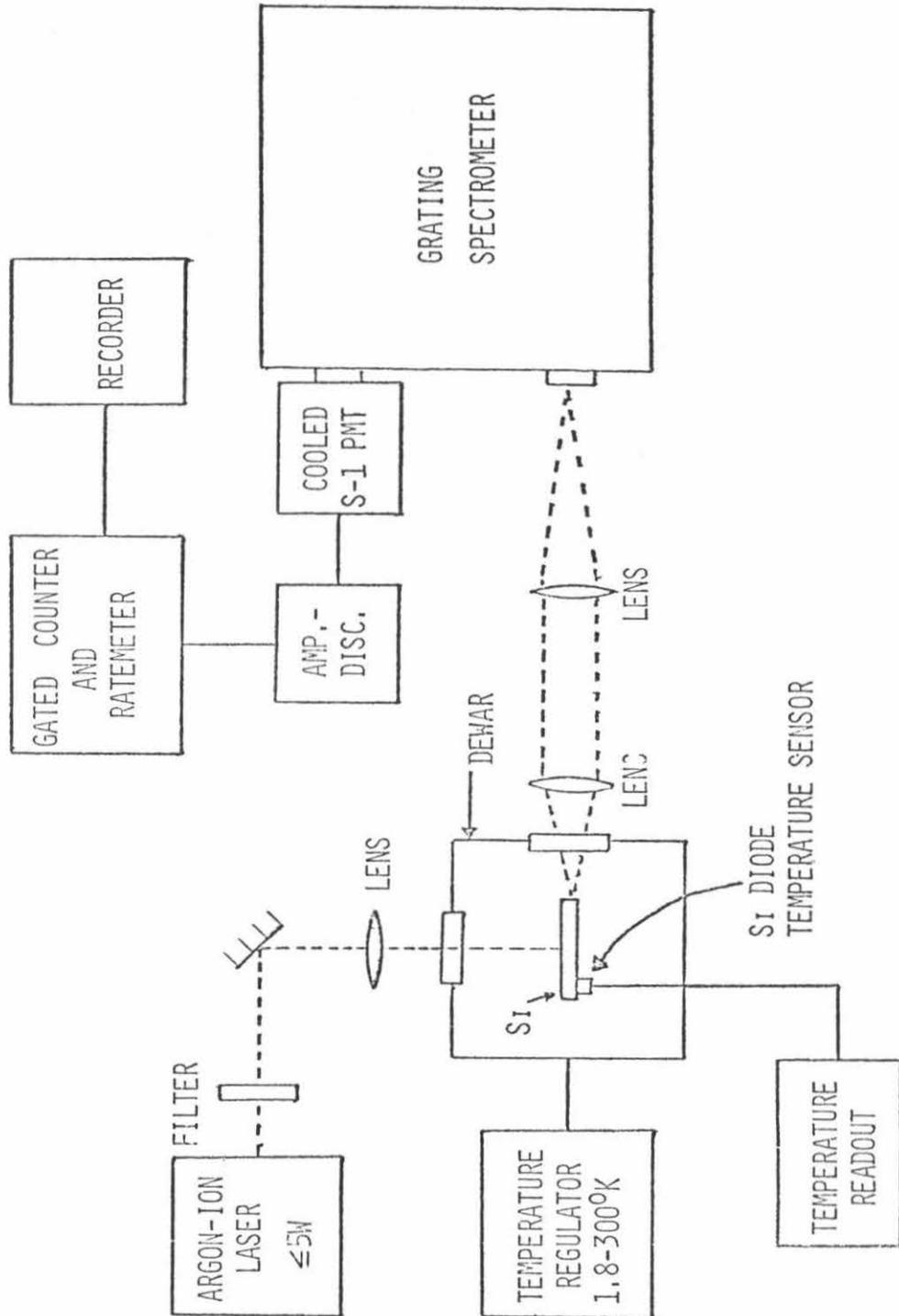
Figure 2.2
Photoluminescence apparatus

the sample through a lens. By moving the lens, the size of the laser spot on the crystal could be changed. For some experiments a GaAs laser diode was used for excitation. The diode was mounted on the sample holder a couple mm from the Si crystal. The spot size was approximately 1 mm as determined by an infrared image converter. The GaAs laser was operated in a pulsed mode, typically with 2 μs pulses and a 4% duty factor. The laser power was measured using a calibrated Si photodiode. The powers quoted for both the Ar-ion and GaAs have not been corrected for reflection losses at the surface of the sample.

The luminescence was collected from the edge of the crystal as shown in Fig. 2.2. The light exists predominantly through the edge due to total-internal reflection within the Si. Two lenses giving a magnification of 3 collected the luminescence and focused it on the entrance slit of the spectrometer. For most of the experiments a double pass Spex 1400-II spectrometer was used although for some experiments a single pass Spex 1269 was used. The output of the spectrometer was detected by a liquid nitrogen cooled S-1 photo-multiplier tube (RCA 7102). A fast amplifier-discriminator at the output of the photomultiplier enabled us to use single-photon-counting techniques. The discriminator pulses were processed by a gated rate-meter giving an analog output proportional to the intensity which was recorded on a strip chart recorder. The dark count with the photo-multiplier cold was about 4 counts per second, which made synchronous detection unnecessary. Consequently, the experiments using the Ar-ion

laser were run CW leading to improved temperature stability.

IV. Experimental Results

The luminescence spectrum for Si:Ga is presented in Fig. 2.3. In this spectrum, we observe transitions from the ground state of the BE, labeled BE(J=0), and from the two excited states of the BE (labeled BE (J=2)). The splitting between the BE(J=0) line and the lowest line of the BE(J=2) doublet is 1.47 meV, and the splitting between the BE(J=2) doublet is 0.33 meV. More important to our discussion here are the three lines labeled b_1, which we will interpret as due to decay of a two exciton complex to a BE. The two lines labeled b_1 (J=2) correspond to transitions with the BE left in an excited state; the line labeled b_1 (J=0) corresponds to a transition in which the BE is left in its ground state. The splittings between the b_1 emission lines are equal to (within the resolution of the experiment, 0.05 meV) the corresponding splittings for the BE emission lines. The interpretation of the b_1 lines as due to recombination of a two exciton complex is further supported by measurements of the pump power dependence of the b_1 and BE line intensities. These measurements show that the intensity ratios of the b_1 lines are independent of pump power; whereas, the ratio of the b_1 line intensities to the BE line intensities increases with pump power. The observation of the complete b_1 triplet conclusively demonstrates that, at least in Si:Ga, a complex of two excitons bound to a single shallow impurity does occur. In Fig. 2.3, we also see an emission line, labeled b_2, which could be interpreted as decay of a three exciton complex. The emission line labeled P is due to an exciton bound to a phosphorus

Figure 2.3

The photoluminescence spectra of Ga doped Si in the
energy range for no-phonon assisted transitions. The lines
labeled BE, b_1, and b_2 are associated with the Ga impurities.
The line labeled P is associated with phosphorous impurities
in the Si.

51
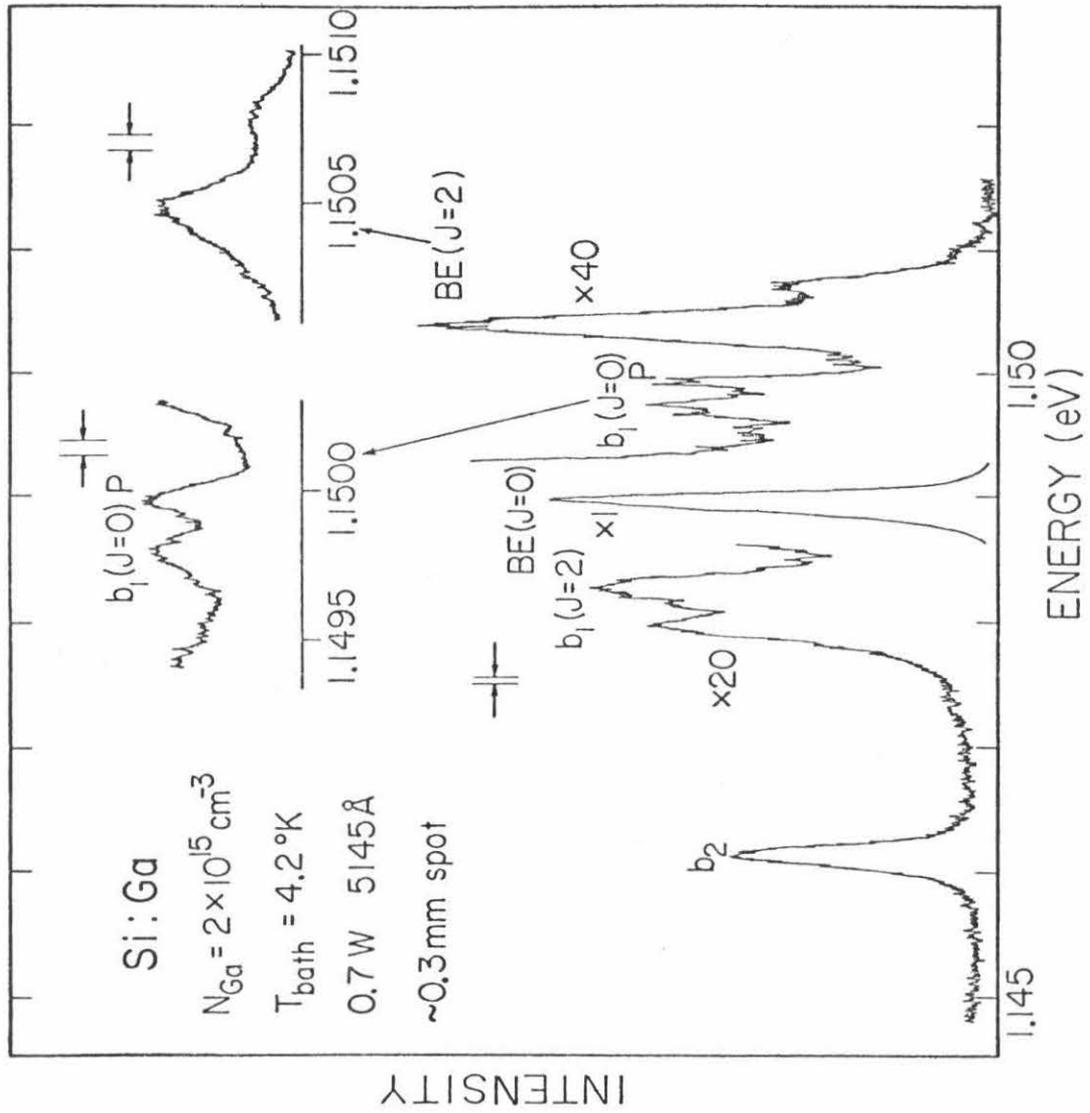
Figure 2.3

impurity [2,3]. Another line at even lower energies not shown in Fig. 2.3 has been observed in the Si:Ga. This line occurs at 1.1441 eV.

The luminescence data for Si:Al are presented in Fig. 2.4. The data are similar to those reported above for Si:Ga. The spectrum shows lines due to BE(J=0) and BE(J=2) states. The splitting between the two components of the BE(J=2) line is about 0.22 meV. At lower energies a broad b_1 line is observed; it is probably made up of the two components of the b_1 (J=2) doublet. The b_1 (J=0) line is not observed, but should occur at an energy indicated by the arrow labeled b_1 (J=0); that is, it is under the much stronger BE (J=0) line and hence difficult to observe. The two other lines, labeled b_2 and b_3, observed at lower energy are associated with the Al impurity. Emission lines labeled P are due to phosphorus impurities [2,3].

The data for Si:In are presented in Fig. 2.5. The data show a similar structure to that observed in Si:Ga and Si:Al. The BE(J=0) line is split from a single BE(J=2) line by about 3.1 meV. (A second BE(J=2) has been seen in absorption at higher energies.) A satellite line is observed 4.0 meV below the BE(J=0) line. This satellite has a lineshape similar to that of the BE(J=2) emission line. It would be tempting to interpret this line as due to the decay of a 2-exciton complex into the BE(J=2); however, other factors rule out this interpretation. Most importantly, the line does not exhibit the pump power dependence expected for a 2-exciton complex. It shows the same dependence on excitation as the BE(J=0) and is even

Figure 2.4

The photoluminescence spectra of Al doped Si in the energy range for no-phonon assisted transitions. The lines labeled BE, b_1, b_2, and b_3 are associated with Al impurities. The lines labeled P are associated with phosphorous impurities in the Si.
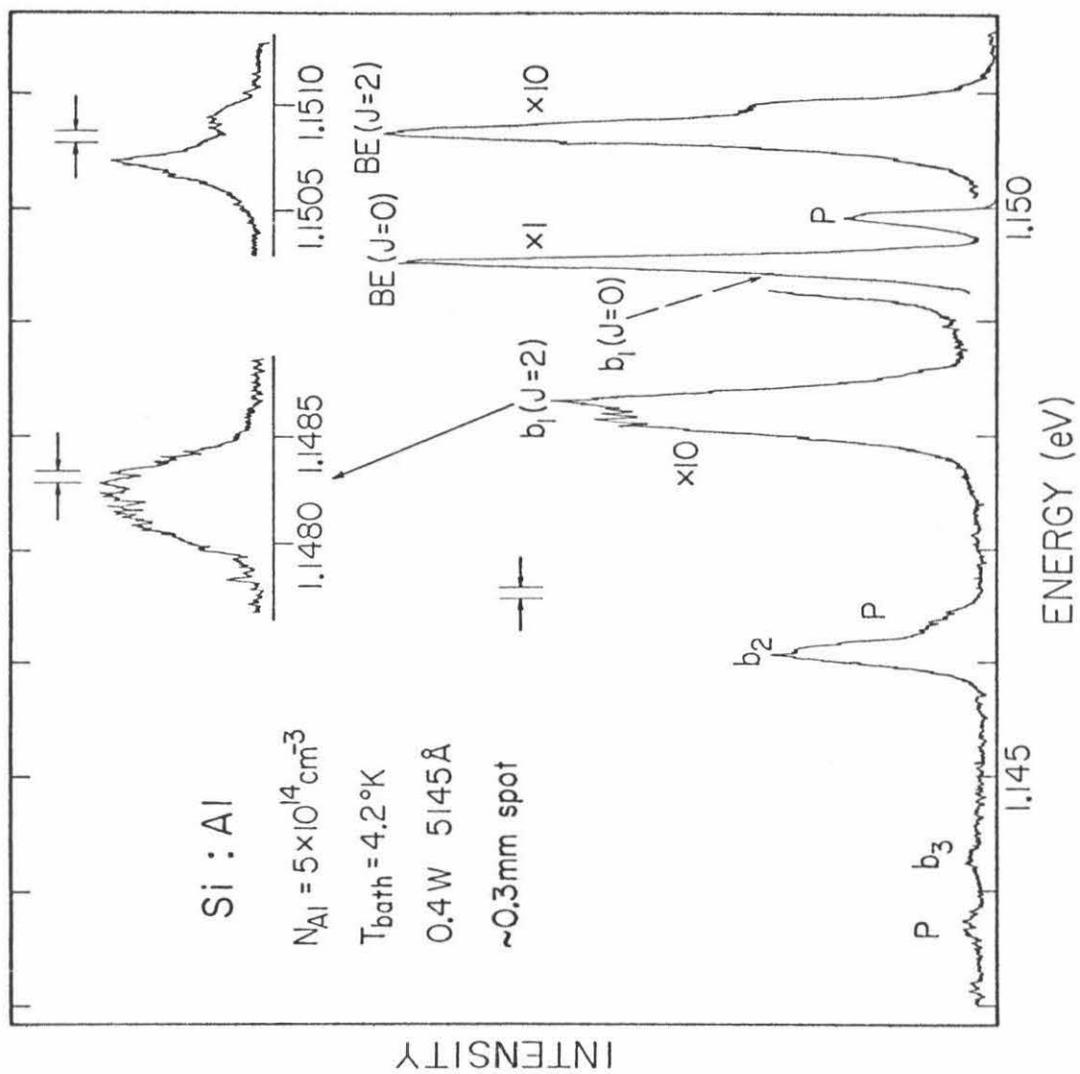
Figure 2.4

Figure 2.5

The photoluminescence spectra of In doped Si in the energy range of the no-phonon assisted transitions. All three lines are associated with In impurities.

56
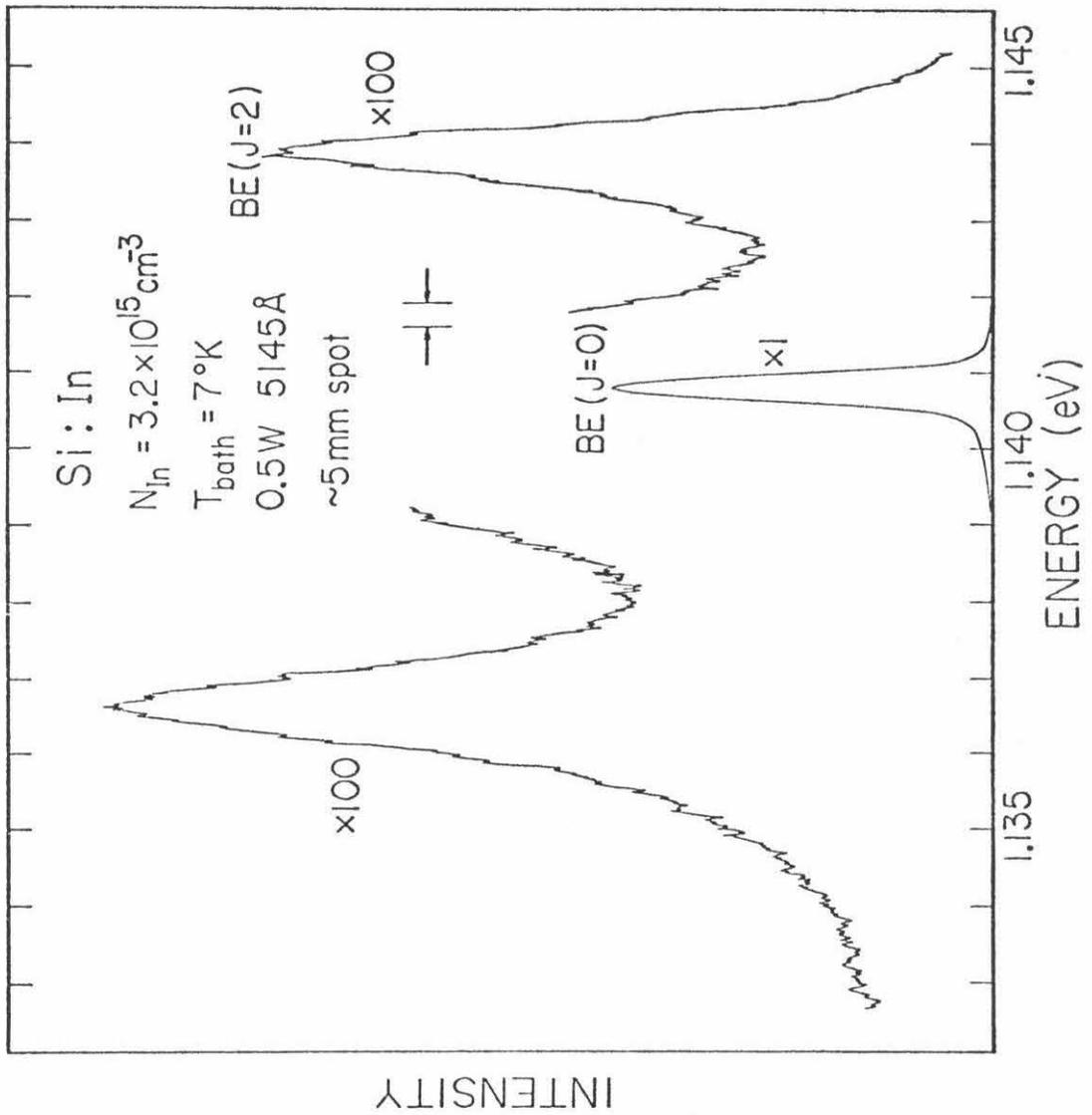
Figure 2.5

seen at low pump powers in heavily doped Si. At the moment the origin of this line is unknown.

V. Discussion and Conclusions

We believe that our experimental data along with that previously reported [9,10] argues strongly for the existence of two-exciton complexes bound to Si:Ga and Si:Al. However, the results are not as conclusive in the case of the b_2, b_3 lines since there is no structure indicating as clearly that the decay is from a three-exciton complex into a two-exciton complex or four-exciton complex into a three-exciton complex. If we take the additional lines to be due to ground state transitions involving a change of one in exciton number, then the energy separations between the free exciton, no-phonon threshold and the satellite line energies give the binding energies of an exciton to a BMEC consisting of zero to three excitons, as discussed in Chapter 1. These line positions along with a line indicating the free exciton threshold and the energy per pair in the electron-hole liquid [18] are given in Fig. 2.6. The data show that for Si:B the binding energy of an additional exciton increases monotonically with complex number. For Si:Al, the first two excitons bind with approximately the same energy while the third and fourth bind with successively larger energy. For Si:Ga, the situation is qualitatively different. The second exciton binds with a smaller binding energy than the first. The binding energy of the second exciton in both Si:Ga and Si:Al is less than in Si:B. Further, it is interesting to note that the b_2 lines for Si:B, Si:Al and Si:Ga all occur at approximately the same energy. The b_3 lines are inverted in order in comparison to the ordering for the b_1 lines. This

Figure 2.6

The position of the no-phonon assisted lines in photo-
luminescence for various lines associated with B, Al, Ga,
and In acceptors in Si. The line labeled FE was obtained
by shifting the position of the TO-phonon assisted line (Ref.
18) due to the FE by the TO-phonon energy of 58 meV (Ref. 3).
The line labeled μ_{EHD} is the chemical potential of the
electron-hole droplet (Ref. 18).
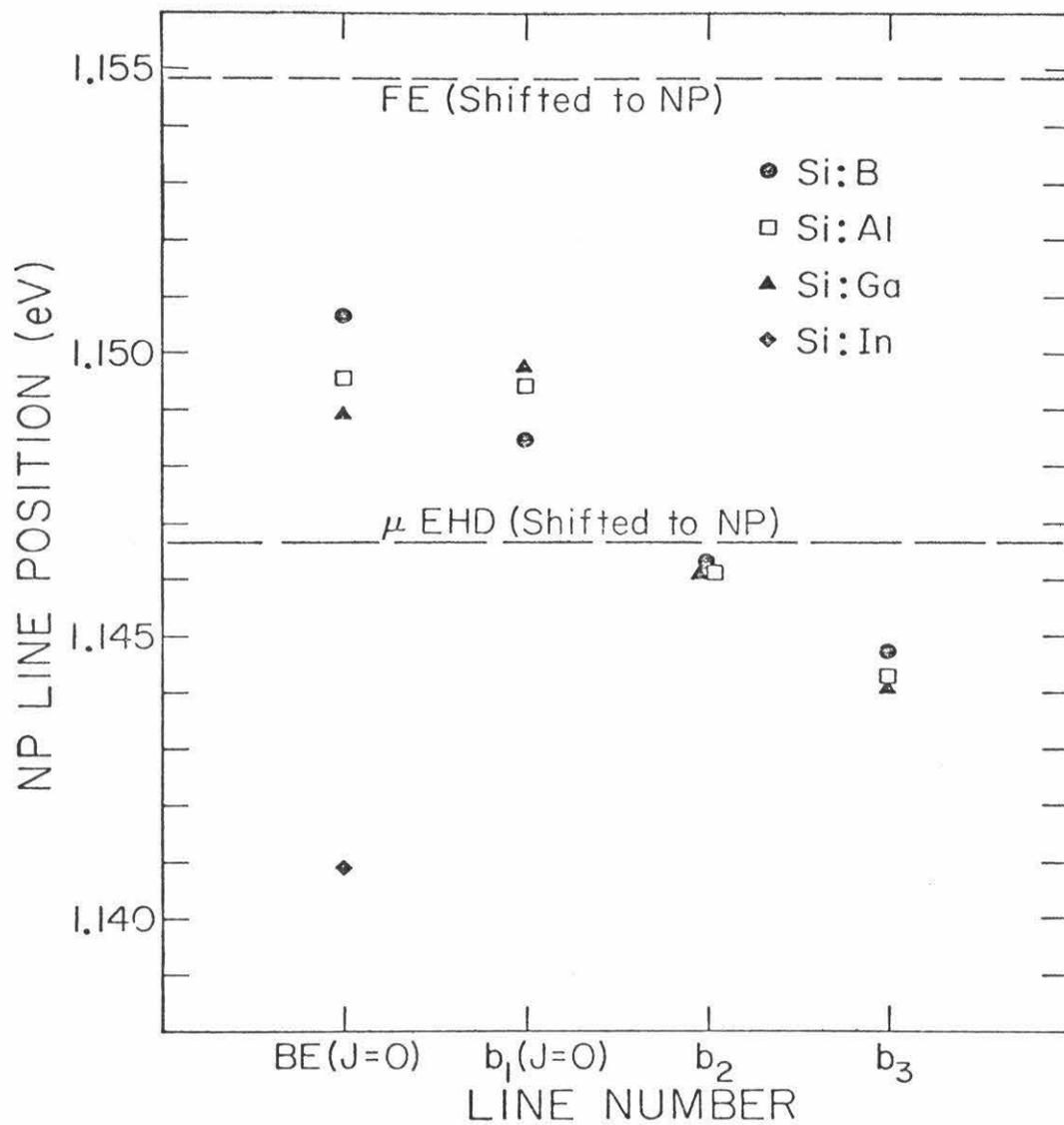
Figure 2.6

suggests that binding energy as a function of exciton number is not simply a monotonic function of the strength of the central cell correction.

These data also show clearly that the binding of the excitons for three and four exciton complexes for B, Al, and Ga are stronger than that for an exciton in the EHD in spite of the fact that the first exciton binds less strongly than a pair in the EHD. The fact that binding energy obtained by interpreting the lines as due to ground-state to ground-state transitions dips substantially below that for the EHD suggests that deeper lines b_2 and b_3 may in fact result from recombination in multiexciton complexes where the complex is left in an excited state. While lines that could be interpreted as ground-state to ground-state for these complexes are not observed, it should be noted that the corresponding $b_1(J=0)$ line is not seen in Si:Al because it is buried under the much larger BE. Furthermore, the ground-state to ground-state transition for the 2-exciton complex in Si:Ga is approximately three times less intense than the associated ground-state to excited-state transitions.

In summary, we have investigated the photoluminescence spectra of Si doped with the acceptors Al, Ga, In. Two excited states of the BE are observed for the Si:Ga and Si:Al. In the Si:Ga we also observe three lines associated with the decay of a two-exciton complex. The fact that these lines mirror the structure of the BE is conclusive evidence that at least two excitons will bind to a Ga impurity in Si.

The data for Si:Al are similar to those of Si:Ga and indicate that two excitons will also bind to an Al impurity. However, no lines attributable to BMEC are observed in luminescence spectra of Si:In. We have also observed two lower energy satellites in Si:Ga and Si:Al presumably due to the decay of larger BMEC. Assuming the lines arise from ground-state to ground-state transitions we find that the work functions of the complexes do not show a simple dependence on either exciton number or the strength of the central cell correction.

References

1. A. S. Kaminskii, Y. E. Pokrovskii, and N. V. Alkeev, Zh. Eksp. Teor. Fix. $\underline{59}$, 1937 (1970) [Sov. Phys. JETP. $\underline{32}$, 1048 (1971)].

2. R. Sauer, Phys. Rev. Lett. $\underline{31}$, 376 (1973).

3. K. Kosai and M. Gershenzon, Phys. Rev. $\underline{B9}$, 223 (1974).

4. R. Sauer and J. Weber, Phys. Rev. Lett., $\underline{36}$, 48 (1976).

5. R. Sauer and J. Weber, Phys. Rev. Lett. $\underline{39}$, 770 (1977).

6. P. J. Dean, D. C. Herbert, D. Bimberg, and W. J. Choyke, Phys. Rev. Lett. $\underline{37}$, 1635 (1976).

7. P. J. Dean, D. C. Herbert, D. Bimberg, and W. J. Choyke, in Proceedings of the 13th International Conference on the Physics of Semiconductors, Rome, 1976, edited by F. G. Fumi (Tipografia Marves, Rome, 1977) p. 1098.

8. M. A. Vouk and E. C. Lightowlers, in Proceedings of the 13th International Conference on the Physics of Semiconductors, Rome, 1976, edited by F. G. Fumi (Tipografia Marves, Rome, 1977) p. 1098.

9. M. L. W. Thewalt, Phys. Rev. Lett. $\underline{38}$, 521 (1977).

10. E. C. Lightowlers and M. O. Henry, J. Phys. $\underline{C10}$, L247 (1977).

11. P. J. Dean, W. F. Flood and G. Kaminsky, Phys. Rev. $\underline{163}$, 721 (1967).

12. D. S. Pan, D. L. Smith, and T. C. McGill, Solid State Commun. $\underline{18}$, 1557 (1976).

13. See, for example, E. U. Condon and G. H. Shortley, Theory of Atomic Spectra (University Press, Cambridge, 1970) p. 287.

14. A. M. White, P. J. Dean and B. Day, J. Phys. $\underline{C7}$, 5002 (1975).

15. M. Schmidt, T. N. Morgan, and W. Schairer, Phys. Rev. $\underline{B11}$, 5002

(1975).

16. K. R. Elliott, G. C. Osbourn, D. L. Smith and T. C. McGill, Phys. Rev. $\underline{B17}$, 1808 (1978).

17. G. Kirczenow, Can. J. Phys. $\underline{55}$, 1787 (1977).

18. R. B. Hammond, T. C. McGill and J. W. Mayer, Phys. Rev. $\underline{B13}$, 3566 (1976).

CHAPTER 3

LIFETIMES OF BE AND BMEC

BOUND TO ACCEPTORS IN Si

I.   Introduction

In the last chapter we found that it is possible to bind at least two excitons to an impurity. There are still other questions concerning the BMEC. Even at high excitation densities we were unable to produce a 2-exciton complex in Si:In. Furthermore, we find that higher excitation densities are needed to produce BMEC for deeper impurities. For example, at 4.2^OK in Si:B, the b_1 line can be as large or larger than the BE, with only modest pump power. For Si:Ga, however, the b_1 is always much smaller than the BE(J=0). Also, it is found that the BE saturates at a lower excitation intensity for boron than for gallium. Aluminum lies in between the other two.

Another observation is that the overall radiative efficiencies of the bound excitons decrease for the deeper impurities. The intensity of the TO-phonon assisted BE replica is significantly lower for a sample of Si:Ga than for one of Si:B under the same excitation conditions. The oscillator strengths of the phonon assisted processes do not change much for the different impurities, however [1]. The variation in radiative efficiencies leads us to conclude that the BE can have very different lifetimes with the deepest impurities having the fastest decay rate.

In Si, BE lifetimes have been measured for the donors Li [2], P [3] and As [4]; among acceptors, only the lifetime for B [3] has been reported. In this chapter, I will present measurements of the BE lifetimes for the four common acceptors in Si (B, Al, Ga and In) and lifetimes of the first two BMEC in Si:Al and Si:Ga. (For Si:In,

we are only able to set an upper limit on the BE lifetime). We find very different lifetimes for the BE associated with the different acceptors; the lifetimes decrease rapidly (by about three orders of magnitude) as the binding energy of the acceptor increases.

The lifetime of the acceptor BE in Si is most likely limited by Auger transitions in which an electron recombines with one of the holes in the BE and the energy is carried off by the second hole. We will compare our measurements with the results of a calculation [5] of transition rates for this process. The calculation accounts for the strong dependence of the BE lifetime on acceptor binding energy and is in approximate quantitative agreement with the measured lifetimes.

II. Experimental Results

The experimental setup is essentially the same as that diagrammed in Fig. 2.2. A GaAs diode laser was used for excitation instead of the argon-ion laser. The laser diode was mounted in the helium dewar, a few mm from the sample. The laser spot was about 1 mm in diameter. The Si crystals were prepared by lapping and etching as discussed in Chapter 2. The boron, gallium and indium doped samples were several mm thick while the Si:Al crystal was about 450 μm thick. Bath temperature was measured with a Ge sensor in the sample block. The spectrometer slits were adjusted to select a narrow wavelength band ($\sim$3Å) centered on the peak of each line. For Si:B the TO assisted lines were measured while for the other crystals the NP luminescence was studied. The gated photon counter (see Fig. 2.2) has an adjustable length gate which can be scanned in time relative to a trigger pulse which is derived from the diode pulsing circuitry. The experiment consists of adjusting the spectrometer to the peak of a line and then scanning the gate to obtain a plot of the luminescence intensity as a function of time after the end of the excitation pulse.

The minimum system response time was tested by measuring the fall time of the laser pulse; it was approximately 5 nsec. In measurements on Si:B, a 200 nsec gate was used; for Si:Al, Si:Ga and Si:In, the 5 nsec gate was used. The laser excitation power was selected so that the BE luminescence dominated the spectrum. Thus, the results should not be complicated by exciton capture and

BMEC decay. The decay of the BE luminescence was exponential for over an order of magnitude drop in the intensity.

The measurements were made at 4.2°K and 10°K. There was a small increase in the observed lifetime as the temperature was raised to 10°K. In the case of Si:B this increase is probably due to the evaporation of excitons off the B impurities and the subsequent "feeding" of the BE by the longer lived FE. (There was a reasonably large free exciton emission signal at 10°K, but this emission signal was very weak compared to the BE emission at 4.2°K.) In the case of Si:Ga, the BE has an excited state 1.47 meV above the ground state. At 10°K this excited state is populated with a probability comparable to that for the ground state. If the Auger rate for the excited state is slower than for the ground state, population of the excited BE state in Si:Ga (as well as exciton evaporation and recapture) can increase the observed lifetime as the temperature is raised.

The measured BE lifetimes for the four acceptors are listed in Table 3.1. We have also listed the decay time for the first two BMEC in Si:Al and Si:Ga. The result for Si:B at 4.2°K is identical to that previously reported [3]. (We did not measure the BMEC decay for Si:B because they are already available in the literature [3].) The BE lifetime in Si:In was shorter than our system response time, and we can only set an upper bound on it.

Table 3.1 Measured lifetimes for bound excitons (BE) and bound multiple exciton complexes for acceptors in Si; b_1 and b_2 label the first and second BMEC, respectively; E_A is the acceptor binding energy and N_A is the acceptor concentration.

	$\tau(4.2^{\circ}K)$	$\tau(10^{\circ}K)$	E_A	N_A	Excitation Conditions
Si:B(BE)	1.0 μsec	1.15 μsec	44.5 meV	$2 \cdot 10^{15} cm^{-3}$	6 μsec at 0.1 watt
Si:Al(BE)	80 nsec		68.5 meV	$5 \cdot 10^{14} cm^{-3}$	350 nsec at 0.2 watt
$b_1(J=2)$	59 nsec			$5 \cdot 10^{14} cm^{-3}$	350 nsec at 0.5 watt
b_2	46 nsec			$5 \cdot 10^{14} cm^{-3}$	350 nsec at 0.5 watt
Si:Ga(BE)	58 nsec	67 nsec	72 meV	$3 \cdot 10^{16} cm^{-3}$	350 nsec at 0.5 watt
$b_1(J=2)$	39 nsec			$2 \cdot 10^{15} cm^{-3}$	300 nsec at 0.5 watt
b_2	35 nsec [a]			$2 \cdot 10^{15} cm^{-3}$	300 nsec at 0.5 watt
Si:In(BE)	<5 nsec		155 meV	$2 \cdot 10^{16}$	200 nsec at 0.5 watt

a) The b_2 line for Si:Ga was very weak and there was a background which decayed with a 47 nsec lifetime beneath it. The presence of the background may cause the measured decay time to be somewhat larger than the actual lifetime.

III. Auger Calculation of BE Lifetimes

From Table 3.1, we see that the BE lifetime decreases rapidly as the acceptor binding energy increases. This behavior is similar to that observed for acceptor BE lifetimes in GaP [6]. This effect can be understood as due to an increased spreading in k-space of the BE wavefunction as the acceptor binding energy increases [6]. This idea has been quantified and calculations of Auger rates for acceptor BE in Si have been carried out [5]. Here I will give only the physical picture and results of the detailed calculation.

From time dependent perturbation theory, the BE Auger transition rate is given by

$$\frac{1}{\tau} = \frac{2\pi}{\hbar} \sum_F | \langle F|V|I \rangle |^2 \, \delta(E_F - E_I) \tag{3.1}$$

Here $|F\rangle$ is the final state which consists of a free hole, $|I\rangle$ is the initial state which consists of two holes and an electron bound to the charged acceptor, and the interaction which leads to the transition, V, is the Coulomb interaction between the carriers.

The final hole state is an eigenstate of wavevector. The possible final states are restricted by energy conservation. The initial BE state is not an eigenstate of wavevector because the carriers are localized in space by the impurity potential. In order for the Auger transition to occur, the initial BE state must have an amplitude to contain wavevectors which are accessible to the final state hole. Because the wavefunction for the holes in

the BE are peaked in k-space at k=0 while the electron is peaked at
the conduction band minimum, the total wavevector for the BE is peaked
at the conduction band minimum. This point is rather far, in k-space,
from the constant energy surface accessible to the final state hole.
Thus, spreading of the BE wavefunction in k-space is essential for the
Auger transition to occur. For the acceptor BE, the holes are more
highly localized in space than the electron and the spreading of the
BE wavefunction in k-space is due primarily to the holes. The extent
of this spreading depends on the impurity; it increases as the binding
energy of the acceptor increases because the holes are more strongly
localized in space for the more tightly bound acceptors.

In principle, it is possible that the Auger transitions are
phonon assisted. If this were the case, the phonon would supply
the wavevector necessary for the transition to occur, and the
transition rate would not depend on the k-space spreading of the
BE wavefunction. Thus, one would expect the phonon assisted Auger
rates to be insensitive to the acceptor type. Since the observed
lifetimes are, in fact, very sensitive to the acceptor type, we
believe the Auger transitions occur without phonon assistance.

The Auger transition rates for the acceptor BE were computed
using wavefunctions obtained from a variational calculation [5]
with a simplified model of the BE. The results of the calculation
are shown in Fig. 3.1. The calculation is seen to describe the
observed dependence of the lifetime on acceptor binding energy
reasonably well. The computed lifetimes are larger than the

Figure 3.1

Bound exciton lifetimes vs impurity binding energy
for the four common acceptors in Si. The solid circles
are measured values and the hollow squares are calcula-
tions of the Auger lifetime. For Si:In, the lifetime
was shorter than our system response time, and we can
only set an upper limit on it.
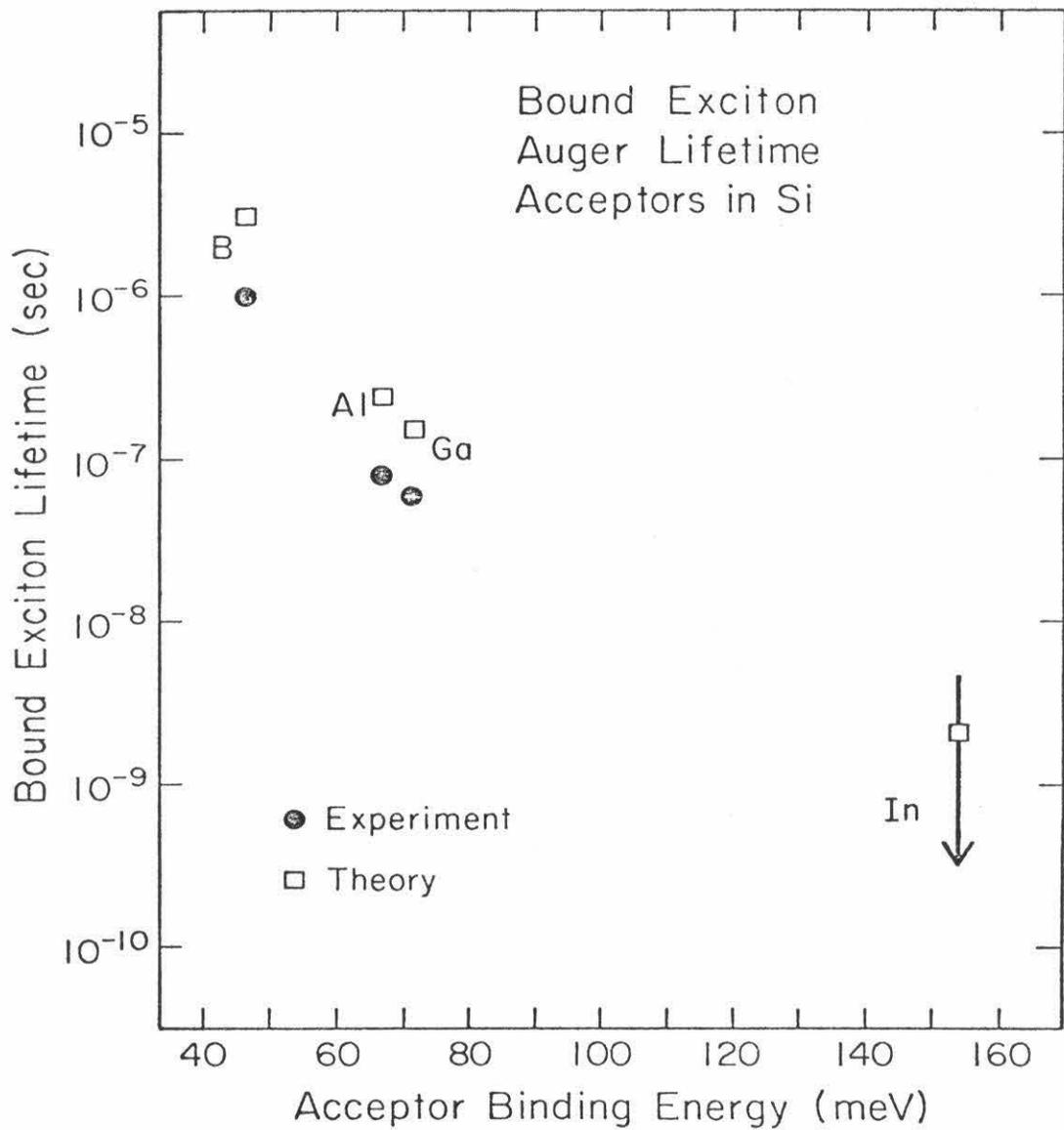
Figure 3.1

experimental values by about a factor of three for all the
impurities. Considering the sensitivity of the calculated lifetimes
on the BE wavefunction, we consider this agreement to be reasonable.

IV.   Conclusions

In conclusion, we see that these measurements answer some
of the questions concerning the systematics of BMEC as a function
of impurity. The deeper impurities give rise to more rapid Auger
rates for BE and BMEC and correspondingly lower radiative effi-
ciencies. Also, the results explain the higher pump powers needed
to make BMEC or saturate the BE in Si with deeper impurities. To
saturate the BE we must supply excitons faster than they decay on
the impurities, which means, of course, that it is more difficult
to saturate the BE if they decay rapidly. Similarly, to make an
m-exciton complex, we need the (m-1)-exciton to live long enough
to capture the next exciton. For the more rapidly decaying com-
plexes this means that a high density of excitons is necessary to
reduce this capture time. This explains the high pump powers
needed to make significant numbers of BMEC in Si:Ga. It also
may explain the absence of 2-exciton complexes in Si:In. The capture
rate per impurity is given by

$$R = n_{ex} v_{th} \sigma_m \quad , \tag{3.2}$$

where n_{ex} is the exciton density, v_{th} the exciton thermal velocity
and σ_m is the cross section for a single m-complex to capture an
exciton making it an (m+1)-complex. For Si:In, σ_0 (capture by
a neutral impurity) has been measured [7], and it has a value of
$\sim 10^{-12} cm^2$ at $2^{\circ}K$, decreasing rapidly at higher temperatures.

If we assume that the capture cross section for a second exciton is about the same as for the first, and take a thermal velocity of 10^6 cm/sec, then we can estimate the formation rate of 2-exciton complexes in Si:In for various exciton densities. In particular in order to form 2-exciton complexes this capture rate must be larger than the BE decay rate. Assuming a 5 nsec BE decay rate and the values quoted above for the other parameters, we find that n_{ex} must be at least 2×10^{14} cm^{-3}. However, we cannot reach this exciton density at 2°K because EHD will grow and maintain a lower density. Therefore, even if two excitons will bind to an indium impurity in silicon, we cannot expect a BMEC to form out of a gas of free excitons.

In summary, we have measured the luminescence lifetimes of BE on the four common acceptors in Si and lifetimes of the first two BMEC in Si:Ga and Si:Al. The BE decay rates increase rapidly as the binding energy of the acceptor increases, there being about a three order of magnitude difference between the rates for B and In. These results are in approximate quantitative agreement with a calculation [5] which assumes that the lifetimes are limited by Auger transitions. Knowledge of the decay rates is important to the understanding of the kinetics of the growth and decay of BMEC. We find that the BE lifetime in Si:In is so short (<5 ns) that it is probably impossible to form 2-exciton complexes on In impurities out of a gas of free excitons.

References

1. P. J. Dean, W. F. Flood and G. Kaminsky, Phys. Rev. 163, 721 (1967).

2. K. Kosai, M. Gershenzon, Phys. Rev. B9, 723 (1974).

3. R. Sauer, Proc. Twelfth Int. Conf. Physics of Semiconductors Stuttgart, 1974), p. 42.

4. D. F. Nelson, J. D. Cuthbert, P. J. Dean, and G. D. Thomas, Phys. Rev. Lett. 17, 1262 (1966).

5. G. C. Osbourn, and D. L. Smith, Phys. Rev. B16, 5426 (1977).

6. P. J. Dean, R. A. Faulkner, S. Kimura, and M. Ilegems, Phys. Rev. B4, 1926 (1971).

7. K. R. Elliott, D. L. Smith, and T. C. McGill, Solid State Commun. 24, 461 (1977).

CHAPTER 4

TEMPERATURE DEPENDENCE AND WORK FUNCTIONS

OF BOUND MULTIEXCITON COMPLEXES IN Si

I. Introduction

In Chapter 2 we saw that the BMEC interpretation has been firmly established for two excitons bound to the acceptors aluminum and gallium [1-3]. However, questions arise in extending the picture to the donors and to the lower energy lines for the acceptors. One question involves the binding energies of excitons to the complexes. In this chapter we will discuss thermodynamic measurements of the work functions, ϕ_m, of the BMEC (m labels the number of pairs in the complex). At temperatures such that the thermalization rate of excitons on and off of a complex is large compared to its decay rate we assume that the complex is in thermal equilibrium with the surrounding gas of FE. This assumption enables us to obtain the work functions from our measurements of the line intensities as a function of temperature.

In the usual interpretation of the lines as corresponding to ground-state to ground-state (G-G) transitions, the binding energy of the last exciton is given by the energy separation between the given BMEC line and the free exciton (FE). However, there is no evidence to support the assumption of G-G transitions. In fact for the 2-exciton complex in Si:Ga the G-G transition is at least three times weaker than the transitions which leave the BE in an excited state [3]. Furthermore, with the usual interpretation for the larger complexes, each additional exciton is bound more tightly than the last. In the context of particular models [4,5] it has been proposed that at least some of the lines are not G-G transitions.

The thermodynamic measurements give us a way of determining the work functions of the BMEC while avoiding questions concerning the final states of the optical transitions and without using a specific model of the structure of the complexes in the interpretation of the data. In contrast to the large "binding energies" obtained by taking spectroscopic differences we find from the thermal data, for the dopants studied here, that the second or third exciton is the most tightly bound and subsequent excitons bind with decreasing energy. Furthermore, none of the measured work functions exceeds that of the EHD [6].

The experiments have been performed on crystals of Si doped with Al, B, Li and P. The position of the G-G transition is known for the m = 2 BMEC [1-3] in Si:Al. For Si:Al our results agree with the previous work for the binding energy of the BE and m=2 BMEC. However, our data show that the m=3 BMEC in Si:Al is bound less tightly than its line position would indicate. Similarly for Si:B the BE and m=2 BMEC have work functions agreeing with their spectroscopic differences. However, the m=3 and m=4 BMEC are bound less strongly than the G-G intepretation of the spectroscopy would indicate and thus correspond to decays into excited states. The thermodynamic value for the BE work function in Si:Li agrees with the spectroscopic difference. Our measurement of the work function of the 2-exciton complex indicates that it decays into an excited state of the BE. We have observed this BE excited state as well as another one in the

Li doped Si. For Si:P we obtain the correct binding energy for the BE and our data show that all of the first four BMEC lines arise from transitions to excited states and are thus less strongly bound than previously believed.

The remainder of this chapter will be organized as follows: In Section II we will describe the method by which work functions are obtained from the temperature data. In Section III we will describe the experimental methods. Section IV will be a presentation of the experimental work functions for BMEC in Si:Al, Si:B, Si:Li and Si:P. Section V will be a discussion of these results and our conclusions.

II. Analysis of the Temperature Data

At sufficiently high temperatures the evaporation rate of excitons off a complex will exceed the recombination rate for pairs within the complex. Under these conditions the complex is in approximate thermal equilibrium with the surrounding gas of free excitons. Thus we can use equilibrium statistics to relate the populations of m-exciton complexes, (m-1)-complexes, and free excitons (FE). An (m-1)-complex plus a FE with wave vector $\bar{k}$ is then viewed as a type of excited state of an m-complex and as such has a probability of being occupied given by

$$P(m-1,\bar{k}) = \frac{g_{m-1}\, g_{ex}}{g_m}\, e^{-(\phi_m + \varepsilon_{\bar{k}})/kT}\, P(m) \quad , \qquad (4.1)$$

where g_m is the degeneracy of an m-complex, g_{ex} is the degeneracy of a FE, ϕ_m is the work function of an m-complex, $\varepsilon_{\bar{k}}$ is the kinetic energy of a FE with wave vector $\bar{k}$, T is the temperature, and $P(m)$ is the probability of finding a complex with m-excitons. Since we are only interested in the density of FE and not their specific $\bar{k}$'s we can average over $\bar{k}$. In integrating over the wave vector of the excitons, we will assume that the FE dispersion curves are described simply by an effective mass, m^*. Actually the FE ground state in Si is split by about .3 meV[7-9]. However, unlike Ge, the splitting does not generate a significant mass reversal[10] and the .3 meV is less than the uncertainties in the present experiments. With

this assumption of a single exciton band and replacing the probabilities with densities, we obtain

$$n_{ex}n_{m-1} = \left(\frac{2\pi m^* kT}{h^2}\right)^{3/2} D_m \, e^{-\phi_m/kT} \, n_m \quad , \tag{4.2}$$

where $D_m \equiv \dfrac{g_{m-1}g_{ex}}{g_m}$, n_{ex} is the density of excitons and n_m is the density of m-complexes. Eq.(4.2) may be rearranged, yielding,

$$\frac{T^{3/2}n_m}{n_{ex}n_{m-1}} = \left(\frac{2\pi m^* k}{h^2}\right)^{3/2} D_m^{-1} \, e^{\phi_m/kT} \quad , \tag{4.3}$$

where now the ratio on the left is accessible to experiment. If we assume that the luminescence intensity of a given line is proportional to the density of the associated complex, then we have

$$\ln\left(\frac{T^{3/2}I_m}{I_{ex}I_{m-1}}\right) \propto \phi_m/kT \quad , \tag{4.4}$$

where I_m is the intensity of the luminescence line due to the decay of an m-complex and I_{ex} is the integrated FE luminescence intensity. Therefore, a graph of the quantity on the left side of Eq. (4.4) versus $1/kT$ will produce a straight line with slope ϕ_m. In the actual experiments, surface excitation was used and the densities in Eq. (4.3) are functions of position within the crystal. At every point in the

crystal Eq. (4.3) holds, however the signal we observe is the integral
of the luminescence over the crystal volume. As long as the
carrier profiles do not change with temperature, then using spatially
integrated luminescence intensities in Eq.(4.4) will not change the
analysis. As we lower the temperature, at some point the recombina-
tion rate of the m-exciton complex will become comparable to its
evaporation rate and thermal equilibrium will no longer exist. To
understand this region, it is necessary to investigate the rate
equations which govern the BMEC. A system of rate equations has been
proposed [11] to describe the BMEC which assumes that each complex
obeys the relation

$$
\frac{dn_m}{dt} = \frac{-n_m}{\tau_m} + \frac{n_{m+1}}{\tau_{m+1}} + n_{m-1} \, n_{ex} \, V_{th} \, \sigma_{m-1} - n_m n_{ex} V_{th} \sigma_m
$$

$$
- n_m \, R_m^{evap} + n_{m+1} \, R_{m+1}^{evap} \quad , \tag{4.5}
$$

where τ_m is the recombinative lifetime for an m-complex, V_{th} is the
exciton thermal velocity, σ_m is the exciton capture cross-section of
an m-complex and R_m^{evap} is the evaporation rate of excitons off an
m-complex. The terms on the righthand side of Eq. (4.5) correspond
to respectively: pair recombination on an m-complex, pair recombina-
tion on an (m+1)-complex (making an m-complex), exciton capture on an

(m-1)-complex (making an m-complex), exciton capture on an m-complex, evaporation of an exciton off an m-complex, and evaporation of an exciton off an (m+1)-complex (making an m-complex). These rate equations assume that when a pair in a complex recombines, the only effect is to reduce the number of pairs by one. However, the dominant decay mechanism for a complex is probably an Auger process [12] which deposits about 1 eV into the BMEC. Since the work functions for these complexes are of order of a few meV, it may be more appropriate to assume that a non-radiative recombination strips all the excitons off the impurity. This would change Eq. (4.5) by eliminating the second term on the righthand side.

If we assume that the rate equations take the form of Eq.(4.5) then the system can be solved for n_m in terms of quantities involving the next smaller complex. If we write the rate equation for (m+1)-complexes the 2nd, 4th and 6th terms in Eq. (4.5) will appear but with the opposite sign, so that adding the two equations causes these terms to cancel out. Extrapolating this idea we find:

$$\sum_{k=m}^{\ell} \frac{dn_k}{dt} = \frac{-n_m}{\tau_m} + \frac{n_\ell}{\tau_\ell} + n_{m-1}n_{ex}V_{th}\sigma_{m-1} - n_\ell n_{ex}V_{th}\sigma_\ell$$

$$- n_m R_m^{evap} + n_{\ell+1}R_{\ell+1}^{evap} \quad . \tag{4.6}$$

In steady state $\frac{dn_k}{dt} = 0$ for all k, and we can let ℓ be large enough so that $n_\ell = 0$, then solving Eq. (4.6) yields

$$\frac{n_m}{n_{m-1}n_{ex}} = \frac{V_{th}\sigma_{m-1}}{1/\tau_m + R_m^{evap}} \qquad . \qquad (4.7)$$

As we mentioned above, it may be appropriate to assume that a non-radiative recombination destroys the complex. This changes Eq. (4.7) to:

$$\frac{n_m}{n_{m-1}n_{ex}} = \frac{V_{th}\sigma_{m-1}}{1/\tau_m + R_m^{evap} + \sum_{k=m+1}^{\ell+1} \frac{n_k}{n_m\tau_k}} \qquad . \qquad (4.8)$$

This extra term in the denominator on the righthand side is usually negligible since $n_{m+1} \ll n_m$ so that $1/\tau_m \gg \frac{n_{m+1}}{n_m\tau_{m+1}}$. Only under near saturation conditions, where $n_{m+1} \sim n_m$, will this term be important.

In either case, (Eq. 4.7 or 4.8) if the temperature is high enough to make the evaporation rate large compared to the recombination terms then we can neglect decay leaving

$$\frac{n_m}{n_{m-1}n_{ex}} = \frac{V_{th}\sigma_{m-1}}{R_m^{evap}} \qquad . \qquad (4.9)$$

Assuming detailed balance for the capture and release of excitons,

Figure 4.1

Graphs of a calculation of the expected temperature dependence of BMEC from Eq. (4.7) for three forms of $\sigma(T)$. The graphs cover a temperature range in which modifications to thermal equilibrium due to finite lifetimes become important.
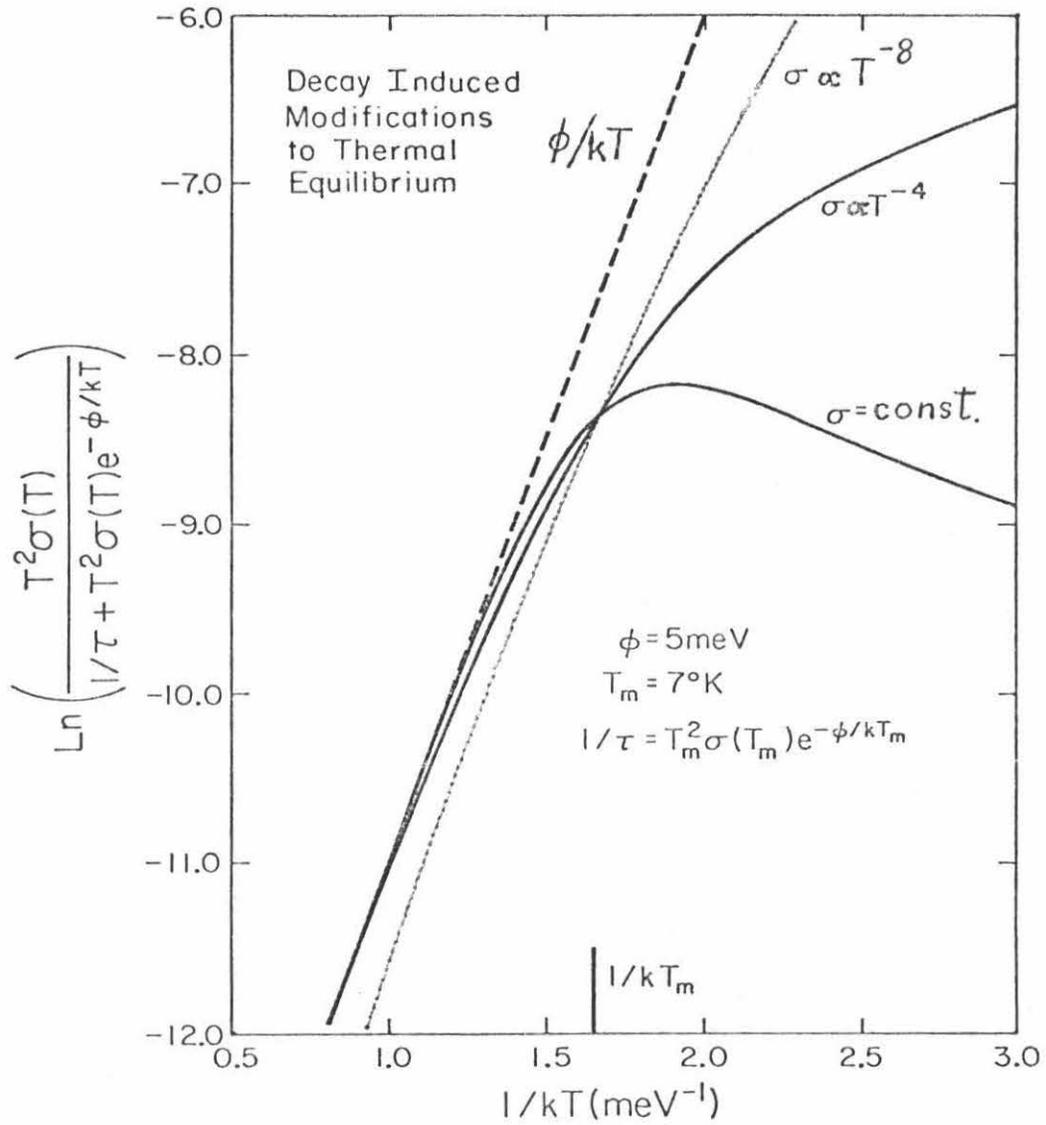
Figure 4.1

$$R_m^{evap} = \left(\frac{2\pi m^* kT}{h^2}\right)^{3/2} D_m V_{th} \sigma_{m-1} \, e^{-\phi_m/kT} \quad , \tag{4.10}$$

and Eq. (4.9) can be reduced to the thermal equilibrium result, Eq. (4.2). However, we should expect deviations from the equilibrium result when $R_m^{evap} \lesssim 1/\tau_m$, as described by Eq. (4.7). At lower temperatures the curve we obtain from the Arrhenius plot will bend down away from the straight line of Eq. (4.4) and become relatively constant. This rounding will appear at about the temperature, T_m, where the evaporation rate equals the decay rate.

$$T_m = \frac{\phi_m}{k\ell n \left[\left(\frac{2\pi m^* kT_m}{h^2}\right)^{3/2} \tau_m D_m V_{th} \sigma_{m-1}\right]} \quad . \tag{4.11}$$

The value of T_m is linear in ϕ_m while depending only logarithmically on the other terms, and, hence is sensitive to ϕ_m and insensitive to the precise values of the other parameters.

In Fig. 4.1 we show how we expect the temperature data to look for three possible forms for the capture cross section. The curves are a graph of the natural logarithm of $T^{3/2}$ times the righthand side of Eq. (4.7) versus $1/kT$. This function, $\ell n \dfrac{T^2 \sigma(T)}{1/\tau + T^2 \sigma(T) \, e^{-\phi/kT}}$, is plotted for $\sigma(T) = $ constant, $(T) \propto T^{-4}$, and $\sigma(T) \propto T^{-8}$. A measurement of $\sigma(T)$ has been made for the BE in Si:In [13], and σ was found to increase rapidly with decreasing temperature. A value of 5 meV was

used for ϕ and T_m was chosen to be 7^0K. Together with $\sigma(T)$ this fixes τ. The dashed line in the figure corresponds to $y = \phi/kT$ and is approached asymptotically by the calculated curves as $T \rightarrow \infty$. We see that curve assuming $\sigma \propto T^{-8}$ shows essentially no rounding at T_m. The experimental data do exhibit breaks, indicating that the cross section does not vary as rapidly as T^{-8}. The graphs assuming $\sigma = $ constant and $\sigma \propto T^{-4}$ both round over near T_m.

III. Experimental Methods

The B, Al, and P doped samples were cut from float zone silicon crystals in which the dopants were introduced during growth. The Si:B and Si:P samples were 3 mm thick while the Si:Al was 450 μm thick. The Si:Li samples were prepared by diffusing Li onto Si crystals. Lithium doped silicon sample No. 1 was prepared from p-type silicon with an initial room temperature resistivity of 15 kΩ-cm. A suspension of Li in mineral oil was painted on both sides of the 1 mm thick crystal and diffused into the silicon at 370^oC for one minute. The crystal was then removed from the furnace and lightly lapped to remove excess Li. A drive-in diffusion at 650^oC for 1 1/2 hours was performed to improve the uniformity of the Li distribution. The other Si:Li sample (No. 2) was prepared from n-type silicon with an initial room temperature resistivity of 80 Ω-cm. The pre-deposition was for one minute at 400^oC. The rest of the preparation was the same as for the first Li-doped sample. The impurity concentration in each of the samples was determined from room temperature resistivity measurements. The crystals were all about one square centimeter in area. The samples were lapped and etched with HNO_3:HF (7:1) to remove surface damage. Immediately before mounting in the dewar the crystals were washed with methanol.

The 5145 $\overset{o}{A}$ line from an argon-ion laser was used for excitation. The excitation was continuous, not chopped, to make accurate measure-

ments of sample temperature possible. The exciting beam was first passed through an infrared filter to remove any extraneous emission lines in the wavelength region of interest. Spot sizes used on the sample ranged between 3 and 8 mm in diameter. The luminescence was collected with a lens and after passing through a filter to remove the visible laser light was focused on the entrance slit of a grating spectrometer. The light was detected with a liquid nitrogen cooled S-1 photomultiplier and processed with photon counting equipment.

The sample temperature was measured with a calibrated silicon diode thermometer soldered directly to the crystal. The FE lineshape was fit for the higher pump powers and the temperature obtained agreed with the sensor reading to within 15%. For the Si:Al sample the intensity ratio between the ground state and excited states of the BE was also measured. The agreement between this measure of the sample temperature and the sensor reading was again to within 15%. Another check on the sensors ability to measure true sample temperature was obtained by observing the sensor reading as liquid helium was allowed to touch the bottom of the crystal. With the sensor attached at the top of the sample, as soon as any portion was immersed in liquid the reading dropped to within $.2^{o}K$ of $4.2^{o}K$ with laser powers typical of those used for these experiments. Thus, the whole crystal was at essentially one temperature and that temperature was accurately measured with the Si sensor. It was found that the

measured work functions depended somewhat on excitation intensity, decreasing 10-20% at high pump densities. This is probably due to inhomogeneous saturation, leading to a temperature dependent carrier profile as discussed in the last section. To reduce this effect, we used as low excitation densities as was feasible for any given line.

Spectra were taken at each temperature and any background was subtracted to obtain the true intensity of the lines. The slits were opened so that the peak intensity was proportional to the integrated intensity of the BMEC lines. For the FE the integrated intensity is proportional to T times the peak intensity [14]. For the BE we have assumed that the density of occupied impurities is small compared to the total impurity density. Therefore we avoided saturating centers when measuring BE work functions.

IV. Experimental Results

A. Si:B and Si:Al

The temperature dependence of the ratios along values of ϕ_m ($\pm.5$ meV for m = 1-3, ± 1 meV for m = 4) for the BE and m = 2-4 BMEC for Si:B are shown in Fig.4.2. At high temperatures the data points fall on a straight line while the curves bend away from the straight line at lower temperatures,. The rounding of the curves is seen to occur somewhere between 7 and 8^oK for m = 2,3 and at a lower temperature for the m = 4 BMEC. These values for T_m are in a range expected from Eq. (4.11).

The uncertainties were assigned by observing that in Fig. 4.1 for σ = constant or $\sigma \propto T^{-4}$ a straight line fit to the high temperature portion of the curve will mis-estimate ϕ by up to about .5 meV. For the larger complexes, (m = 4,5) we have data over a limited temperature range and uncertainties of ± 1 meV are assumed.

The rounding is again apparent in Fig.4.3 which shows the data and the values of ϕ_m for the BE and m = 2,3 BMEC in Si;Al. Using Eq.(4.11) we can estimate the temperature, T_m, at which the curves should bend away from the straight line. Assuming $\tau_1 = 8\times10^{-8}$ sec.,[12] $V_{th} = 2\times10^6$ cm/sec, $m^* = 0.6\, m_o$, $\sigma_o = 10^{-13}$cm^2 [13], and $\phi_1 = 5.1$ meV, we can estimate T_m for the BE in Si:Al and obtain $T_1 = 6.5^oK$, in agreement with the data.

Fig. 4.4 is a graph of our results for work functions of BMEC

Figure 4.2

The temperature dependence of m = 1-4 BMEC lines in
Si:B. Here ϕ_m is the work function obtained from the
straight line fit to the data.
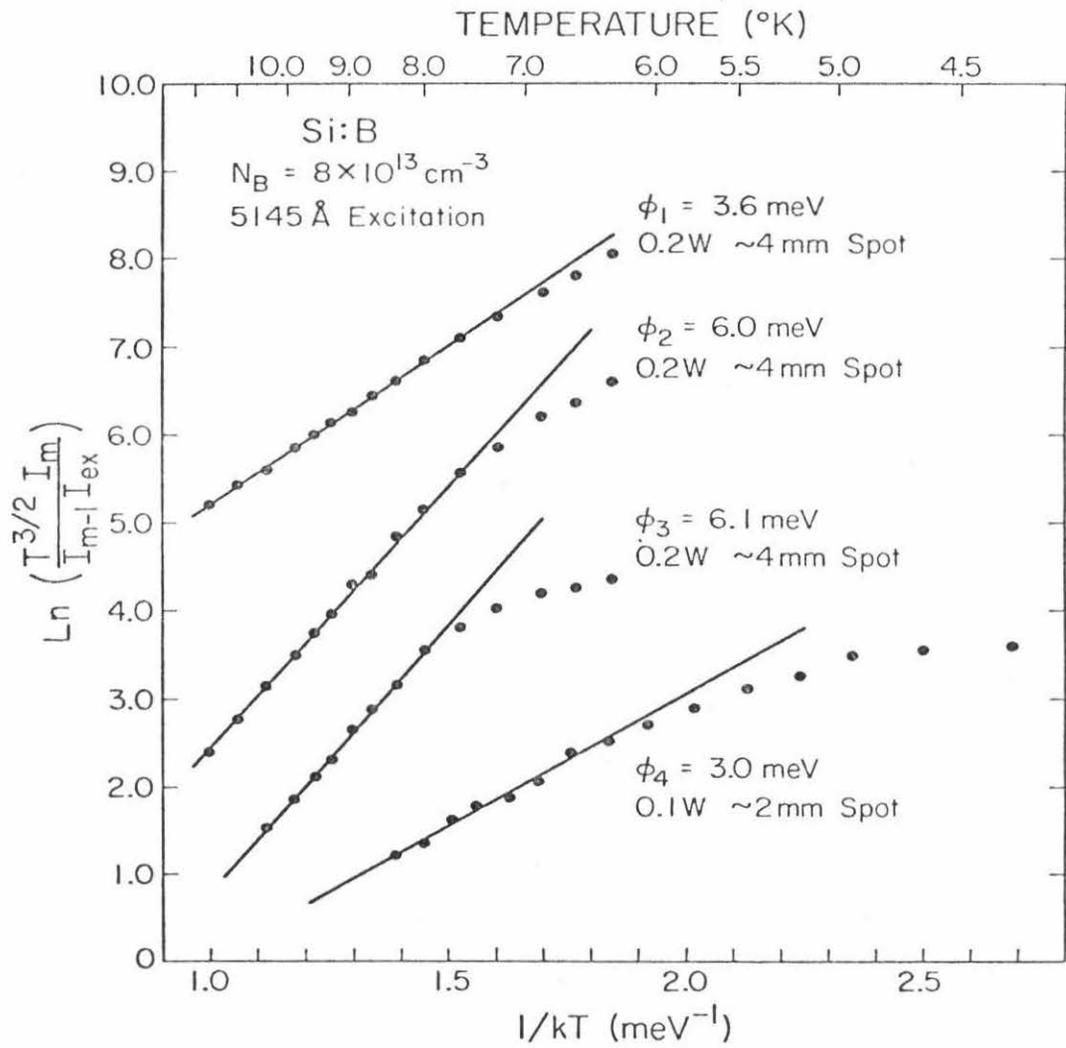
Figure 4.2

Figure 4.3

The temperature dependence of m = 1-3 BMEC lines in Si:Al. Here ϕ_m is the work function obtained from the straight line fit to the data.
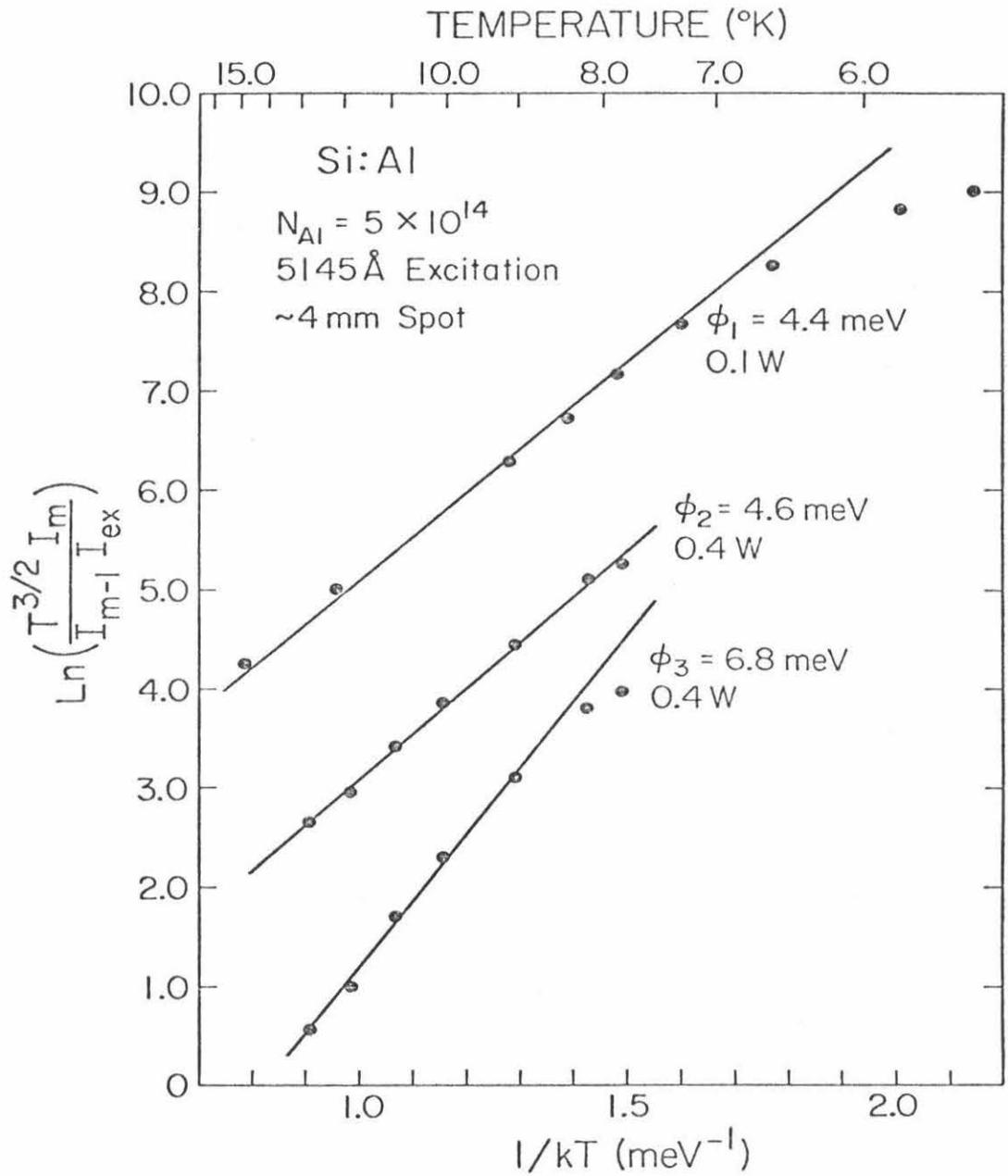
Figure 4.3

in Si:Al and Si:B, as well as the values one obtains by taking spectroscopic differences ($\delta_m \equiv h\nu_{ex} - h\nu_m$), as a function of the number of pairs on the impurity (m). We know that the BE lines arise from G-G transitions and, therefore, the work functions, ϕ_1, and the spectroscopic differences, δ_1, are equal. We see in the figure that for both boron and aluminum ϕ_1 equals δ_1 to within the experimental uncertainties. (The uncertainty in δ_m is $\pm.3$ meV, arising mainly from the uncertainty in the FE edge.) The position of the G-G transition for a 2-exciton complex in Si:Al has been established independently[1-3]. Thus we can determine ϕ_2 spectro-scopically and the thermodynamic value is in agreement with the spectroscopic result. We also see that $\phi_2 = \delta_2$ for Si:B, which indicates that the m = 2 BMEC line is a G-G transition. For both Si:Al and Si:B $\phi_3 < \delta_3$, and the difference is larger than the experimental uncertainties, indicating that the m = 3 BMEC lines arise from a transition leaving the 2-exciton complex in an excited state. The value for ϕ_4 in Si:B is considerably less than δ_4, again indicating an excited state. One possible explanation for the substantial decrease in work function for the fourth exciton in Si:B is that this last pair puts a fifth hole into the complex but all four Γ_8 hole states are already occupied. The envelope function will be forced to change in order to accommodate the fifth hole, possibly leading to weaker binding.

Figure 4.4

The thermodynamic work functions and no-phonon spectro-
scopic differences as a function of the number of pairs on
the site for BMEC in Si:B and Si:Al. The spectroscopic dif-
ferences were obtained assuming a no-phonon FE threshold of
1154.6±.3 meV. For Si:Al the m=2 G-G transition is used for
the spectroscopic difference. The energy of this transition
is inferred from the position of the transitions leaving the
BE in an excited state (Ref. 1-3). The dashed line indicates
the work function of the electron-hole droplet (Ref. 6).
The experimental uncertainties in the thermodynamic numbers
are ±.5 meV for m=1-3 and ±1 meV for m=4.
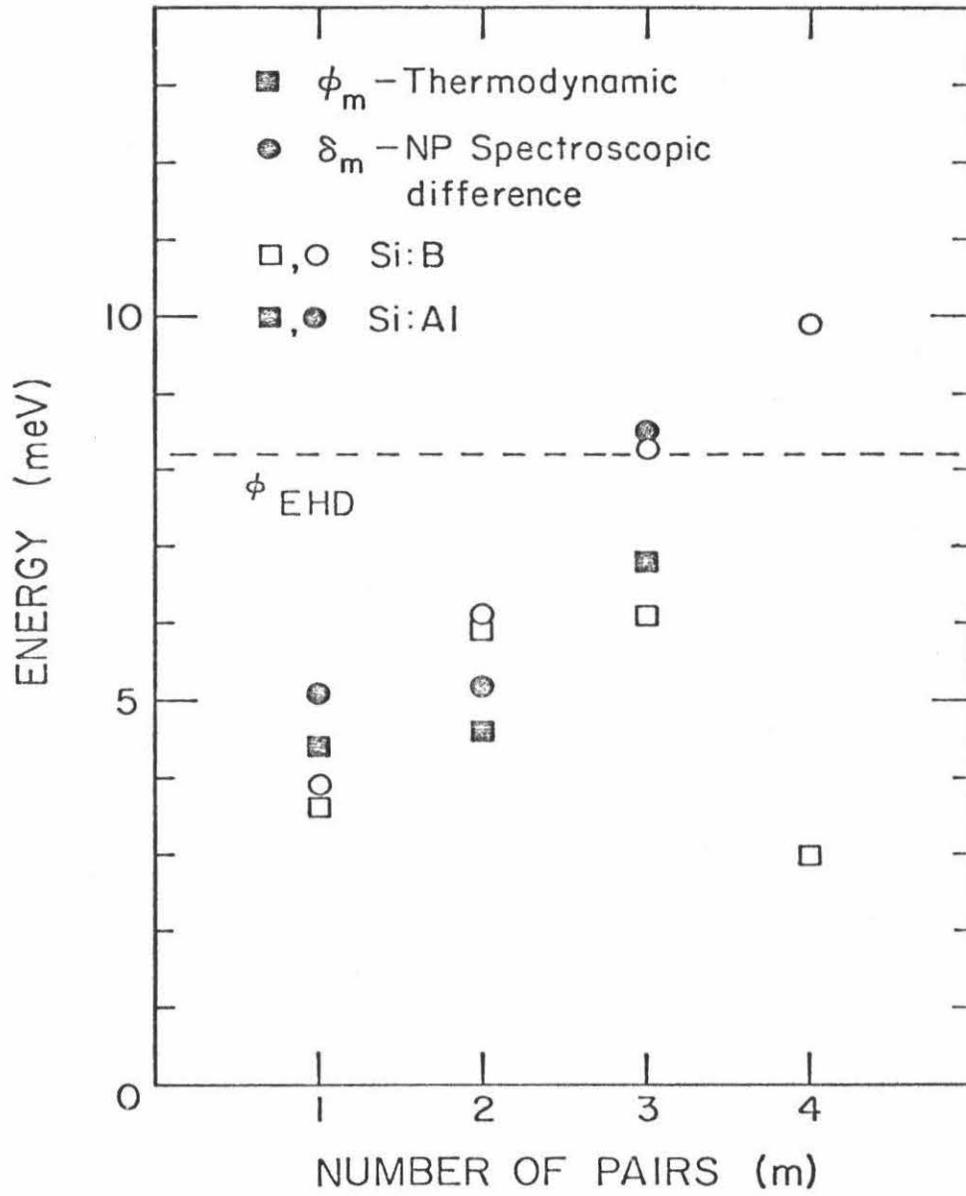
Figure 4.4

For Si:Al and Si:B we have found that wherever ϕ_m is known independently (the two BE and the m = 2 BMEC in Si:Al) the thermodynamic determination is in agreement with the previous result. However, for m = 3,4 we find that the work functions are less than the corresponding spectroscopic differences. This implies that the luminescence lines are due to transitions which leave the final complex in an excited state. The energies of these excited states are given by $\delta_m - \phi_m$.

B. Si:Li

The temperature data and values of ϕ_m for the BE and m = 2 BMEC in Si:Li are shown in Fig.4.5. As for Si:B and Si:Al we find that $\phi_1 = \delta_1$ in Si:Li (δ_1 = 3.4 meV [15]). Again this was to be expected since the BE is known to be a G-G transition. However, in contrast to the two acceptors, we find that $\phi_2 < \delta_2$ (δ_2 = 6.1 meV [15]). The data for the m = 3 and larger complexes did not show a break until about 9^oK or higher. By these temperatures the lines were too weak to obtain reliable measurements of ϕ, but the values for T_m indicate that the larger complexes may have work functions that are at least as large as ϕ_2.

We see that Si:Li is qualitatively different from Si:B and Si:Al in that $\phi_2 < \delta_2$. The m=2 BMEC line corresponds to a transition which leaves the BE in an excited state, with an energy $\delta_2 - \phi_2$ = 2.5 meV above the ground state. Spectra of Si:Li are

Figure 4.5

The temperature dependence of m=1,2 BMEC lines in Si:Li. Here ϕ_m is the work function obtained from the straight line fit to the data. The data for m=1 were obtained from sample No. 2 (N_{Li} = 1.2x10^{15}cm^{-3}) with 100 mW of excitation and a 2 mm spot size. The data for m=2 were obtained from two different experiments. The data for 9°K and higher in temperature were taken on sample No. 2 with 600 mW of excitation and a 3 mm spot size. The data for 9°K and lower were taken on sample No. 1 (N_{Li} = 1x10^{13}cm^{-3}) with 200 mW of excitation and a 5 mm spot size. The two sets of data were shifted vertically to match the 9°K data points from each experiment.
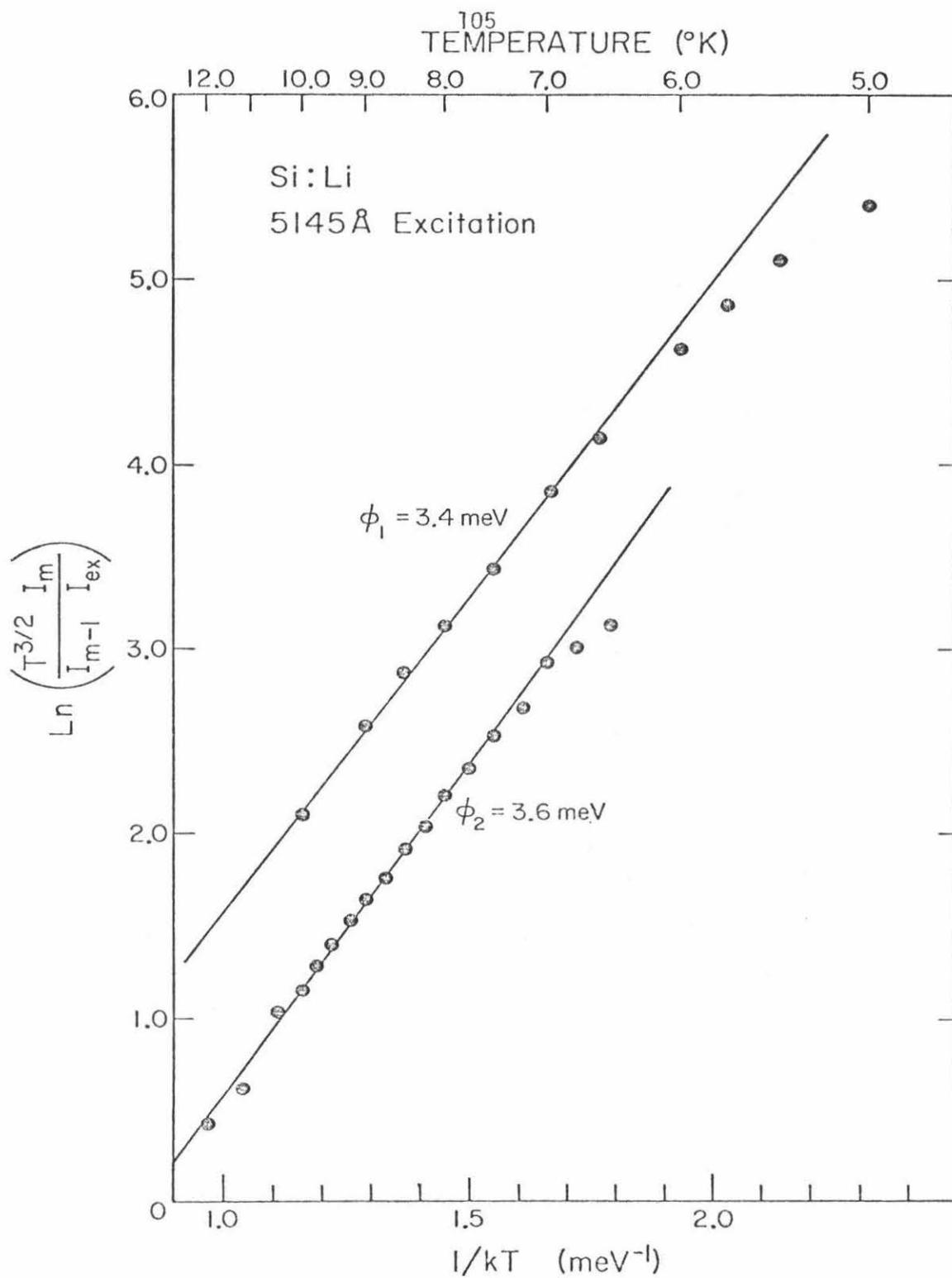
Figure 4.5

Figure 4.6

Photoluminescence spectra at three temperatures of Li-doped Si in the energy range for TO and LO phonon assisted transitions. The lines labeled BE are associated with the Li impurities. The thermal data predict the existence of an excited state of the BE at the position indicated by the arrow. The line labeled P is associated with phosphorous impurities and the line labeled FE is the free exciton luminescence.
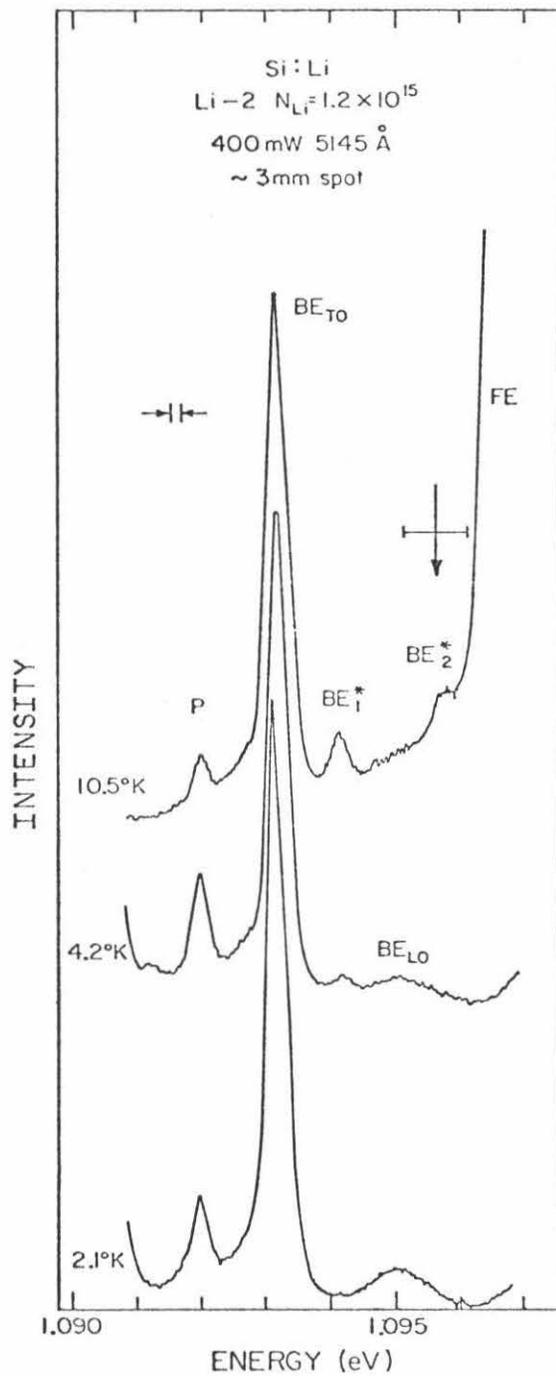
Figure 4.6

shown in Fig.4.6 and we see in the upper spectrum (10.5°K) a
luminescence line, labelled BE_2^*, corresponding to an excited state
of the BE with the expected energy (indicated by the arrow). We
know that this line at 1.09589 eV is an excited state of the BE
because it is not present in the two lower spectra taken at 4.2
and 2.1°K, in accordance with a Boltzmann factor. In addition to the
1.09589 eV line and the BE_{TO} and BE_{LO} (the line labelled P is due to
phosphorous impurities) we see a line at 1.09451 eV, labelled BE_1^*.
This line is large at 10.5°K, smaller (relative to the BE) at
4.2°K, and entirely absent in the 2.1°K spectra. This dependence
on temperature indicates that it is also an excited state of the BE,
0.94 meV above the ground state. In Si:Li we have observed two
excited states of the BE, one of which is positioned correctly to
be the final state in the radiative decay of the 2-exciton complex.
The G-G transition for this complex would lie 3.6 meV below the FE
and be buried under the BE line.

C. Si:P

The data and values of ϕ_m for Si:P are given in Fig. 4.7. The
work functions ϕ_m and spectroscopic differences, δ_m, as well as the
spectroscopic differences, to the β-lines, δ_m^β, are plotted in Fig.4.8
as a function of the number of pairs on the impurity. The β-lines
are interpreted as G-G transitions in the shell model[5], making
the δ_m^β ($\delta_m^\beta \equiv h\nu_{ex} - h\nu_{\beta_{m-1}}$, $\delta_1^\beta \equiv \delta_1$), the work functions of the com-
plexes in this model. We find that $\phi_1 = \delta_1 = \delta_1^\beta$ as expected. For

Figure 4.7

The temperature dependence of m=1-5 BMEC lines in Si:P.
Here ϕ_m is the work function obtained from the straight line
fit to the data.
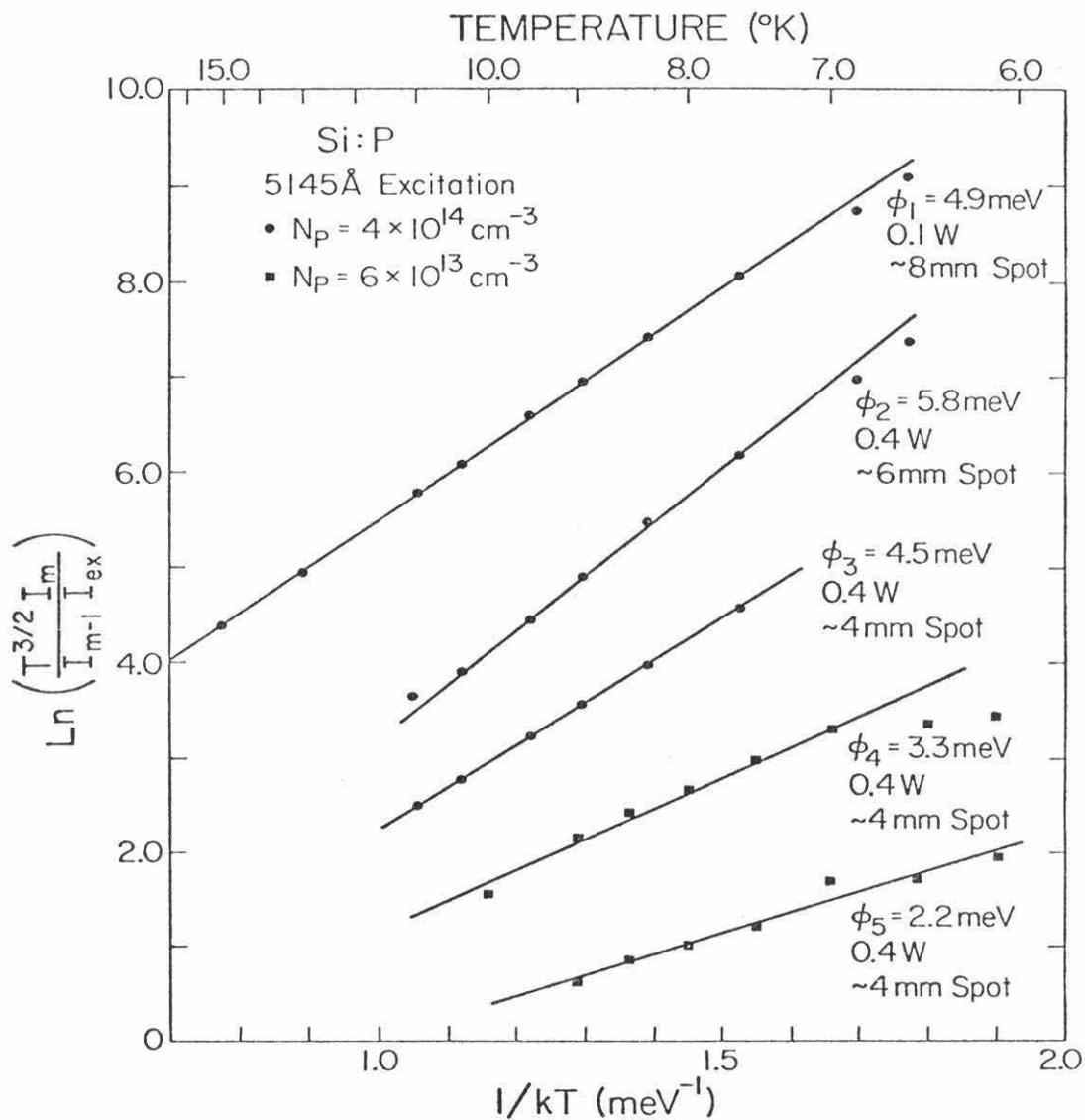
Figure 4.7

Figure 4.8

The thermodynamic work functions, no-phonon spectroscopic differences, and spectroscopic differences to the β-lines (Ref. 17) as a function of the number of pairs on the site for BMEC in Si:P. The no-phonon spectroscopic differences were obtained by assuming a no-phonon FE threshold of $1154.6\pm.3$ meV and the β-series spectroscopic differences were obtained from the data in Ref. 1. The dashed line indicates the work function of the electron-hole droplet (Ref. 6). The experimental uncertainties in the thermodynamic numbers are $\pm.5$ meV for m=1-3 and ±1 meV for m=4,5.
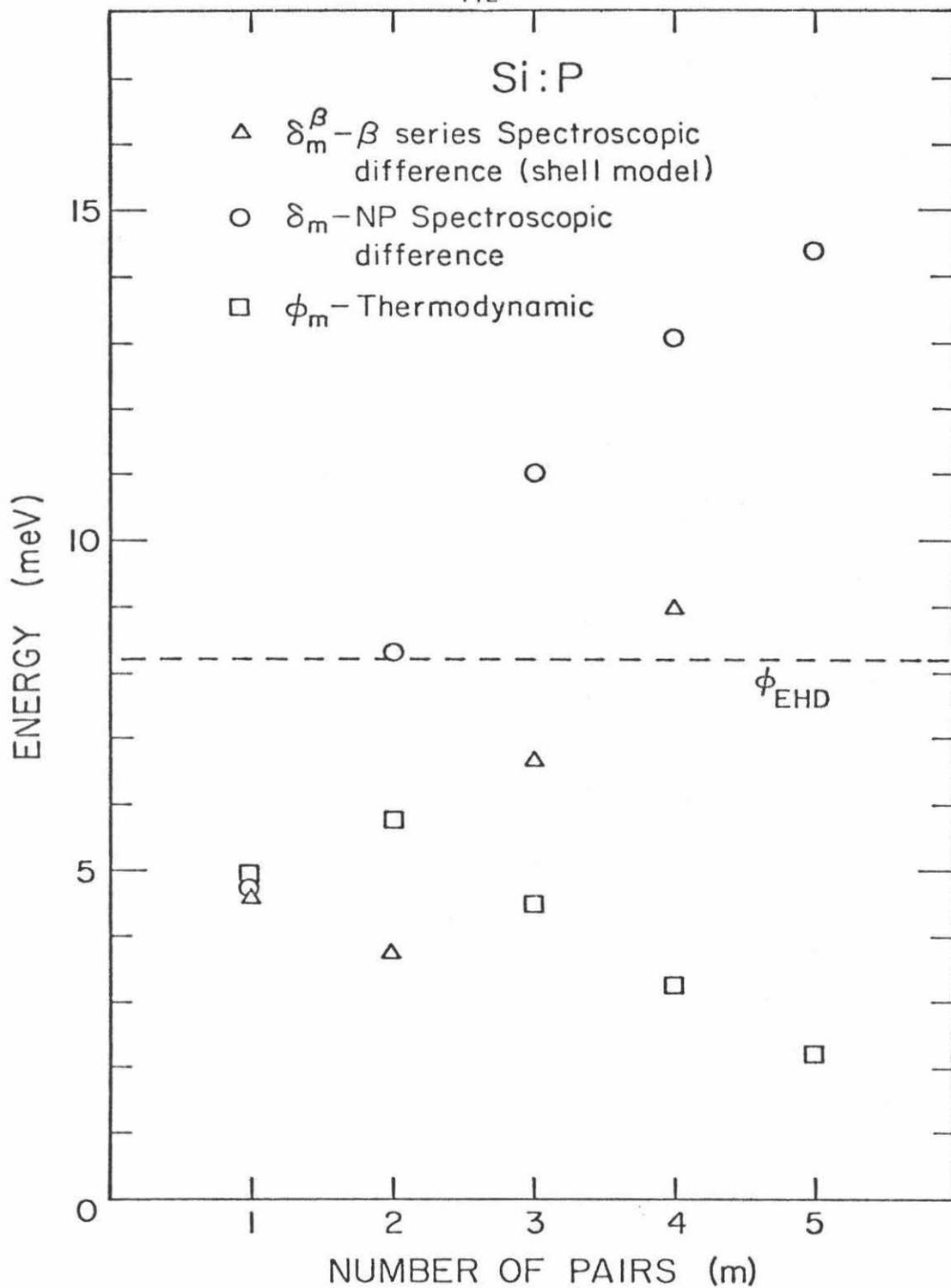
Figure 4.8

the 2-exciton complex, $\phi_2 < \delta_2$ as we found for Si:Li. However, the graph shows that $\phi_2 > \delta_2^\beta$ which indicates that the β_1 line does not arise from the decay of a 2-exciton complex bound to a phosphorous impurity. For m > 2 the ϕ_m decrease as the number of pairs on the impurity increases. This is in contrast to the behavior of δ_m and δ_m^β which both increase for increasing m. None of the measured ϕ_m exceed ϕ_{EHD} while both δ_m and δ_m^β are greater than ϕ_{EHD} for sufficiently large m.

Since $\delta_2 > \phi_2$ the m-2 BMEC transition we observe in Si:P must leave the BE in an excited state as in Si:Li. There are two excited states of the phosphorous BE observed in absorption and high temperature luminescence spectra. Neither of these lines have the correct energy. However, we expect to see the G-G transition at $h\nu_{ex} - \phi_2$. Fig.4.9 is a spectrum taken on Si:P in the TO phonon region. The sample was prepared from ultra-high purity ($N_A - N_D = 2 \times 10^{11}$) Si by transmutation doping [16]. The lines are labelled after Ref. 17. (α_m is the m-exciton complex line). The arrow indicates the expected position of the G-G transition for the decay of a 2-exciton complex. There is a small line with energy 1.09058 eV at this position. The m=2 BMEC on boron lies at about this energy; however, the boron content of this sample is very low. We do not know whether the observed line is due to P or whether the P-related transition is being masked by the m=2 boron line.

Figure 4.9

Photoluminescence spectrum of P-doped Si in the energy range for TO and LO phonon assisted transitions. The lines labeled with α's and β's (Ref. 17) are associated with the P impurities. The thermal data predict the existence of the G-G transition for the m=2 BMEC decay at the position indicated by the arrow.
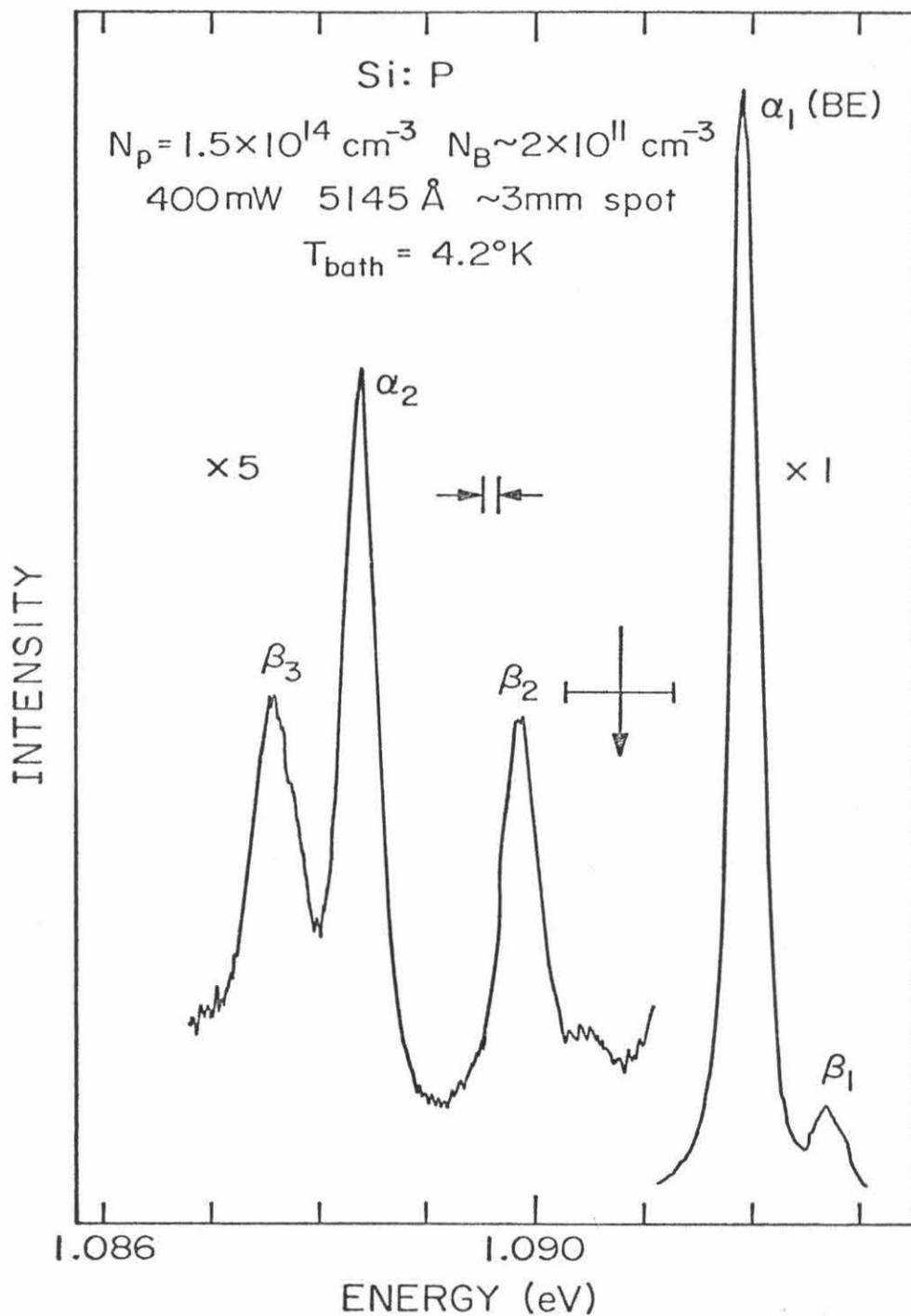
Figure 4.9

V. Discussion and Conclusions

We have measured the temperature dependence of BMEC lines in Si doped with B, Al, Li and P. At the higher temperatures we assume that the complexes come into thermal equilibrium with the surrounding exciton gas. This assumption allows us to extract values for the work functions of the BMEC from the thermal data. We interpret the lower temperature data in terms of a system of rate equations and we see the expected transition to thermal equilibrium as the temperature is raised.

In all cases where the work functions are known independently, (m=2 for Si:Al and the four BE), the values of ϕ_m obtained from the thermal data are in agreement with the previous results. We also find that for the m=2 BMEC in Si:B $\phi_2 = \delta_2$, indicating that the line is a G-G transition. For the other lines measured, we find that $\phi_m < \delta_m$. This suggests that ground-state to excited-state transitions are being observed. For Si:Li the temperature dependence of the m=2 BMEC predicts that the BE has an excited state about 2.5 meV above the ground state. This has been confirmed by our observation of an excited state of the BE at the expected position in high temperature luminescence spectra. We also see a line in spectra of Si:P which is positioned correctly to be the G-G

transition of the m=2 BMEC, though we have not yet made this iden-
tification with certainty. Its small size and the general lack of
lines due to G-G transitions for the BMEC are consistent with data
for Si:Ga in which the G-G transition for the m=2 BMEC is at least
a factor of three smaller than the transitions leaving the BE in
an excited state.

We find that the dependence of the measured work functions on
the number of excitons in the complex is very different from that
of the corresponding spectroscopic differences. In general the
spectroscopic differences increase with the size of the complex while
the values of ϕ_m show that for Si:Al and Si:B, the binding increases
for m going from 1 to 3 and then decreases for m=4 in Si:B. For Si:P
and Si:Li, ϕ_m increases for m going from 1 to 2, then decreases for m
going from 3 to 5 in Si:P. The decrease in ϕ_m for m=4 in Si:B may
be due to the necessity of changing the envelope function when the
fifth hole is added.

Our data answer some of the questions involving the work func-
tions of BMEC but raise some interesting new questions. All of the
measured work functions are less than ϕ_{EHD}. In the limit of large
m, however, we expect ϕ_m to approach ϕ_{EHD}. We have not been able
to measure the work functions for large enough complexes to observe
this limiting behavior. It may be possible to understand the approach
to ϕ_{EHD} in terms of a surface energy correction to the droplet work

function for very small drops. We also do not have a clear under-
standing of the decrease in ϕ_m for m ranging from 2-5 in Si:P. The
difficulty in minimizing the electron-electron interaction when the
fourth electron is added to the complex may contribute to the de-
crease in work function going from m=2 to m=3 in Si:P.

As well as the dependence of the work functions on the size
of the BMEC, another question these data raise concerns the nature
of the final states of the optical transitions. We find that in
general the observed lines involve transitions which leave the
complex in an excited state. In only a few cases (aside from the
BE) are G-G transitions observed. However, a background is often
observed beneath the BMEC lines [15], and it could arise from a
superposition of G-G and other transitions which are too weak to
appear as discrete lines. We are still left with the question of
why the complexes seem to decay predominantly into one particular
excited state when the final complex probably has many excited
states. In some cases the remaining complex is left with enough
energy to kick off one or more excitons. We know that the excited
states must have lifetimes of at least a picosecond to give the ob-
served linewidths.

In conclusion we have used a thermodynamic method to measure the
binding energies of the last exciton for BMEC in Si:Al, Si:B,
Si:Li and Si:P. For the larger complexes the work functions we

measure are considerably smaller than the corresponding spectro-
scopic differences. Interpreting the BMEC lines as being due to
G-G transitions leads to work functions which increase monotonically
for the larger complexes; whereas, we find that the second exciton
in Si:P and third in Si:B are the most tightly bound and each
succeeding exciton is bound with less energy than the last. We
find that, in general, the optical transitions leave the remaining
complexes in excited states.

References

1. M.L.W. Thewalt, Phys. Rev. Lett. 38, 521 (1977); and Can. J. Phys. 55, 1463 (1977).

2. E. C. Lightowlers and M. O. Henry, J. Phys. C10, L247 (1977).

3. S. A. Lyon, D. L. Smith, and T. C. McGill, Phys. Rev. B17, 2620 (1978).

4. T. N. Morgan, in Proceedings of the Thirteenth International Conference on the Physics of Semiconductors, Rome, 1976, edited by F. G. Fumi (Tipografia Marves, Rome, 1977), p. 825.

5. G. Kirczenow, Solid State Commun. 21, 713 (1977).

6. R. B. Hammond, T. C. McGill, and J. W. Mayer, Phys. Rev. B13, 3566 (1976).

7. R. B. Hammond, D. L. Smith and T. C. McGill, Phys. Rev. Lett. 35, 1535 (1975).

8. M. Capizzi, J. C. Merle, P. Fiorini, and A. Frova, Solid State Commun. 24, 451 (1977).

9. R. B. Hammond and R. N. Silver, Solid State Commun. (to be published).

10. M. Altarelli and N. O. Lipari, Phys. Rev. B15, 4898 (1977).

11. R. N. Silver, Phys. Rev. B11, 1569 (1975).

12. S. A. Lyon, G. C. Osbourn, D. L. Smith and T. C. McGill, Solid State Commun. 23, 425 (1977).

13. K. R. Elliott, D. L. Smith, and T. C. McGill, Solid State Commun. 24, 461 (1977).

14. The integrated intensity of the FE is given by
$$I_{ex} = I_o \int_0^\infty (h\nu)^{1/2} e^{-h\nu/kT} d\nu, \text{ or } I_{ex} \propto I_o(kT)^{3/2}.$$ The
intensity at the peak of the FE luminescence line is pro-
portional to $I_o(kT)^{1/2}$. Therefore $I_{ex} \propto T \times I_{peak}$.

15. K. Kosai and M. Gershenzon, Phys. Rev. B9, 723 (1974).

16. A. Hunter, et al, (unpublished).

17. M.L.W. Thewalt, Solid State Commun. 21, 937 (1977).

PART II

CHAPTER 5

CLOUD MODEL FOR THE DECAY

OF EHD IN PURE AND DOPED Ge

I. Introduction

As discussed in Chapter 1, the existence of electron-hole-droplets in semiconductors is now well established. Their equilibrium properties have been studied extensively, especially in Ge. However, there are still questions concerning the transient behavior of the drops in Ge. Numerous investigations have been made of the growth and decay of EHD [1-10]. The kinetics have been studied with both surface [8] and volume excitation [9]. In the volume-excitation experiments [9] the EHD are observed to grow from a super-saturated FE gas in agreement with the predictions of nucleation theory [11,12]. The surface excitation experiments are less well understood. They are complicated by the transport of carriers into the crystal. The EHD appear to be formed in a dense plasma at the surface under the laser spot and then move into the sample forming a "cloud" of droplets with a diameter of 1 mm or more.

Similarly, at high excitation densities the decay of EHD is complex. The drops are in a gas of free excitons and their decays are coupled. The general system of equations which must be solved is,

$$\frac{d\nu_i}{dt} = \frac{-\nu_i}{\tau} - aT^2 \nu_i^{2/3} e^{-\phi_{EHD}/kT} + bn_{ex}(r_i)\nu_i^{2/3} \qquad (5.1a)$$

for each droplet, labelled by i, and

$$\frac{\partial n_{ex}(r)}{\partial t} = D\nabla^2 n_{ex}(r) - \frac{n_{ex}(r)}{\tau_{ex}} + \left(aT^2 \nu_i^{2/3} e^{-\phi_{EHD}/kT} - bn_{ex}(r)\nu_i^{2/3} \right) \delta(r-r_i)$$

$$(5.1b)$$

for the FE, where ν_i is the number of electron-hole pairs in the ith EHD located at r_i, τ and τ_{ex} are respectively the EHD and FE recombination lifetimes, a is the Richardson-Dushman constant [14], T is the temperature, $n_{ex}(r)$ is the density of FE at the point r, and D is the exciton diffusivity. The constant b is equal to $\pi v_{th}(4\pi n_0/3)^{-2/3}$ where v_{th} is the average thermal velocity of the excitons, and n_0 is the density of pairs in an EHD. The three terms on the righthand side of Eq. 5.1a are the recombination rate for pairs in the EHD, the FE evaporation rate off EHD, and the exciton capture rate on EHD, respectively.

Even in principle the system of equations 5.1a,b is insoluble since we have no way of determining the position of each EHD. Some simplifying assumptions are necessary to obtain tractable equations. Pokrovskii [13] and Hensel [3] have proposed a model which has been used to describe the decay of the EHD in the surface-excitation experiments. This average or "single drop" picture is based on the assumption of a uniform number density of identical drops, N, through-out the crystal and a uniform exciton density $\bar{n}_{ex}$. Then the system of equations 5.1a,b reduces to two average equations. For droplets we have,

$$\frac{d\nu}{dt} = \frac{-\nu}{\tau} - aT^2\nu^{2/3} e^{-\phi_{EHD}/kT} + b\bar{n}_{ex}\nu^{2/3} \quad , \tag{5.2a}$$

and for FE,

$$\frac{d\bar{n}_{ex}}{dt} = \frac{-\bar{n}_{ex}}{\tau_{ex}} + aT^2N\nu^{2/3} e^{-\phi_{EHD}/kT} - b\bar{n}_{ex}N\nu^{2/3} \quad , \tag{5.2b}$$

where ν is the average number of electron-hole pairs in an EHD. Usually the further approximation is made that $\bar{n}_{ex}$ is zero, i.e., the EHD are evaporating in a "vacuum", and thus the exciton capture rate is zero. This decouples Eq. 5.2a from the excitons and allows an analytic solution,

$$\nu(t) = \nu(o) \; \frac{e^{(t_c - t)/3\tau} - 1}{e^{t_c/3\tau} - 1} \quad , \tag{5.3}$$

with

$$t_c = 3\tau \; \ell n \left(1 + \frac{\nu(o)^{1/3}}{aT^2\tau e^{-\phi_{EHD}/kT}} \right) . \tag{5.4}$$

At low temperatures the evaporation rate is very small making $t_c \gg 3\tau$, and the decay is nearly exponential with a lifetime, τ. At higher temperatures, the decay is faster than this exponential and is characterized by the cut-off time, t_c. By adjusting t_c it is possible to fit a wide range of experimental data with this model. However, t_c is found to be a function of excitation intensity. At relatively high excitation [5,6] the values of t_c needed to fit the data lead to values for $\nu(o)^{1/3}$ and consequently initial drop radii which are much larger than those deduced from other experiments [15]. From fits to the decay transients drop radii of several hundred microns are obtained, while light-scattering experiments show that the drops are less than ten microns in size [2,10,16]. Furthermore, we know from infrared absorption measurements that at all but the lowest

excitation intensities the EHD form a cloud with interdrop distances small compared to the FE diffusion length [16]. We expect that the FE density in the body of the cloud to be near the thermodynamic equilibrium value, not zero. The resulting recapture of excitons should reduce the net evaporation and its effect on the decays at high temperatures.

In this chapter a new model will be introduced which overcomes some of the deficiencies in the single drop picture. Instead of assuming the EHD are spread throughout the crystal, the new model assumes that there is a uniform density of drops within some region (the cloud) and none outside. The FE density inside the cloud is determined by solving the diffusion equation around an "average drop". The diffusion equation is again solved to determine the exciton profile outside the cloud. By incorporating the experimental fact that the EHD form a cloud, and including the diffusion of excitons, it is possible to fit the data at all pump powers and temperatures without invoking the unphysically large drops. From a fit to the EHD decay it accurately predicts the FE luminescence decay. Furthermore, it is possible to include the effects of doping on the EHD luminescence transients by decreasing the FE diffusion length.

II. Description of the Model

Fig. 5.1 is a schematic illustration of the basic ideas under-
lying the cloud model. The small circles represent droplets and the
dots excitons. The cloud is assumed to be a hard-edged sphere in
that there is a uniform density of EHD's within some radius R_c and none
outside. We know that this is somewhat idealized in that the cloud's
shape is much more complicated [16,17] and the EHD may be in motion[20].
However, the model retains the essential idea that there is a bounded
region in which droplets are relatively close together, and the
exciton density is consequently non-negligible. Within the cloud it
is assumed that these excitons have an average density $(\overline{n}_{ex})$ which
is determined by conditions in the body of the cloud. Since the EHD's
are taken to be occupying a region within an infinite medium, there
is an exciton diffusion tail extending out from the surface of the
cloud, the density being pinned to $\overline{n}_{ex}$ at the surface and going to
zero at infinity. In the figure this is shown as a decreasing
density of dots (excitons) moving out from the cloud. This diffusion
of excitons away from the cloud provides one means of decay, since
it is assumed that they are supplied by the evaporation of droplets
at the surface, making the cloud shrink.

The inset in Fig.5.1 depicts the situation in the body of the
cloud and is the basis for the calculation of the average exciton
density. The close proximity of the droplets, interdrop distances
being much less than an exciton diffusion length for pure material,
implies that each drop on the average only supplies excitons to its

Figure 5.1

Schematic illustration of the cloud of electron-hole-droplets and free-excitons. The radius of the cloud is R_c. Inset shows an enlarged view of an electron-hole droplet surrounded by neighboring electron-hole droplets. The central electron-hole-droplet needs to supply excitons only into the volume bounded by R_s (dashed line).

SCHEMATIC OF CLOUD
OF
# ELECTRON-HOLE DROPLETS

o – ELECTRON-HOLE DROPLET
· – EXCITON
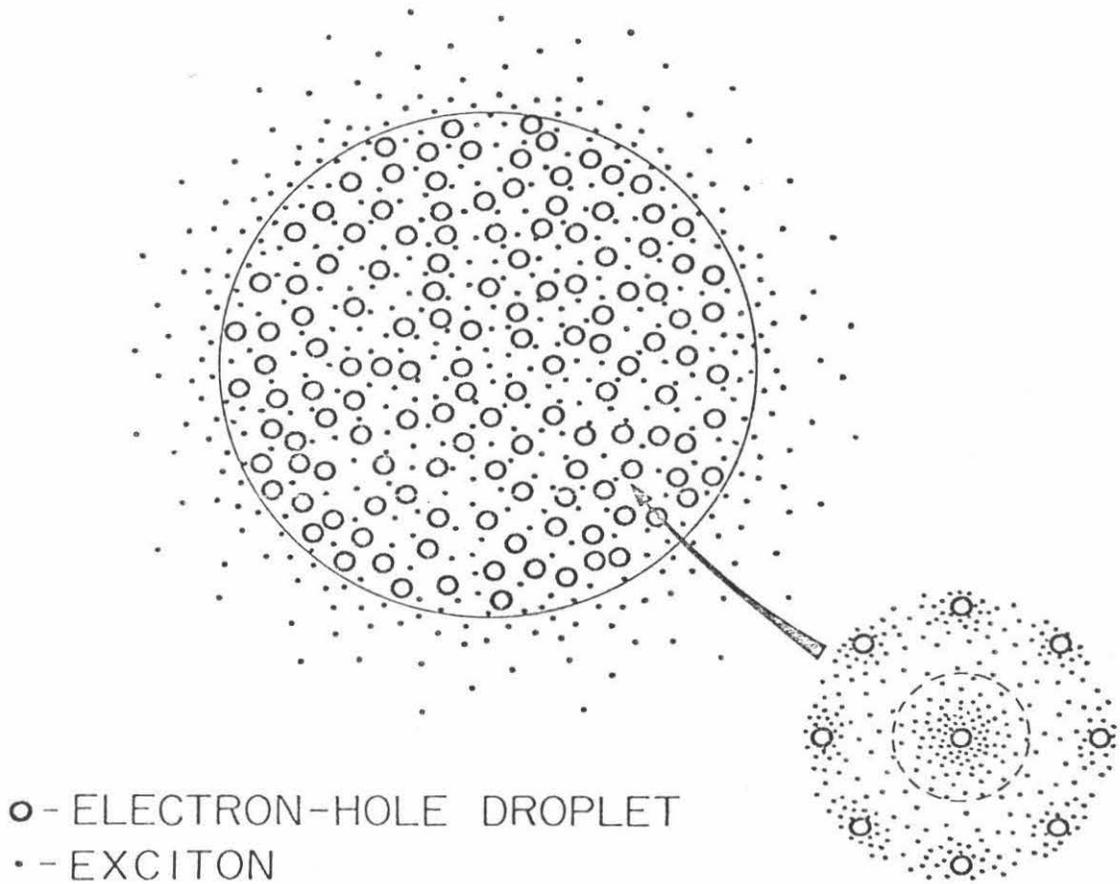
Figure 5.1

immediate vicinity. Each droplet is assigned a spherical volume of radius R_s as shown in the figure by the dashed line, and the condition is imposed that the net flux of excitons across these boundaries is zero. This is in contrast to a single drop picture in which the excitons outside the drop would have a boundary condition at infinity. Solving the diffusion equation within the region bounded by R_s and averaging the exciton density over this volume gives the average exciton density within the cloud. Each droplet in the body of the cloud now shrinks as pairs within it and the excitons inside its region recombine. Thus the number of pairs bound in droplets and the associated luminescence signal decrease both through the shrinking of individual droplets and of the cloud as a whole. This approach allows us to treat both evaporation and backflow for an EHD as well as the escape of excitons from the cloud; two important aspects of the problem which are neglected in the single-drop model.

The differential equation describing the decay of the cloud is determined by equating the rate of change of the total number of pairs in the cloud to the sum of the recombination rate for pairs bound in droplets, the recombination rate for excitons within the cloud, and the diffusion current of excitons away from the cloud at its surface.

$$\frac{d}{dt}(V_c N_0 + V_c \bar{n}_{ex}) = \frac{-V_c N_0}{\tau} - \frac{V_c \bar{n}_{ex}}{\tau_{ex}} - J_D\Big|_{R_c} \quad , \qquad (5.5)$$

where V_c is the volume of the cloud, N_0 the density of pairs bound

in EHD's (EHD density x fill factor), and J_D the diffusion current of
free excitons, here evaluated at the radius of the cloud, R_c. Dis-
tributing the time derivative we obtain two terms one describing
the change in V_c and the other change in total density of pairs. If
we assume that recombination only affects the density of pairs in
the cloud without changing its size while exciton diffusion causes
the cloud to shrink but only perturbs the pair density slightly near
the surface, then Eq. (5.5) separates giving

$$(N_o + \overline{n}_{ex}) \frac{dR_c}{dt} = \left| D\nabla n_{ex} \right|_{R_c} \quad , \tag{5.6}$$

and

$$\frac{d}{dt} (N_o + \overline{n}_{ex}) = - \left(\frac{N_o}{\tau} + \frac{\overline{n}_{ex}}{\tau_{ex}} \right) \quad , \tag{5.7}$$

where D is the exciton diffusivity, and thus $-D\nabla n_{ex}\big|_{R_c}$ is the exciton
flux evaluated at the surface of the cloud. Thus, there are essen-
tially two problems which must be solved. One is the shrinking of the
cloud due to the diffusion of excitons away from its surface (Eq. 5.6).
The other concerns the calculation of the exciton profile around each
droplet. From this part we obtain $\overline{n}_{ex}$, which is used in the solution
of Eq. (5.7) for EHD within the cloud as well as in Eq. (5.6) for
the cloud's surface.

To obtain the exciton diffusion current on the righthand side of

Eq. (5.6) we need to solve the diffusion equation governing the FE's outside the EHD cloud,

$$\frac{\partial n_{ex}}{\partial t} = D\nabla^2 n_{ex} - n_{ex}/\tau_{ex} \quad , \tag{5.8}$$

where n_{ex} is a function of both t and the distance r from the center of the cloud. The boundary conditions to be satisfied are

$$n_{ex} = \bar{n}_{ex}$$

$$\text{at } r = R_c(t) \quad , \tag{5.9}$$

and

$$n_{ex} = 0$$

$$\text{at } r = \infty \quad . \tag{5.10}$$

Equation (5.8) is coupled to Eq. (5.6) for R_c through boundary condition Eq. (5.9). These equations can be solved for $\frac{dR_c}{dt}$ in terms of $R_c(t)$ and $\bar{n}_{ex}(t)$.

We can rearrange Eq. (5.7) as

$$\frac{dN_0}{dt} = -\frac{N_0}{\tau} - \left(\frac{d\bar{n}_{ex}}{dt} + \frac{\bar{n}_{ex}}{\tau_{ex}}\right) \quad , \tag{5.11}$$

where the term in parentheses on the right is the average exciton

generation rate, which is just the net evaporation rate per unit volume after the end of the excitation pulse. Therefore, to determine the decay of EHD and FE inside the cloud, it is necessary to solve the exciton diffusion Eq. (5.8) for the region surrounding a given droplet with two boundary conditions. First, at the surface of the drop, $r = R_D(t)$, diffusion current away from the droplet equals net evaporation rate, or

$$-4\pi R_D^2 D \frac{\partial n_{ex}}{\partial r}\bigg|_{R_D} = aT^2 e^{-\phi_{EHD}/kT} v^{2/3} - 4\pi R_D^2 n_{ex} v_{th} \quad . \qquad (5.12)$$

Second, no exciton diffusion current flows across R_s, that is,

$$\nabla n_{ex} = 0$$

$$at \ r = R_s(t) \quad . \qquad (5.13)$$

The only time dependent part of N_o is the droplet radius, R_D, which is related to the diffusion current away from droplets by Eq. (5.11). The exciton diffusion equation can be solved to obtain this current which when substituted into Eq. (5.11) yields dR_D/dt as a function of time.

From the two parts of the problem, Eq. (5.6) and (5.7), two equations are obtained

$$\frac{dR_D}{dt} = f(R_D) \quad , \qquad (5.14)$$

and

$$\frac{dR_c}{dt} = g(R_D, R_c) \quad . \tag{5.15}$$

The functions f and g will be derived in the next section. A straightforward numerical integration of f and g yields $R_D(t)$ and $R_c(t)$. From $R_D(t)$ and $R_c(t)$ we obtain

$$I_{EHD} \sim R_c(t)^3 \cdot F(t) \quad , \tag{5.16}$$

and

$$I_{FE}(t) \sim \frac{4}{3} \pi R_c^3 \bar{n}_{ex}(t) + M_{ex}(t) \quad , \tag{5.17}$$

where M_{ex} is the number of excitons outside the cloud and F is the fill factor. To determine M_{ex} we numerically integrate the source - sink equation with respect to time

$$M_{ex} = \int_0^t \left(4\pi R_c^2 |D\nabla n_{ex}|_{R_c} \frac{-M_{ex}}{\tau_{ex}} \right) dt' + M_{ex}(o) \quad , \tag{5.18}$$

Where $M_{ex}(o)$, the number of excitons outside the cloud at t = 0, is calculated from the initial conditions.

During the laser pulse, a generation term must be added to the lefthand side of Eq. (5.12). This generation term drives the exciton gradient at each droplet surface positive so that excitons can flow into droplets during the time the laser is on. It is obvious that since we have not introduced the generation term, we cannot start

out with the correct initial condition. In fact, our solution assumes an initial condition such that the exciton gradient is negative at the surface of each droplet. However, since FE decay is fast, we expect the exciton density to relax from that at the end of the laser pulse to the one we assume in about one exciton lifetime. This relaxation can be observed in the FE transient in Fig. 5.3. Thus, our solution should be accurate to describe the decay transients after about one exciton lifetime from the end of the laser pulse.

III. Detailed Mathematical Formulation of Model

In this section the forms of $f(R_D)$ and $g(R_D,R_c)$ in Eq. (5.14) and (5.15) will be derived. First we will solve Eq. (5.11) for the interior of the cloud in order to obtain $\bar{n}_{ex}(t)$ and $N_o(t)$. As explained in the last section, we assume that each droplet has a volume associated with it and that there is no net flow of excitons across the surface of this volume. We take this region to be a sphere of radius R_s defined by

$$R_S = \left(\frac{R_D^3(t=0)}{F(t=0)} \right)^{1/3} .$$
(5.19)

The decay of a single drop is governed by

$$\frac{d}{dt} (n_o V_D) = \frac{-n_o V_D}{\tau} - J_D \Big|_{R_D} ,$$
(5.20)

with n_o the density of pairs in an EHD, V_D the average volume of a drop, and J_D the exciton diffusion current, here evaluated at the surface of the drop. Since n_o is independent of time, we have

$$\frac{dR_D}{dt} = \frac{-R_D}{3\tau} - \frac{F_D\big|_{R_D}}{n_o} ,$$
(5.21)

where F_D is the flux of free excitons away from the surface. To find F_D we must solve the diffusion equation for the excitons with boundary conditions at R_D and R_S

$$\frac{\partial n_{ex}}{\partial t} = D\nabla^2 n_{ex} - \frac{n_{ex}}{\tau_{ex}} \tag{5.22}$$

At $r = R_s$, $\frac{\partial n_{ex}}{\partial r} = 0$. At the surface of the drop, evaporation must balance backflow plus diffusion current away from the drop. In equilibrium, however, the backflow just balances the evaporation. So at $r = R_D$,

$$v_{th} n^o_{ex}(T) = v_{th} n_{ex}(r) + F_D \tag{5.23}$$

where v_{th} is the exciton thermal velocity and $n^o_{ex}(T)$ is the measured density of excitons in equilibrium with droplets as a function of temperature.

Defining $q = rn_{ex}$ and using the assumed spherical symmetry, the diffusion equation becomes

$$\frac{\partial q}{\partial t} = D \frac{\partial^2 q}{\partial r^2} - q/\tau_{ex} \quad . \tag{5.24}$$

Since we are in the interior of the cloud (and the fill factor is large enough for the cloud concept to be meaningful) q varies slowly with time, and we can make an adiabatic assumption that $\frac{\partial q}{\partial t} = 0$. This removes the explicit time dependence of $n_{ex}(r)$ though it still has an implicit time dependence through the boundary condition at R_D. The diffusion equation, Eq. (5.24), has solutions of the form

$$n_{ex}(r) = q/r = \frac{R_D}{r} a_1 n_{ex}^0 (a_2 e^{-(r-R_D)/\ell_{ex}} + e^{(r-R_D)/\ell_{ex}}) \quad , \quad (5.25)$$

where ℓ_{ex} is the exciton diffusion length, $\ell_{ex} \equiv \sqrt{D\tau_{ex}}$, and a_1, a_2 are determined by the boundary conditions at R_D and R_s. If we let

$$\beta = v_{th} R_D/D \quad , \quad (5.26)$$

which is just the ratio of drop radius to exciton mean free path, and

$$\gamma = e^{(R_s - R_D)/\ell_{ex}} \quad , \quad (5.27)$$

then

$$a_2 = \gamma^2 \frac{R_s - \ell_{ex}}{R_s + \ell_{ex}} \quad , \quad (5.28)$$

and

$$a_1 = \frac{\beta}{(\beta+1)(a_2+1) + \frac{R_D}{\ell_{ex}}(a_2-1)} \quad . \quad (5.29)$$

This gives

$$\frac{F_D\big|_{R_D}}{n_0} = Da_1 \frac{n_{ex}^0}{n_0} \left(\frac{a_2+1}{R_D} + \frac{a_2-1}{\ell_{ex}} \right) \quad . \quad (5.30)$$

Substituting Eq. (5.30) into Eq. (5.21) we obtain

$$\frac{dR_D}{dt} = f(R_D) \quad , \quad (5.31)$$

with

$$f(R_D) \equiv - \frac{R_D}{3\tau} + Da_1 \frac{n_{ex}^0}{n_0} \left(\frac{a_2+1}{R_D} + \frac{a_2-1}{\ell_{ex}} \right) \, , \tag{5.32}$$

which is Eq. (5.14) in the last section. This equation is integrated numerically since a_1 and a_2 are complicated functions of R_D. From Eq. (5.25) we obtain

$$\frac{\bar{n}_{ex}}{n_{ex}^0} \equiv \frac{\int_{R_D}^{R_s} 4\pi r^2 n_{ex}(r)dr}{\frac{4\pi}{3} R_s^3 n_{ex}^0} = \frac{3a_1 R_D \ell_{ex}}{R_s^3} \left[(a_2-1)(R_s-\ell_{ex}) + 2a_2 \, \ell_{ex} \right], \tag{5.33}$$

and

$$N_0 = \left(R_D/R_s \right)^3 \quad . \tag{5.34}$$

Now with $\bar{n}_{ex}$ and N_0 we can go back to the problem of the cloud as a whole. We need to determine the exciton diffusion profile outside the cloud to find $F_D\big|_{R_c}$, the flux of excitons at its surface. We have

$$\frac{\partial n_{ex}}{\partial t} = D\nabla^2 n_{ex} - \frac{n_{ex}}{\tau_{ex}} \qquad (r > R_c(t)) \quad , \tag{5.35}$$

and

$$\frac{\partial n_{ex}}{\partial t} = D\nabla^2 n_{ex} - \frac{n_{ex}}{\tau_{ex}} + \frac{3v_{th} \cdot F}{R_D} \left(n_{ex}^0 - n_{ex} \right) \quad (r \lesssim R_c(t)) \quad . \tag{5.36}$$

The first of these equations holds for excitons completely outside the region in which there are droplets ($r > R_c$). The second equation is for excitons just inside the edge of the cloud with the last term corresponding to the net evaporation of excitons per unit volume. This term leads to an average effective diffusion length for excitons within the cloud which is much smaller than ℓ_{ex} and thus the perturbation in exciton concentration due to the cloud's surface extends in only a small distance.

In solving these equations, we must match the two solutions at $r = R_c(t)$ with boundary conditions $n_{ex} = 0$ as $r \to \infty$ and $n_{ex} \to \bar{n}_{ex}$ as $r \to 0$. Deep inside the cloud $\bar{n}_{ex}$ satisfies the equation

$$\frac{\partial \bar{n}_{ex}}{\partial t} = \frac{-\bar{n}_{ex}}{\tau_{ex}} + \frac{3Fv_{th}}{R_D} \left(n_{ex}^0 - \bar{n}_{ex} \right) . \tag{5.37}$$

Defining $w \equiv \bar{n}_{ex} - n_{ex}$, and an effective lifetime due to capture by droplets $\tau_c \equiv R_D/(3 F v_{th})$, then subtracting Eq. (5.36) from Eq. (5.37) yields

$$\frac{\partial w}{\partial t} = D\nabla^2 w - w\left(\frac{1}{\tau_{ex}} + \frac{1}{\tau_c}\right) . \tag{5.38}$$

For reasonable parameters (see Table 5.1) $\tau_{ex}/\tau_c \sim 100$, and the effective diffusion length,

$$\ell_{ef} \equiv \sqrt{\frac{D\tau_{ex}\tau_c}{(\tau_{ex} + \tau_c)}} , \tag{5.39}$$

is given approximately by

$$\ell_{ef} \approx \sqrt{D\tau_c}$$

and is quite short, $\ell_{ex}/\ell_{ef} \approx 10$. Thus, the perturbation in exciton density due to the cloud's surface extends in only a short distance. Furthermore, τ_c is so short that the exciton profile within the cloud can react very rapidly to the motion of the surface as the cloud shrinks. This allows us to make an adiabatic approximation, setting $\partial w/\partial t = 0$ in the frame of reference of the cloud's surface and reducing the equation to steady state. Using spherical symmetry the resulting equation is readily solved, giving:

$$w(r) = \frac{R_c}{r} w(R_c) \left[\frac{e^{r/\ell_{ef}} - e^{-r/\ell_{ef}}}{e^{R_c/\ell_{ef}} - e^{-R_c/\ell_{ef}}} \right] \qquad (r \leq R_c(t)) , \qquad (5.40)$$

where the second term in the numerator keeps the solution finite at the origin and $w(R_c)$ must be determined by matching to the outside solution.

The solution to the equation for $r > R_c(t)$ is complicated by the fact that the exciton lifetime is too long to allow us to make the simple adiabatic assumption in this region we used in the $r \lesssim R_c$ case. Here the exciton profile does not simply move with the cloud's surface but it changes depending upon the velocity of the surface.

Assuming spherical symmetry and defining, $u \equiv \dfrac{rn_{ex}}{R_c(t)}$ and

$v \equiv \dfrac{-\partial R_c}{\partial t}$, we can reduce the equation for $r > R_c$ to a one-dimensional form,

$$\frac{\partial u}{\partial t} = D \frac{\partial^2 u}{\partial r^2} - u(\frac{1}{\tau_{ex}} - v/R_c) \quad . \tag{5.41}$$

Now we transform to the frame stationary with respect to the cloud's surface by defining

$$x \equiv r - R_c(t) \quad . \tag{5.42}$$

Defining $\tau' \equiv \dfrac{R_c - \tau_{ex} v}{R_c \tau_{ex}}$, the resulting equation is

$$\frac{\partial u}{\partial t} = D \frac{\partial^2 u}{\partial x^2} - v \frac{\partial u}{\partial x} - u/\tau' \qquad (x > 0) \quad . \tag{5.43}$$

Thus, to find $F_D \big|_{R_c}$, we must solve this equation subject to the boundary conditions that the inside and outside solutions match at R_c and that the density of excitons is zero at infinity.

$$\bar{n}_{ex} - w(R_c) = u(x=0) \quad ; \tag{5.44}$$

$$- \frac{\partial w}{\partial r}\bigg|_{R_c} = \frac{\partial}{\partial x} \left(\frac{u}{R_c + x}\right)\bigg|_{x=0} \quad , \tag{5.45}$$

and

$$u(\infty) = 0 \quad . \tag{5.46}$$

The transformation has taken some of the time dependence out of u. The parts still left are

$$\frac{\partial n_{ex}(R_c)}{\partial t} \quad , \quad \frac{\partial v}{\partial t} \quad , \quad \text{and} \quad \frac{\partial \tau'}{\partial t} \quad .$$

If we assume that these terms are small, then we can make the adiabatic assumption and say $\partial u / \partial t = 0$. This assumption allows an analytic solution to Eq. (5.43).

Defining:

$$\ell' \equiv \frac{2D}{\sqrt{v^2 + 4D/\tau'} - v} \qquad , \qquad (5.47)$$

the solution is

$$n_{ex}(r) = R_c(t) n_{ex}(R_c) \frac{e^{(R_c - r)/\ell'}}{r} \qquad . \qquad (5.48)$$

Matching the inside solution, Eq. (5.40), to the outside solution and using the fact that $R_c \gg \ell_{ef}$, gives

$$n_{ex}(R_c) = \bar{n}_{ex} \frac{\ell'}{\ell' + \ell_{ef}} \left(1 - \frac{\ell_{ef}}{R_c} \right) \qquad . \qquad (5.49)$$

Balancing the density of carriers inside with the flux out gives

$$\frac{-dR_c}{dt} = \frac{Dn_{ex}(R_c)}{N_0 + n_{ex}(R_c)} \left(1/\ell' + 1/R_c \right) \quad . \qquad (5.50)$$

where $\partial \ell'/\partial t$ has been ignored since it is small when the adiabatic approximation is valid. Defining

$$\alpha \equiv \frac{2(N_0 + n_{ex}(R_c))}{n_{ex}(R_c)} \qquad , \qquad (5.51)$$

we get the solution (ignoring the slight dependence on v of $n_{ex}(R_c)$)

$$\frac{dR_c}{dt} = g(R_D, R_c) \quad , \tag{5.52}$$

with

$$g(R_D, R_c) \equiv \frac{-2}{\alpha+2} \frac{\ell_{ex}}{\tau_{ex}} \left(\frac{\ell_{ex}}{R_c} + \sqrt{\frac{\alpha+2 - 2(\ell_{ex}/R_c)^2}{\alpha}} \right) \tag{5.53}$$

This is the equation given in the last section (5.15). N_o and $\bar{n}_{ex}$ are functions of R_D and thus α is a function of $R_D(t)$.

Thus we have reduced the problem to two consecutive numerical integrations. First Eqs. (5.31) and (5.32) are integrated to obtain $R_D(t)$, and from it $\bar{n}_{ex}(t)$ (Eq. (5.33)) and $N_o(t)$ (Eq. (5.34)) may be found. These functions are then used in the integration of Eqs. (5.52) and (5.53) to find $R_c(t)$. It is most convenient to calculate the exciton luminescence by breaking it up into the contribution from excitons within the cloud and the contribution from those outside (Eq. 5.17). The source-sink equation (Eq. (5.18)) is used to find the term arising from excitons outside the cloud. This avoids the problem of a careful calculation of the exciton profile which would be needed for a spatial integration to determine I_{FE}. The effective diffusion length, ℓ', is a good characterization of the diffusion profile near the cloud's surface since it arises from the surface moving past some excitons and thus giving less slope to the profile than just ℓ_{ex}. However, far from the cloud edge the exciton profile is not a simple exponential due to the acceleration of the

surface of the cloud.

The theoretical curves were calculated with initial conditions chosen so as to avoid transients at the beginning. Thus, it was assumed that the cloud and droplet edges have a finite velocity at $t = 0$. This was found by determining the diffusion profiles within the cloud to get $\bar{n}_{ex}$, and then solving self-consistently for $\partial R_c/\partial t$. The self-consistent approach is necessary to correctly include the dependence of $n_{ex}(R_c)$ on v. The number of excitons outside the cloud at the beginning of the calculation, $M_{ex}(o)$, is determined by spatially integrating the solutions for $n_{ex}(r)$ at $t = 0$.

IV. Results of Calculation and Comparison with Experiments

In this section, the calculated decay transients of the EHD and FE intensity will be presented and compared to experimental data.

The theoretical curves presented in Fig. 5.2 were calculated for three different initial cloud radii. Values of the parameters used in the calculation are listed in Table 5.1 along with the values of the same parameters reported in the literature. Figure 5.2(a) shows the calculated EHD luminescence decay transient, normalized to unity at the start of the decay. The corresponding curves for the FE are shown in Figure 5.2(b). At 4.2^OK, an increase of $R_c(o)$ causes the decay to be longer, because for larger $R_c(o)$ the initial surface to volume ratio is smaller, and this lessens the importance of exciton diffusion away from the cloud. Spatially-resolved optical absorption experiments at 4.2^OK [21] show that different initial $R_c(o)$ can be created by using different excitation powers. It can be seen in Figure 5.2(b) that there are clear differences between the three FE curves making them a sensitive, independent check on the model. In particular, these results are very different from the solutions to the average rate equations in which there is no boundary to the region occupied by EHD's. Experimental results of the EHD and FE decay transients after long (100 μsec) excitation pulses for two different pump powers are also shown in Figure 5.2. It can be seen that excellent agreement is obtained for both the EHD and the FE curves when reasonable values for the parameters are used in the

calculation. There are several points that should be noted however. First, parameters can offset each other to some extent, e.g., reducing the exciton diffusion length slows down the decays, but this may be offset by increasing the equilibrium density of excitons. Whenever possible, values for the parameters determined from independent measurements have been used to reduce the number of fitting parameters. Second, optical absorption experiments have shown that exciton recombination current at the Ge surface is non-negligible at $4.2^{o}K$ [21]. Furthermore, recent pictures of the cloud in Ge have shown that it has a complicated shape which is only roughly hemispherical [17]. Thus, our model is qualitatively correct in that the essential physics has been retained, but it is difficult to get accurate quantitative results from the fits. Since the cloud is not simple in shape, R_c is an average cloud radius characterizing the volume to surface ratio. Figure 5.2(c) shows plots of $R_c(t)$ corresponding to the cases shown in (a) and (b). At $4.2^{o}K$, it is seen that the shrinking of the cloud of EHD's is as important as the shrinking of individual droplets in causing the decay in the droplet luminescence intensity. This collapse of the EHD cloud has been observed in temporally and spatially resolved absorption experiments [21].

Our model also correctly describes the EHD decay at $2^{o}K$. The cloud radius, R_c, does not change noticeably with time because $\bar{n}_{ex}$ is so small that FE recombination current cannot significantly affect EHD decay.

Figure 5.2

Results of calculations of the model for 4.2°K. The parameters used are appropriate for pure Ge and are given in Table 5.1. The initial radii of the cloud for curves 1, 2 and 3 are 1.0, 1.4 and 1.8 mm, respectively. Experimental results for high-purity Ge are shown for comparison; pump-powers used are (▲) 0.14 W and (●) 0.09W. (Experimental results from M. Chen.)
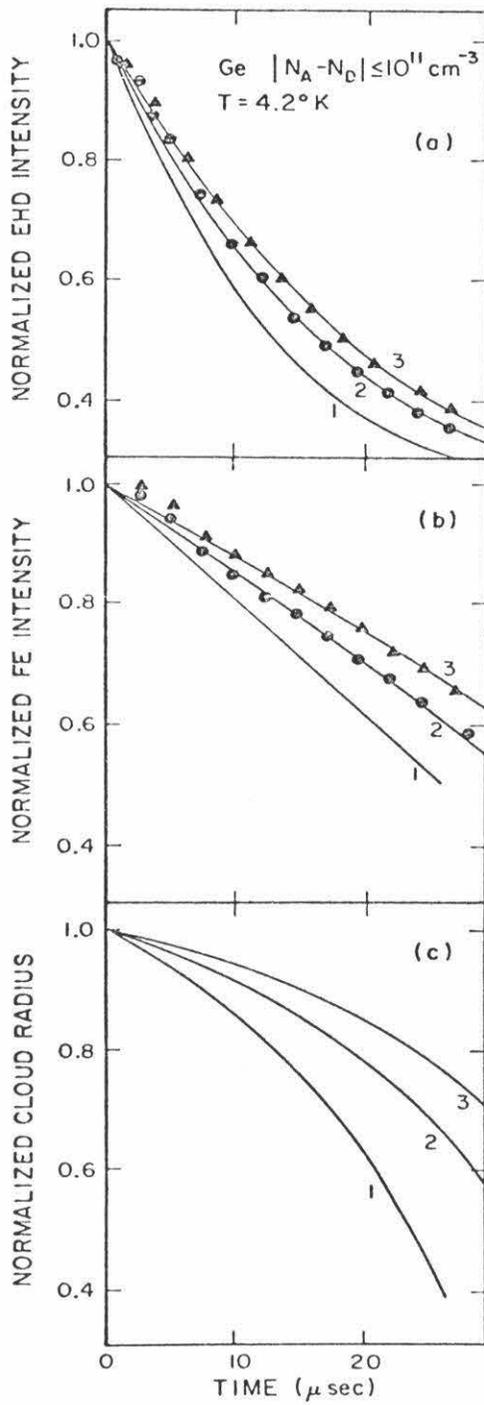
Figure 5.2

Table 5.1. Values of parameters used in the model

Parameter	Values used in calculations for Fig. 7	Values found in the literature
EHD lifetime, τ	37 μsec	36-45 μsec [a-c]
FE lifetime, τ_{ex}	7 μsec	6-8 μsec [c-d]
Equilibrium density of FE, n_{ex}^0		
2°K	7×10^{11} cm^{-3}	7×10^{11} cm^{-3} [e]
4.2°K	3×10^{14} cm^{-3}	5×10^{14} cm^{-3} [e]
Pair density in the EHD, n_0		
2°K	2×10^{17} cm^{-3}	2.1×10^{17} cm^{-3} [e]
4.2°K	2×10^{17} cm^{-3}	2.4×10^{17} cm^{-3} [e]
Initial EHD radius, $R_D(0)$		
2°K	2 μm	2 μm [f]
4.2°K	10 μm	~10 μm [g]
FE diffusion length, ℓ_{ex}	0.8 mm	~ 1 mm [h,i]
Fill factor, F	2%	1-2% [f,j]
Initial cloud radius, $R_s(0)$	1.4 - 1.8 mm	1-2 mm [k,j]

a. Ref. 3

b. Ref. 4

c. Ref. 5

d. V. Marello, T. C. McGill and J. W. Mayer, Phys. Rev. B13, 1607 (1976).

e. G. A. Thomas, A. Frova, J. C. Hensel, R. E. Miller and P. A. Lee, Phys. Rev. B13, 1692 (1976).

f. J. M. Worlock, T. C. Damen, K. L. Shaklee and J. P. Gordon, Phys. Rev. Lett. 33, 771 (1974).

g. Ref. 10

h. Ref. 13

i. Ref. 20

j. Ref. 19

k. Ref. 16

Under the same excitation conditions, the initial cloud radius, initial fill factor, and exciton diffusion length can be different in pure Ge and Ge doped with about $10^{15} cm^{-3}$ of impurities. Spatial luminescence intensity scans show that the cloud of EHD's does not penetrate as deeply in lightly doped Ge as in pure Ge[20,21], so $R_c(o)$ should be smaller in lightly doped Ge compared to pure Ge. This fact, coupled with the observation that the total luminescence intensities from pure and doped Ge do not differ significantly, implies a larger fill factor in doped Ge. Neutral impurity scattering of excitons can significantly alter the exciton diffusion length at the $10^{15} cm^{-3}$ doping level. Figure 5.3 shows calculations for $4.2^{\circ}K$ for various initial cloud radii, fill factors, and exciton diffusion lengths. For curve 1, an initial radius of 0.5 mm was assumed, and the fill factor has been increased to 10% in keeping with the greater confinement of the EHD's. The exciton diffusion length, ℓ_{ex}, is still 0.8 mm. The decay is seen to be slower in this case compared to pure Ge (Figure 5.2(a)) but is still far from being exponential. Curve 2 assumes $R_c(o) = 0.5$ mm, fill factor = 2% and $\ell_{ex} = 0.016$ mm. Comparison of curves 1 and 2 shows the much greater importance of diffusion length over fill factor in slowing down the decay. Curve 3 incorporates all the expected changes for doped Ge with $R_c(o) = 0.5$ mm, $\ell_{ex} = 0.016$ mm, and a fill factor of 10%. As can be seen from the figure, altering the parameters to those for doped Ge dramatically changes the decay curves, causing the luminescence transients to become nearly exponential for temperatures

as high as 4.2^{o}K. Excellent agreement with the experimental data, shown as dots in Figure 5.3(a), is obtained. It should be noted that the value for exciton diffusion length in the doped material was determined through fitting the luminescence decays and has not been determined independently. Figure 5.3(b) shows the calculated decay curves for FE corresponding to the cases in Figure 5.3(a). The decay time of the FE is controlled by the evaporation of excitons from droplets and is, therefore, directly related to the EHD life-time. For the case corresponding to lightly doped Ge, curve 3, the FE decay is expected to be very slow compared to pure Ge. Figure 5.3(c) shows the calculated $R_c(t)$ using the same parameters as those used for the corresponding curves in Figures 5.3(a) and (b). These curves illustrate clearly that reducing the diffusion length stops the escape of excitons from the cloud and the reduction of R_c with time. Merely increasing the fill factor as for curve 1 does not accomplish this, and consequently the calculated decay is much too fast compared to experiment. The net evaporation of excitons from droplets must be shut off in order to account for the long decays observed for lightly doped Ge.

The reduction of free exciton diffusion length in doped Ge implies a short exciton diffusion tail and, therefore, fewer excitons around each drop. Thus, it is expected that the relative EHD to FE intensity should be small while EHD's are decaying. This reduction of FE intensity for doped Ge is observed experimentally.

Figure 5.3

Results of calculations of the Model for 4.2^{O}K.
Curve 1: FE diffusion length - 0.8 mm, fill factor = 10%.
Curve 2: FE diffusion length - 0.016 mm, fill factor = 2%.
Curve 3: FE diffusion length = 0.016 mm, fill factor = 10%.
Initial cloud radius for all three curves is 0.5 mm, all
other parameters are the same as those for pure Ge given in
the text. Experimental results of the luminescence intensity
decay of the EHD in a Ge sample with $4 \times 10^{15} cm^3$ are shown as
the dots. (Experimental results from M. Chen.)
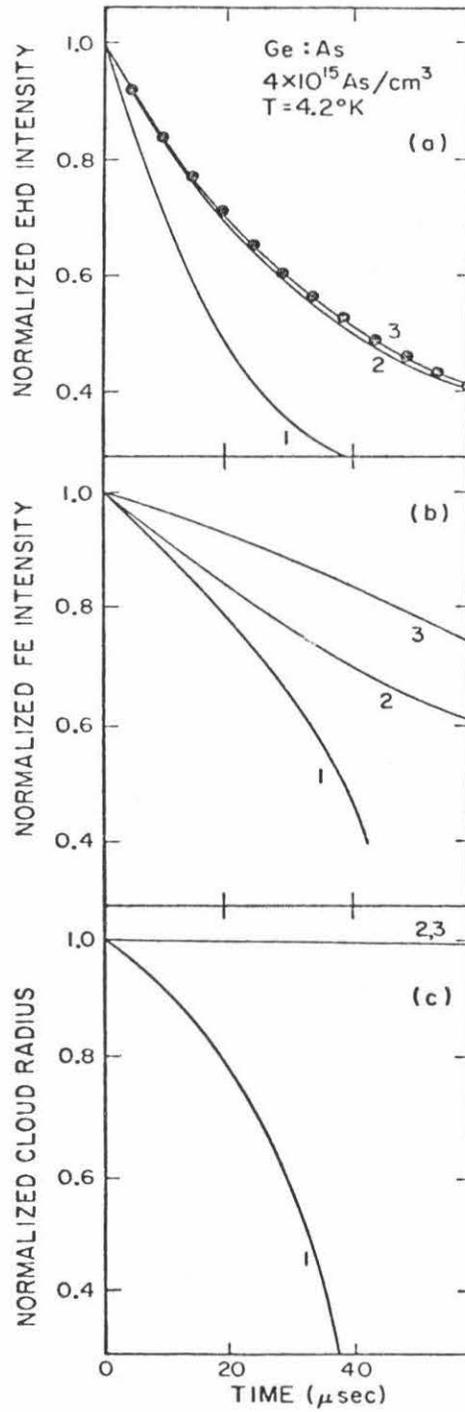
Figure 5.3

Our model predicts, as observed experimentally, that the decay of the EHD in lightly doped Ge at 2^{O}K should be determined by the recombinative lifetime of the EHD.

V.   Summary and Conclusion

It has become apparent that the single-drop model is unable to account for the EHD decay transients observed in many experiments. For high excitation intensities and temperatures, unphysical parameters are needed to fit the data. We have developed a new model for the EHD luminescence intensity decay which takes into account both the existence of a cloud of droplets and exciton emission and capture by droplets. This model simultaneously gives excellent fits to both the EHD and FE decay transients. In the case of pure Ge at $4.2^{o}K$, evaporation from the droplets in the cloud keeps the exciton density inside the cloud at approximately the equilibrium density after the excitation is turned off. This exciton density implies that backflow is large within the cloud. This high backflow rate causes the observed EHD decay times at $4.2^{o}K$ in pure Ge to be longer than expected from the independent droplet model. The decay of the luminescence is due to a combination of the shrinking of individual droplets and the shrinking of the cloud as a whole. Pump-power dependence of the decay time is a consequence of the different initial cloud radii generated by different pump conditions.

For the lightly doped Ge the FE exciton diffusion length is reduced from that in pure Ge. This change in diffusion length can produce a large reduction in the rate of FE evaporation from the droplets. At sufficiently small diffusion lengths the droplets in our model act independently. The cloud does not shrink, since

excitons are not supplied to a substantial region outside the cloud or for that matter in between droplets. Furthermore, the evaporation of excitons from a given drop is nearly cancelled by the recapture of those excitons by the same drop before they can diffuse away. This reduction in net evaporation accounts for the nearly exponential behavior of the EHD decay transients in lightly doped Ge at high temperatures.

References

1. C. D. Jeffries, Science 189, 955 (1975), and references contained therein.

2. K. L. Shaklee, in Proceedings of Third International Conference on Light Scattering in Solids, Campinas, Brazil, 1975, edited by M. Balkanshi, R. C. C. Lute, and S. P. S. Porto (Flammarion Sciences Press, Paris, 1976) p. 160.

3. J. C. Hensel, T. G. Phillips and T. M. Rice, Phys. Rev. Lett. 30, 227 (1973).

4. C. Benoit a la Guillaume, M. Capizzi, B. Etienne and M. Voos, Solid State Commun. 15, 1031 (1974).

5. R. M. Westervelt, T. K. Lo, J. L. Staehli and C. D. Jeffries, Phys. Rev. Lett. 32, 1051 (1974).

6. B. M. Ashkinadze and I. M. Fishman, Fiz. Tekh. Poluprovodn. 11, 408 (1977) [Sov. Phys. Semicond. 11, 235 (1977)].

7. K. Fujii and E. Otsuka, Solid State Commun. 14, 763 (1974).

8. J. Shah, A. H. Dayem, M. Voos and R. N. Silver, Solid State Commun. 19, 603, (1976).

9. J. L. Staehli, Phys. Status Solidi B75, 451 (1976).

10. V. S. Bagaev, N. A. Penin, N. N. Sibel'din and V. A. Tsvetkov, Fiz. Tverd. Tela. 15, 3259 (1973) [Sov. Phys. Solid State 15, 2179 (1974)].

11. R. N. Silver, Phys. Rev. B11, 1569 and B12, 5689 (1975).

12. R. M. Westervelt, Phys. Status Solidi b74, 727 and b76, 31 (1976).

13. Y. E. Pokrovskii, Phys. Status Solidi $\underline{a11}$, 385 (1972).

14. To apply to the excitons, the Richardson-Dushman Constant for metals is corrected for exciton mass, binding energy and degeneracy. In addition, a factor $(36)^{1/3} n_o^{2/3}$ is incorporated in which converts $v^{2/3}$ to the droplet surface area.

15. J. M. Hvam and O. Christensen, Solid State Commun. $\underline{15}$, 929 (1974).

16. J.C.V. Mattos, K. L. Shaklee, M. Voos, T. C. Damen and J. M. Worlock, Phys. Rev. $\underline{B13}$, 5603 (1976), and references contained therein.

17. J. P. Wolfe, M. Greenstein, and J. Arzegian, Bull. A.P.S. $\underline{23}$, 422 (1978).

18. J. Doehler, J.C.V. Mattos and J. M. Worlock, Phys. Rev. Lett. $\underline{38}$, 726 (1977).

19. K. R. Elliott, D. L. Smith and T. C. McGill (to be published).

20. R. W. Martin, Phys. Status Solidi $\underline{B61}$, 223 (1974).

21. M. Chen (unpublished).